

# UC Irvine

## UC Irvine Electronic Theses and Dissertations

### Title

Mitochondrial Akt1 Signaling Enhanced iPSC Reprogramming- Mechanism of Mitochondrial Akt1-PDH E3 Subunit Interaction

### Permalink

<https://escholarship.org/uc/item/1f06484r>

### Author

CHEN, YU-HAN

### Publication Date

2016

### Copyright Information

This work is made available under the terms of a Creative Commons Attribution-NonCommercial-NoDerivatives License, available at <https://creativecommons.org/licenses/by-nc-nd/4.0/>

Peer reviewed|Thesis/dissertation

UNIVERSITY OF CALIFORNIA,  
IRVINE

Mitochondrial Akt1 Signaling Enhanced iPSC Reprogramming  
- Mechanism of Mitochondrial Akt1-PDH E3 subunit Interaction

DISSERTATION

Submitted in partial satisfaction of the requirements  
for the degree of

DOCTOR OF PHILOSOPHY

in Physiology and Biophysics

by

Yu-Han Hank Chen

Dissertation Committee:  
Professor Ping H. Wang, Chair  
Professor Lan Huang  
Professor Rongsheng Jin  
Professor Bogi Andersen  
Assistant Professor Qin Yang

2016



# DEDICATION

To

My late Grandmoms and Uncle Donny,

My wonderful parents,  
Sister Emily, Brother in Law Joe and Nephew Matthew,  
And Bother James

# TABLE OF CONTENTS

	Page
LIST OF FIGURES	iv
LIST OF TABLES	vi
ACKNOWLEDGMENTS	vii
CURRICULUM VITAE	ix
ABSTRACT OF THE DISSERTATION	xi
CHAPTER 1: Introduction	1
CHAPTER 2: Mitochondrial Akt1 Signaling Enhanced iPSC Reprogramming Efficiency	
Introduction	13
Materials and Methods	14
Results	21
Discussion	26
CHAPTER 3: Mitochondrial Akt1 Modulated Cellular Metabolism	
Introduction	39
Materials and Methods	42
Results	45
Discussion	47
CHAPTER 4: Mechanism of Mitochondrial Akt1-PDH E3 subunit Interaction	
Introduction	57
Materials and Methods	59
Results	67
Discussion	75
CONCLUSION	93
REFERENCES	96

## LIST OF FIGURES

		Page
Figure 1.1	Mouse preimplantation development	12
Figure 2.1	The two mitochondria-targeting Akt constructs	30
Figure 2.2	The scheme of mouse iPSC induction procedure	31
Figure 2.3	Morphologies of reprogrammed cells from MEF or HDF-N	31
Figure 2.4	Mitochondrial Akt1 enhanced mouse iPSC reprogramming efficiency	32
Figure 2.5	The mouse iPSCs expressed embryonic stem cell markers	34
Figure 2.6	The reprogrammed cells may differentiate into cell lineages of three germ layers	35
Figure 2.7	Methylation of Oct4 and Nanog promoters in mouse iPSCs	37
Figure 2.8	Mitochondrial Akt1 modulated cellular respiration in the resulting iPSC	38
Figure 3.1	The scheme of metabolite extraction from mouse embryonic fibroblast	51
Figure 3.2	The mass spectrums of extracted metabolites from cells with or without external control	52
Figure 3.3	Mitochondrial Akt1 modulated cellular bioenergetics of mouse embryonic Fibroblast	55
Figure 3.4	Activation of mitochondrial Akt1 signaling reduced ROS and apoptosis Levels under stress conditions	56
Figure 4.1	The simulation model of interactionn of Akt1–E3 by Brownian dynamics	79
Figure 4.2	The results of recombinant protein purifications	80
Figure 4.3	Both recombinant wild type and mutant E3s bind to recombinant constitutively active Akt1 in a pulldown assay	81
Figure 4.4	Binding region mapped by FBS	82
Figure 4.5	FindBindSite predicted interaction model shows partial agreement with Brownian Dynamics simulated model	83

		Page
Figure 4.6	In vitro pulldown assay reveals some small molecule compounds disrupted Akt1-E3 interaction	84
Figure 4.7	Compound NSC 34766 and NSC 628725 reduced the amount of bound Akt1 on E3	85
Figure 4.8	The expression of a constitutively active mitochondria-targeting Akt1 increased PDH activity	86
Figure 4.9	Compound NSC 628725 Incubation Reduced PDH Activity	87

## LIST OF TABLES

		Page
Table 4.1	List of small molecular compounds obtained via FBS and pharmacophore studies	90
Table 4.2	List of 19 compounds obtained from NCI/DTP for Akt1-E3 pulldown Assay	91
Table 4.3	The effects of small molecular compounds on Akt1-E3 interaction	92



## ACKNOWLEDGMENTS

I would like to express my appreciation to my committee chair, Dr. Ping H. Wang, who is always busy but can still spare some time to discuss with me. He is always patient and kind to lead me through the difficulties during research. I appreciate his attitude towards research and teaching. Without his guidance and persistent help, this dissertation would not have been possible.

I would also like to thank my committee members, Dr. Rongsheng Jin, Dr. Lan Huang, Dr. Qin Yang and Dr. Bogi Andersen, who have been giving their constructive opinions and suggestions to the current dissertation. Without their suggestions and help, this project would not have achieved such far.

I would also like to thank my mentor in the laboratory, Dr. Yumay Chen, who is knowledgeable and always ready for a new adventure in research. Her strong confidence and knowledgeable bench work have inspired me to pursuit a new page of scientific career.

A special thanks would be given to Dr. Brian A. Pedersen, who is another mentor to me in the laboratory. He is always reachable, knowledgeable, logical and patient. Through every discussion with him, I understand what is the so called paragon of a scientist. I appreciate his passion and attitude towards sciences. His logical thinking and enthusiasm for learning new things have inspired my motivation to become a scientist like him.

A thank you is also given to the people who have contributed to the current dissertation. James B. Fields from Dr. Douglas Tobias group at Department of Chemistry and Hubert Li from Dr. Nagarajan Vaidehi group at Department of Immunology at City of Hope. Without their professional knowledge, we would not have reached this far.

Many thanks are given to those who have accompanied me during my 7 years at UC Irvine and reached such far. The National Taiwan University group at City of Hope, Dr. YunRu Chen, Dr. Chun-Ting Cheng, Dr. Ching-Ying Kuo, Yi-Ying Chung, Wei-Le Wang, Joanna Lin, Dr. Ting-Yu Lin, Dr. Tsung-Chin Lin, Dr. Alice Su, Dr. Superching and Yu-Cheng Lin, thank you for being such a nice supporting group during my stay in America and providing so much entertainment when I feel alone. The UC Irvine Ping Wang group, Dr. Hsin-Bang Leu, Dr. Jia-Ying Yang, Dr. Puya Yarzdi, Jared Tylor, Chia-Hsuan Wu, Chung-Hsuan Kao, Dr. Weiwen Wang, Dr. Wu Deng, Dr. Hsiao-Chen Lee, Dr. Wenjun Fan, Dr. Chin-Sung Kuo, Dr. Min Liu, Dr. Chin-Hsung Kuo, Charity Juang, and Matthew Funsten, thank you for the contribution to the laboratory environment. The UC Irvine Stem Cell group, Tauen Lim, Linan Liu, Christina Tu, Dr. Chinhui Hsiang, You-Hsing Sung, Vanessa Scarfone, Marek Mandau, and Christopher Ottm, thank you for providing supportive knowledge and technique platforms. The UC Irvine doctorate friends, Dr. Ian Ho, Dr. Ming-Je Sung, Dr. Alice Chien, thank you for providing supportive energies during every stressful events.

Lastly, I would like to express my deepest appreciation to my parents. Thank you for being so supportive in every single occasion in the past 34 years. Without your efforts, I would not even have reached so far and done this dissertation. My American dream costs you a lot, not just money but also efforts. I would dedicate what I have been trained in the past 7 years to where it is supposed to be applied. Also, thanks are given to all my families in the United States of America and Taiwan, Emily Chen Liao, Joe Liao & Matthew Liao, and James Chen. Auntie Lee Chiou, Auntie Grace and Uncle Alex, and Uncle Paul. Cousins, Alice Hsu and her families, Bill Chiou and his families, Craig Chiou and his families, Julia Lin and her families, Edward Chen and his families, Monica Chen Mah and her families, Jerry Lin, Elaine Lin, George Lin, Yvonne Chen, Stephanie Lin, Peggy Chu and Steven Lin.

Figure 1.1 in this dissertation was referenced from the journal of Trends in Cell Biology, Volume 25, Issue 2, page 82–91, February 2015. Permission to use copyrighted material was granted from the publisher.

Financial supports for this dissertation were provided by National Institutes of Health R01HL096987, Ko Family Foundation, and Oxnard Foundation (to Ping H. Wang) and California Institute of Regenerative Medicine Training Grant TG2-01152 (Yu-Han Chen).

# CURRICULUM VITAE

## Yu-Han Hank Chen

- 2006 B.S. in Clinical Laboratory Sciences and Molecular Biotechnology, National Taiwan University, Taiwan
- 2006-2008 Military Service, Taiwan
- 2008-2009 Research Assistant, Institute of Biological Chemistry, Dr. Ruey-Hwa Chen's group  
Academia Sinica, Taiwan
- 2011 M.S. in Biotechnology, University of California, Irvine
- 2016 Ph.D. in Physiology and Biophysics,  
University of California, Irvine

## HONORS AND SCHOLARSHIPS

- 2012 Oral Presentation at American Diabetes Association Conference, Philadelphia
- 2014 California Institute of Regenerative Medicine (CIRM) Training Grant
- 2016 Oral Presentation at American Diabetes Association Conference, New Orleans

## FIELD OF STUDY

Stem Cell Biology, Mitochondria, Cellular Metabolism, Cell Signaling Transduction

## PUBLICATIONS

1. Pedersen BA, Wang W, Taylor JF, Khattab OS, Chen YH, Edwards RA, Yazdi PG, Wang PH. Hepatic proteomic analysis revealed altered metabolic pathways in insulin resistant Akt1(+/-)/Akt2(-/-) mice. *Metabolism*. 2015;64(12):1694-703. doi: 10.1016/j.metabol.2015.09.008.
2. Yazdi PG, Pedersen BA, Taylor JF, Khattab OS, Chen YH, Chen Y, Jacobsen SE, Wang P: Increasing Nucleosome Occupancy Is Correlated with an Increasing Mutation Rate so Long as DNA Repair Machinery Is Intact. *PLoS One*. 2015;10(8):e0136574. doi: 10.1371/journal.pone.0136574.
3. Yazdi PG, Pedersen BA, Taylor JF, Khattab OS, Chen YH, Chen Y, Jacobsen SE, Wang PH: Nucleosome Organization in Human Embryonic Stem Cells. *PLoS One*. 2015;10(8):e0136314. doi: 10.1371/journal.pone.0136314.
4. Deng W, Leu HB, Chen Y, Chen YH, Epperson CM, Juang C, Wang PH: Protein Kinase B (PKB/AKT1) Formed Signaling Complexes with Mitochondrial Proteins and Prevented Glycolytic

Energy Dysfunction in Cultured Cardiomyocytes During Ischemia-Reperfusion Injury. *Endocrinology*. 2014; 155(5):1618–1628.

5. Wu PR, Tsai PI, Chen GC, Chou HJ, Huang YP, Chen YH, Lin MY, Kimchi A, Chien CT, Chen RH: DAPK activates MARK1/2 to regulate microtubule assembly, neuronal differentiation, and tau toxicity. *Cell Death Differ*. 2011; 18(9):1507-20.

# **ABSTRACT OF THE DISSERTATION**

Mitochondrial Akt1 Signaling Enhanced iPSC Reprogramming  
- Mechanism of Mitochondrial Akt1-PDH E3 subunit Interaction

By

Yu-Han Hank Chen

Doctor of Philosophy in Physiology and Biophysics

University of California, Irvine, 2016

Professor Ping H. Wang, Chair

Embryonic stem cells (ESC) are distinguished by their capacity for self-renewal and differentiation, abilities that are foundational to emerging research on cell-based therapies and regenerative medicine. The mechanisms underlying stem cell pluripotency and differentiation however, remain poorly understood. The discovery of induced pluripotent stem cells (iPSCs) advanced our understanding of pluripotency and broadened the applications of stem cell; it also bypassed the ethical issue of using embryonic stem cells. Although the technique has been broadly applied and modified in the last decade, the mechanistic details remain elusive. It has been demonstrated that activation of phosphatidylinositol-3 kinase/Akt signaling enhanced stem cell pluripotency and iPSC reprogramming. Activation of Akt1 has been reported translocating from cytoplasm to mitochondria. However, the roles of mitochondrial Akt1 plays in the regulation of stem cell pluripotency and iPSC reprogramming have not yet been determined. Using Yamanaka factor reprogramming, we demonstrated that activation of mitochondrial Akt1 signaling enhanced reprogramming efficiency. In addition, we also observed that the DNA methylation status at the OCT4 and NANOG promoters of the resulting Yamanaka factors-

mitochondrial Akt1-reprogrammed cell displayed a more profound de-methylation profile. We also demonstrated that the resulting Yamanaka-mitochondrial Akt1-reprogrammed cells displayed a respiration profile more similar to that in ESCs. Increasing evidence has implicated the importance of mitochondria and cellular metabolism in iPSC reprogramming. Interestingly, we observed that activation of mitochondrial Akt1 signaling reduced cellular oxygen consumption, NADH levels and maintained ATP levels, leading to lower reactive oxygen species production and lower apoptosis levels under stress conditions. We further identified the interaction of Akt1 with pyruvate dehydrogenase (PDH) complex (PDC) in mitochondria, that the dihydrolipoamide dehydrogenase (E3) subunit of the PDC preferentially bound to Akt1. The activation of mitochondrial Akt1 signaling enhanced PDH activity. Using computational method, we identified a protein-protein interaction site on Akt1 and further screened and obtained two potential small molecule compounds, NSC 34766 and NSC 628725, that may bind to Akt1 via this site. Follow up studies indicated that the compounds disrupted the Akt1-E3 interaction and reduced the effects of mitochondrial Akt1 and insulin on PDH activity.

# CHAPTER 1

## Introduction

### 1.1. An Embryonic Stem Cell

Embryonic stem cell (ESC) is a unique type of cell that can divide symmetrically to give rise to a pair of identical daughter cells, which is known as self-renewal capacity. Under certain conditions, ESC can also divide asymmetrically to give rise to two different types of daughter cells, which is called differentiation. The differentiation capacity is unique to all types of stem cells, which allows them to participate in tissue repair or the replacement of damaged cells in physiological setting. For example, haematopoietic stem cells (HSCs) and intestinal epithelial stem cells are required throughout life to replenish cells that turnover in their respective tissues. The proper regulation of stem cell function is important to the development and maintenance of healthy tissues.

During multicellular animal development, the creation of the zygote from the fertilization brings the presence of stem cell. This zygote can proliferate and differentiate into all of the embryonic cell lineages, and as a result, give rise to an organism. The embryo can differentiate into two lineages: (1) the inner cell mass (ICM) and (2) the trophectoderm (TE). The ICM is the location in which the pluripotent cells were identified, and the TE can form an extraembryonic epithelial layer that helps support the ICM (Figure 1.1). The capacity of an embryo forming into both the ICM and the TE, and later into whole organism is termed totipotency. Embryonic cells within the first couple of cell divisions after fertilization are the only cells that are totipotent. On the other hand, the ICM can give rise to all three germ layers but cannot form an organism

without the support from the TE. The ability of the ICM cells to develop into any cell from three germ layers is termed pluripotency. At a later stage of development, ESC is replaced by other types of stem cells, which reside in various tissues and organs in order to replenish the cells and tissue for the maintenance of healthy tissues. These stem cells are named differently depending on which tissues that they reside in, but are generally named adult stem cells or somatic stem cells. Their differentiation capacity is, however, more restricted than ESC and can only give rise to the cell lineages comprising the tissues that they are resided in, and therefore is termed multipotency.

## **1.2. History of Pluripotent Stem Cell Studies**

The studies of pluripotency began three decades ago. Pluripotency was first described in mouse teratocarcinomas studies<sup>1,2</sup>. Embryonal carcinoma (EC) cells were named after the observation that transplantation of a single cell isolated from mouse teratocarcinomas *in vivo* could result in a teratocarcinoma containing a range of differentiated tissues<sup>3</sup>. EC cell culture was later established, and its differentiation property was analyzed and described in culture and in generation of the chimera mice<sup>4-9</sup>. With all the technique platforms and experiences established from EC studies, the EC homolog in early embryonic cell populations were soon isolated from late blastocyst stage (embryonic day 4.0 [E4.0]) and termed embryonic stem (ES) cell<sup>10</sup>.

## **1.3. Pluripotency and Signaling Pathways**

The pluripotency and differentiation of stem cells need to be well-regulated to match the changing growth and regeneration demands of the tissues. Since the discoveries of murine and



human ESC, efforts have been focused on the mechanisms of the regulation of stem cell fate. Understanding the mechanisms regulating stem cell functions is important for normal tissue homeostasis and stem cell application. Somatic stem cells are often quiescent in adult tissues, entering the cell cycle periodically to maintain tissue homeostasis. The physiological cues regulating somatic stem cell functions can be divided into intrinsic and extrinsic mechanisms.

Increasing numbers of studies indicate that both extrinsic and intrinsic mechanisms play fundamental roles in regulating stem cell proliferation and cell fate decisions. The intrinsic mechanisms regulate stem cell functions through transcription factors and epigenetic factors. The extrinsic mechanisms from the local environment, such as short-range signals from the niche and long-range humoral signals, have also been implicated in stem cell functions<sup>11-13</sup>. The activation of intracellular signaling by extrinsic mechanisms has been demonstrated to regulate stem cell proliferation and cell fate specification.

### **1.3.1 LIF/JAK/STAT Signaling**

In earlier studies, leukemia inhibitory factor (LIF) was identified as one of the soluble pluripotency factors used for murine ESC maintenance in culture<sup>14,15</sup>. The binding of LIF to its heteromeric receptor LIFR $\beta$ /gp130 triggers the Janus kinase/STAT (JAK/STAT) signaling pathway, which activates target genes transcription that are responsible for the maintenance of pluripotent state<sup>16</sup>. The significance of STAT3 in regulating ESC pluripotency was demonstrated by a report that the stable expression of a STAT3F dominant negative mutant induced ESC differentiation<sup>17,18</sup>. Myc is one of the target genes of STAT3 and has been implicated in stem cell self-renewal<sup>19,20</sup>. Alternatively, JAK can also activate the Ras/ERK and phosphatidylinositol-3 kinase (PI3K) pathways, which are also implicated in the regulation of stem cell fate. These

studies imply that the murine ESC fate may be modulated through LIF/JAK/STAT3 signaling axis.

### **1.3.2 Wnt/ $\beta$ -catenin Signaling**

Wnt signaling is identified by its roles in carcinogenesis and embryonic development, such as cell proliferation, cell migration, and cell fate decision. Canonical Wnt signaling transmits signals from the plasma membrane to the nucleus via  $\beta$ -catenin. When Wnt signaling is inactivated, the free cytoplasmic  $\beta$ -catenin is phosphorylated by adenomatous polyposis coli (APC)/Axin/glycogen synthase kinase 3 (GSK3) protein complex. Phosphorylated  $\beta$ -catenin is marked for degradation through the ubiquitin-dependent pathway and as a result, the level of  $\beta$ -catenin is low. On the other hand, in the presence of Wnt ligand, the degradation of  $\beta$ -catenin is suppressed and it accumulates in the cytoplasm and then translocates to the nucleus, where it collaborates with T-cell factor (TCF) in stimulating the expression of a set of target genes, including pluripotency genes Oct4 and Nanog<sup>21</sup>. Both murine and human ESC can be maintained undifferentiated by the administration of a GSK3 inhibitor, which activated the Wnt signaling and sustained the expression of Oct4, Rex-1 and Nanog<sup>22</sup>. These results suggest that the Wnt signaling may modulate ESC pluripotency through regulating the expressions of pluripotent genes. The role of the Wnt signaling in regulating stem cell fate decisions is not restricted to ESC. The overexpression of activated  $\beta$ -catenin increased expression of HoxB4 and Notch1 and promoted growth of HSCs and maintained the immature phenotype of HSCs in long-term cultures. The ectopic expression of axin or a frizzled ligand-binding domain, on the other hand, resulted in the inhibition of HSC growth<sup>23</sup>. These studies further provide evidences supporting the role of the Wnt signaling in regulating cell proliferation and stem cell fate decisions.

### **1.3.3 BMP Signaling**

The basic fibroblast growth factor (bFGF) belongs to the FGF protein family, the signaling of which is involved in angiogenesis, wound healing, embryonic development and endocrine signaling pathways. Although bFGF is routinely used in the human ESC culture to maintain its pluripotency<sup>24-26</sup>, the mechanistic details of bFGF-activated signaling is poorly understood. The administration of bFGF in conjunction of the suppression of BMP signaling sustained undifferentiated proliferation of human ESC<sup>27</sup>. Bone morphogenetic proteins (BMPs) were originally identified by their capacities to induce ectopic bone formation<sup>28</sup>. BMPs belong to the transforming growth factor- $\beta$  (TGF- $\beta$ ) superfamily of proteins and its signaling functions similarly to the aforementioned LIF/JAK/STAT signaling via receptor-mediated intracellular signaling and subsequently regulates target gene transcription. The canonical BMP signaling is mediated through the translocation of the complex formed by phosphorylated R-Smads (Smad1, Smad5, or Smad8) and Smad 4 from cytoplasm to nucleus, and regulates target gene transcription. The role of BMP signaling in the regulation of ESC pluripotency has recently been implicated<sup>29</sup>. However, BMP signaling functions differently in murine and human ESCs and the current studies indicated that it plays different roles in different stem cell populations, suggesting additional crosstalk with other signaling pathways exists. Therefore, the precise role of BMP signaling in the regulation of ESC pluripotency requires more investigation.

#### **1.3.4 PI3K/AKT Signaling and Stem Cell Pluripotency**

Identification of the PI3K/Akt pathway can be traced back to 1980s<sup>30</sup> and the functions of PI3K has been implicated in cell growth, proliferation, differentiation, motility, survival and intracellular trafficking. PI3K can be activated via various stimuli, such as receptor tyrosine kinases, B and T cell receptors, cytokine receptors, and G-protein-coupled receptors. PI3Ks bind to these receptors via their regulatory subunit or adapter proteins such as insulin receptor

substrate (IRS) proteins. Activated receptors triggers the activation of class IA PI3Ks, leading to the production of phosphatidylinositol (3,4,5)-trisphosphate (PIP3) from phosphatidylinositol (3,4)-bisphosphate (PIP2) lipids through its catalytic subunit. Akt binds to PIP3 at the plasma membrane through its pleckstrin homology (PH) domain, leading to the access of T308 in the activation loop for phosphoinositide dependent kinase 1 (PDK1). This results in the partial activation through T308 phosphorylation by PDK1<sup>31</sup>. Further phosphorylation of Akt at S473 in the carboxy-terminal hydrophobic domain, either by mTOR<sup>32</sup> or by DNA-PK<sup>33</sup>, leads to full activation of Akt.

Interestingly, the activation of PI3K/Akt signaling is accompanied with embryo development. Previous studies had shown that expression of the p85 and p110 subunits of PI3K and Akt are observed from the 1-cell through the blastocyst stage of murine preimplantation embryo development. In addition, phosphorylated Akt was detected throughout murine preimplantation development, suggesting its activity is required for embryo development. In accordance, inhibition of Akt activity resulted in blastocyst hatching delay, a developmental step that facilitates implantation<sup>34</sup>.

The role of PI3K/Akt signaling has also been implicated in the regulation of stem cell proliferation and pluripotency. The inhibition of PI3K signaling by LY294002 inhibitor reduced murine ESC self-renewal<sup>35</sup>, indicating the significance of PI3K signaling in the regulation of murine ESC pluripotency and self-renewal. This notion can further be supported by another study investigating the downstream signaling axis of PI3K. Watanabe et al. reported that the expression of a constitutively active Akt substitutes the LIF-dependency of mouse and primate ESC, suggesting that the PI3K/Akt signaling axis may sustain ESC pluripotency<sup>36</sup>. The capacity of stem cells to self-renew allows them to maintain their population for use in specific situations,

such as damage repair. Takahashi et al. demonstrated that the activation of PI3K/Akt signaling was required for the proliferative and tumorigenic activities of the ES cells<sup>37</sup>. Collectively, these studies suggest PI3K/Akt signaling may regulate ESC proliferation and pluripotency, which are important for ESC function. The significance of PI3K/Akt signaling in regulating stem cell pluripotency can further be demonstrated by transcription profiling of human ESC. Armstrong et al. ran analyses on gene expression, western blotting, flow cytometry and antibody array in human ESC upon differentiation and demonstrated that the components of PI3K/Akt signaling was decreased during differentiation<sup>38</sup>.

The significance of PI3K/Akt signaling was also demonstrated in alternative studies. Phosphatase and tensin homolog (PTEN) is a tumor suppressor that negatively regulates intracellular levels of PIP3 and leading to negative regulation on Akt activity. Primordial germ cells (PGCs) are germ cell precursors that emerge around E7.5 and exist transiently in embryos<sup>39</sup>. Previous studies had shown that PGCs can give rise to testicular teratomas composed of various differentiated cell types when engrafted into adult testis<sup>40,41</sup>. In another study, Kimura et al. reported that the specific deletion of PTEN gene in PGCs caused testicular teratomas in male newborn mice<sup>42</sup>. These results suggest that some type of pluripotent cell in PGCs exists and that the specific PTEN deficiency in PGCs results in a condition favoring the growth of this type of pluripotent cell. This type of cell was established later and named pluripotent embryonic germ (EG) cell<sup>43,44</sup>. Kimura et al. also demonstrated that PTEN-null PGCs in culture had enhanced proliferation capacity and enhanced pluripotent embryonic germ (EG) cell colony formation. These observations indirectly provide evidence supporting the essential role of Akt in the regulation of proliferation and pluripotency of pluripotent cells. In summary, the above studies reflect that PI3K/Akt signaling is closely associated with stem cell function and cell fate decision.

Collectively, these studies indicate the significance of extrinsic mechanism mediating through signaling pathways in the regulation of stem cell fate decision. Understanding the molecular mechanism by which pluripotency is maintained in ESC is important for the development of improved methods to their derivation, culture and application for therapeutic uses.

#### **1.4. Mitochondria and Stem cell**

Although the role of PI3K/Akt signaling has been intensively investigated in stem cell, the majority of the reports are focusing on cytosolic Akt. Several studies, however, reported a different pool of Akt upon PI3K activation<sup>45-47</sup>. Similarly, our group previously identified the translocation of Akt1 from cytoplasm to mitochondria upon activation<sup>47</sup>. Interestingly, in our preliminary study, we also identified the mitochondrial pool of Akt1 after serum stimulation in human ESCs. This observation raises interesting questions regarding the function of Akt1 inside mitochondria of ESCs.

The mitochondrion is a double-membraned organelle found in eukaryotes and contains its own genome. Mitochondrion is believed to be evolved from bacteria because their genomes show high similarity, which is the hypothesis of endosymbiosis. The mitochondrial circular genomic DNA resides in the matrix and consists of 37 genes, 13 of which encode for proteins integrated in mitochondrial inner membrane, while others encode for mitochondrial tRNAs and rRNAs<sup>48</sup>. It is estimated to have a proteome of ~1000-1500 proteins<sup>49</sup>, and the majority of them are encoded from cell nucleus. It is a specialized organelle that regulates various cellular functions. The most known function of mitochondrion is its role in energy production through a series of coupled biochemical reactions, which compose the tricarboxylic acid (TCA) cycle.

Other important functions mediated by mitochondrion include cellular metabolism, reactive oxygen species, apoptosis, calcium signaling, and mitophagy.

The roles of mitochondrion in stem cells, however, are just being to be investigated recently. Studies showed that ESC contains less amounts of mitochondria with immature cristae structure. Upon differentiation, however, the number of mitochondrion increased and they developed into larger sizes with distinct cristae. This was demonstrated by increased mitochondria DNA copies upon ESC differentiation. The distribution of mitochondria in stem cell was shown to be perinuclear and later changed to homogenous or aggregated when differentiated. However, the interpretations of these morphological differences between undifferentiated stem cell and differentiated cell remained to be established.

Besides the morphological differences of mitochondrion between undifferentiated and differentiated status, ESCs are also demonstrated to be metabolically different from the differentiated counterparts. ESCs reside in hypoxic environment during embryo development; it is therefore, that embryonic cell relies on anaerobic metabolism to generate energy<sup>50,51</sup>. The mutations in four glycolytic enzymes resulted in early postimplantation lethality<sup>52-55</sup>. Upon differentiation, however, metabolic shifting was observed<sup>56-58</sup>. The development of mature mitochondrial cristae potentially fulfills the higher demand of mitochondrial respiration in differentiated cell, which supports the metabolic shift from glycolysis to oxidative phosphorylation (OXOPHOS). The inhibition of mitochondrial OXOPHOS complex III increased Nanog expression and reduced gene profile associated with differentiation in hESCs<sup>59</sup>. Collectively, these results suggest that mitochondria-mediated metabolism plays a role during embryo development and stem cell fate decision. The role of Akt1 in the mitochondria of ESC, however, has not been heavily addressed and remains to be investigated.

## 1.5. Mitochondrial Akt1

The mitochondrion plays significant functions in the eukaryotic cell, such as bioenergetics, metabolism, the regulation of reactive oxygen species (ROS), apoptosis, calcium signaling, and mitophagy. The mitochondrion contains its own circular genome, however, the majorities of mitochondrial proteins are encoded in the nucleus and then transport into mitochondrion. Mitochondria protein translocation pathways of mitochondrion have been intensively studied in the past two decades. Most mitochondria proteins contain a mitochondria targeting presequence at the amino-terminus of the precursor protein and these presequences are tightly associated with the protein transport process<sup>60</sup>. However, there is a significant fraction of mitochondrial proteins (about 30%) that do not contain typical amino-terminal presequences. These proteins can be found at the outer membrane, intermembrane space and the inner membrane. Their translocation mechanisms are not quite understood but could be associated with an internal peptide segment rather than an amino-terminal presequence.

In a recent report, Akt was found to be accumulated in the mitochondrial matrix upon stimulation<sup>61</sup> and known Akt substrates are being reported in the mitochondrion, such as glycogen synthesis kinase  $\beta$ <sup>45,62-65</sup>, hexokinase II<sup>46,66-68</sup>, and  $\beta$ -subunit of complex V<sup>47,61,69</sup>, suggesting that Akt plays a regulatory role in mitochondrion. To date, the physiological functions of mitochondrial Akt have been studied in different studies. The impairment of mitochondrial Akt1 translocation and activation has been implicated in diabetic myocardium<sup>69</sup>. The activation of mitochondrial Akt1 mediated anti-apoptotic effect in cardiac muscle cell<sup>70</sup>. The activation of mitoK<sub>ATP</sub> channels elicits strong cardioprotection against Ca<sup>2+</sup> overload and ischemic injury and is associated with phosphorylated Akt translocation to mitochondria<sup>71</sup>. Akt1



intra-mitochondrial-cycling is central for redox modulation of cell cycle progression<sup>72</sup>. Although increasing evidences suggest the function of Akt1 in mitochondria, the detailed route of Akt translocation is still poorly understood and probably is associated with heat shock protein 90 activity<sup>73</sup>.

### **1.6. Mitochondrial Akt1 signaling in human ESC (hESC)**

To study the role of mitochondrial Akt1 in ESC, we first transduced hESC (H1) with an adenoviral vector carrying mitochondria-targeting constitutively active Akt1 (mito-Akt1). From preliminary protein expression study analyzed by western blot, we found that Oct4 and Sox2 levels were higher in the mito-Akt1-transduced group. On the other hand, the transduction of a lentiviral vector carrying mitochondria-targeting dominant negative Akt1 (mito-dnAkt1) in hESC resulted in the loss of pluripotency markers, such Oct4, stage specific embryonic antigen-4 (SSEA4) and alkaline phosphatase (AP). These results indicate a role of mitochondrial Akt1 in the regulation of hESC pluripotency. The pluripotency could be “induced” by the expression of pluripotency-associated factors was revealed in the recent reports<sup>74,75</sup>. Our preliminary results indicate that activation of mitochondrial Akt1 signaling may sustain the expression of pluripotency factors, suggesting it is associated with pluripotency. We therefore hypothesized that activation of mitochondrial Akt1 signaling may enhance iPSC reprogramming.

## Figures

Figure 1.1

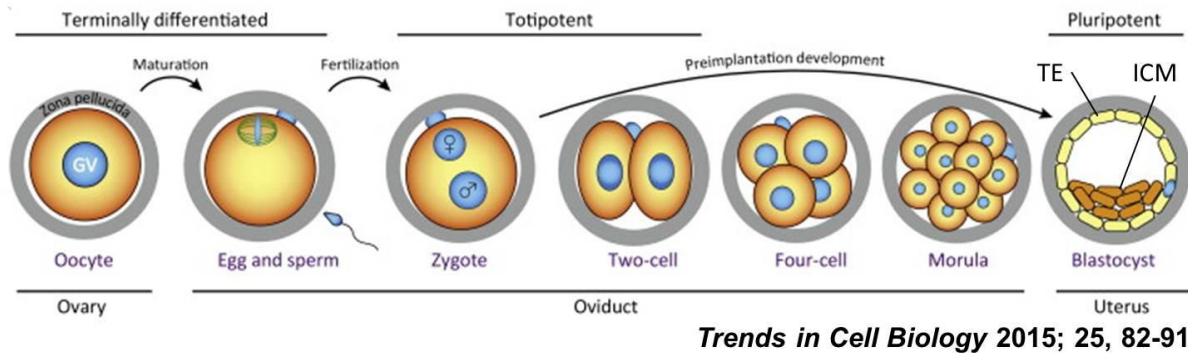


Figure 1.1 Mouse preimplantation development. Totipotent cells only exist in the early stage of embryonic cells. When entering blastocyst stage, embryo differentiated in to inner cell mass (ICM) and trophectoderm (TE). ICM is the source of PSCs. (Figure was referenced from Trends in Cell Biology, Volume 25, Issue 2, Pages 82-91 (February 2015) DOI:

10.1016/j.tcb.2014.09.006<sup>76</sup>)

## CHAPTER 2

### Mitochondrial Akt1 Signaling Enhanced iPSC Reprogramming Efficiency

#### Introduction

#### Induced Pluripotent Stem Cells (iPSC)

Studies regarding the regulation of stem cell fate have been emphasized for years not only because of its significance in embryo development but also because maintaining stem cells in a pluripotent state has its broad implications to the emerging field of regenerative medicine. Regenerative medicine involves replacing or regenerating damaged or diseased human cells, tissues, or organs, to restore or establish normal function<sup>77</sup>. The use of human-derived pluripotent stem cells to replace damaged tissues, therefore, becomes an integral part of regenerative medicine.

Human tissue-derived stem cells have been applied to different areas of tissue regeneration, such as adipose-derived stem cells<sup>78,79</sup>. The spectrum of the application, however, is restricted because these tissue stem cells are multipotent rather than pluripotent. Multipotent stem cells, such as adipose stem cell and satellite cell, have more limited differentiation potency than pluripotent stem cells (PSCs). The limitation to differentiate only into restricted lineages is a major hurdle for broader applications. The discoveries of cell reprogramming by somatic cell nuclear transfer (SCNT)<sup>80,81</sup> and cell fusion with ES cells<sup>82,83</sup> ignited the fire of later great discovery. From these observations, Takahashi et al. hypothesized that the factors that are important for maintaining ESC pluripotency may be required to induce pluripotency in somatic

cells. In search for these “required factors,” they reported that the ectopic expression of four transcription factors, OCT4, SOX2, KLF4, and c-MYC (OSKM), in fibroblast transformed the cell morphology to a state resembling an embryonic stem cell. Molecular characterization further indicated that these cells shifted their gene expression profile from the fibroblast state to a state similar to the embryonic stem cell. Differentiation studies also demonstrated that these cells are able to differentiate *in vitro* and *in vivo* and can give rise to chimeric mice, suggesting they are functionally similar to pluripotent embryonic stem cells. Therefore, they named it the induced pluripotent stem cell (iPSC)<sup>74,75</sup>.

The implication from these studies suggests that the ectopic expression of OSKM in somatic cells may reverse somatic gene expression profile back the profile similar to ESC. However, there are still questions remained that not all pluripotency-associated factors can drive the reprogramming and not all transduced cells can be reprogrammed. Therefore, the mechanisms behind OSKM-reprogramming remain to be investigated. On the other hand, these studies also implied that iPSC reprogramming could be enhanced with the factors that could facilitate the “effects” of OSKM or the pluripotency. Our preliminary observation of “pro-pluripotency” effect of mitochondrial Akt1 signaling, therefore, becomes an interesting hypothesis to further dig in. Herein, we hypothesize that mitochondrial Akt1 signaling may enhance iPSC reprogramming.

## **Materials and Methods**

### **Reagents**

Knockout serum replacement (KOSR), Knockout DMEM/F-12 medium, fetal bovine serum (FBS), Glutamax, non-essential amino acids, Dulbecco’s modified eagle medium-

GlutaMax,  $\beta$ -mercaptoethanol, basic fibroblast growth factors (bFGF), leukemia inhibitory factor (LIF), collagenase IV, 0.25% trypsin/EDTA, MitoTracker®, Fluorophore 2nd antibodies, were purchased from Invitrogen (Carlsbad, CA, USA). Rho kinase (ROCK) inhibitor was from Calbiochem (Gibbstown, NJ, USA). Immobilon-P membranes were from Millipore Co. (Bedford, MA). Anti-SRY (sex determining region Y)-box 2 (SOX2), anti-Oct3/4, anti-Klf4, anti-cMyc, anti-Nanog, anti-SSEA1, anti-beta tubulin 3, anti-alpha-fetoprotein, anti-desmin were purchased from GeneTex Inc. (Irvine, CA). Anti- $\beta$  actin, anti- $\alpha$ -actinin anti-phospho-Akt1 and anti-Akt antibodies were purchased from Santa Cruz Biolabs (Santa Cruz, CA). Anti-porin antibody was purchased from MitoSciences (Eugene, Oregon, CA). The rest of antibodies were purchased from Cell Signaling Technology, Santa Cruz Biolabs or GeneTex Inc. RNeasy kit was from QIAGEN (Valencia, CA, USA). Human gene 1.0 ST microarray was purchased from Affymetrix (Santa Clara, CA, USA). All other chemicals were purchased from Sigma or Fisher Scientific. H9 hESCs were obtained from WiCell (Madison, WI) and human fibroblasts were from ScienCell Research Laboratories (Carlsbad, CA).

### **Cell Culture and Transduction of Viral Constructs**

Undifferentiated hESC H9 line were maintained on mouse embryo fibroblast feeder layer in DMEM/F12 supplemented with 20% (vol/vol) KnockOut serum replacement, 0.1 mM nonessential amino acids, 2mM Glutamax, 0.1 mM 2-mercaptoethanol, and 4 ng/ml bFGF. Cultures were manually passaged with collagenase IV at a 1:2–1:4 split ratio every 5–7 days. To infect adenoviral vectors, hES cells were first passaged to Matrigel (BD Biosciences) in MEF-conditioned medium supplemented with 4ng/ml bFGF to remove MEF feeders. hESC were treated with rho kinase (ROCK) inhibitor for at least 1 hour before passaging with 0.25% trypsin

from matrigel to matrigel. Adenovirus was added twice at 8 and 24 hours after passage. The experimental procedure and protocol were approved by the Human Stem Cell Research Oversight Committee at the University of California, Irvine.

Mouse embryonic fibroblasts (MEF) were isolated from E13.5 embryos by standard isolation procedures. Mouse embryonic stem cells were derived from C57BL/6 mice. MEF (MEF $\epsilon$ A) transgenic for the reprogramming factors were a kind gift from Dr. Konrad Hochedlinger (Boston, MA). MEF were cultured in Dulbecco's Modified Eagle Medium (DMEM) containing 10% fetal bovine serum (FBS), 1% non-essential amino acid (NEAA), and 1% sodium pyruvate (MEF media). Mouse embryonic/induced pluripotent stem cells were cultured in DMEM containing 15% FBS, 1% NEAA, 1% sodium pyruvate and 55 $\mu$ M  $\beta$ -mercaptoethanol, supplemented with 10ng/ml leukemia inhibitory factor (LIF) (ES media). All cells were incubated at 37°C, 5% CO<sub>2</sub>. Neonate human dermal fibroblasts (HDFN) were purchased from ScienCell (#2310).

To study mitochondrial Akt signaling, we generated different Akt constructs, including a constitutively active and a dominant negative Akt1. To build a constitutively active Akt1, we cloned murine Akt1 and mutated Thr308 and Ser473 to aspartic acid (D) to mimic phosphorylated Akt1. To build a dominant negative Akt1, we used the murine Akt1 from before but mutated Lys179 to methionine (M)<sup>84</sup>. To target Akt1 expression specific to mitochondria, we fused a mitochondrial targeting sequence (MSVLTPLLLRGLTGSARRLPVPRAKIHSL) at the amino terminus of both constitutively active Akt1 and dominant negative Akt1. In addition, we attached an HA-tag at the amino terminus of constitutively active Akt1 and a His-tag at the

carboxyl terminus of dominant negative Akt1 (Figure 2.1A and B). The constitutively active Akt1 construct was cloned into adenoviral vector (mito-Akt1)<sup>70,85</sup> (AdEasy Adenoviral Vector Systems, Agilent Technologies) and the dominant negative Akt1 was cloned into a Tet-on inducible lentiviral vector (mito-dnAkt1)<sup>85</sup>. Control adenovirus and lentivirus respectively expressed green fluorescent protein (Ad-GFP) and red fluorescent protein (lenti-RFP). Transgene expression was verified previously with different approaches<sup>70,85</sup>. In current dissertation, we verified the expression in MEF by immunofluorescence staining studies. The transgene expression was examined with anti-HA or anti-His antibodies and co-immunostained with MitoTracker® Green FM (ThermoFisher Scientific) (Figure 2.1C and D).

### **Reprogramming of Fibroblasts**

Plasmid DNA encoding the Yamanaka factors were purchased from Addgene and plasmid DNA were prepared using QIAGEN Plasmid Midi Kit. Retroviruses carrying Yamanaka factors were produced according to the original literature<sup>74,75</sup>. Reprogramming protocol is referenced from the original literature and summarized in Figure 2.2. For retroviral vector reprogramming,  $5 \times 10^4$ /well P3-6 MEF were plated on 6 well plate on day 0. Retroviral vectors carrying Oct4, Sox2, Klf4 and c-Myc were spinoculated at 1200g, 120 minutes, room temperature on day 1 and day 2. Adenoviral vectors carrying either mito-Akt1 or GFP (control) were added on day 3. From day 4-7, cells were incubated with media supplemented with 2mM valproic acid. Adenoviral vectors carrying either mito-Akt1 or GFP (control) were added again on day 8. Cells were trypsinized and counted, equal number of cells was plated into each well of a 6 well plate or 10 cm dish of feeders on day 9. From day 9 to 20, cells were maintained in ES media. For doxycycline-induced reprogramming, P3-6 MEF $\epsilon$ A carrying polycistronic cassette expressing

Oct4, Sox2, Klf4 and c-Myc were plated at  $5 \times 10^4$  cell/well on 6-well plate on day 0. Four factors expression was induced with  $2 \mu\text{g/ml}$  doxycycline in mouse ES media throughout the whole procedure as described previously<sup>86-88</sup>. Adenoviral vectors carrying either mito-Akt1 or GFP (control) were added on day 2 and day 6. Cells were trypsinized and counted, and equal number of cells was plated into each well of a 6 well plate or 10 cm dish of feeders on day 7. From day 7 to 20, cells were maintained in mouse ES media.

### **Alkaline Phosphatase and Immunofluorescence Staining**

For alkaline phosphatase (AP) staining, paraformaldehyde-fixed cells were rinsed with deionized water and stained with FastRed/Napthol or nitroblue tetrazolium/5-Bromo-4-chloro-3-indolyl phosphate (NBT/BCIP). For immunofluorescence staining, paraformaldehyde-fixed cells were rinsed with PBS and blocked with 10% normal goat serum. After blocking, cells were incubated with indicated primary antibodies overnight at  $4^\circ\text{C}$ , followed by PBS wash and 1 hour incubation with conjugated secondary antibodies, counter-stained with DAPI, and analyzed with an Eclipse Ti fluorescence microscope (Nikon). To visualize the effect of insulin on Akt1 subcellular localization, MEFs were fixed with 4% paraformaldehyde for 30 min at room temperature. After washing with PBS, cells were treated with 0.05% saponin in ddH<sub>2</sub>O for 20 min and blocked with 10% normal sera for 30 min. The fixed cells were incubated with specific primary antibodies overnight at  $4^\circ\text{C}$ , conjugated secondary antibodies for 1 hour, counter-stained with DAPI, and analyzed with Eclipse Ti fluorescence microscope (Nikon).

### ***In Vitro* and *In Vivo* Differentiation Assay**



For *in vitro* differentiation assay, induced pluripotent stem cells were trypsinized into cell chunks and grown in suspension culture in low-attachment plates for 10 days. This was followed by plating into 6-well plates or 10 cm dishes and grown for another 5-7 days. iPSC-derived cells were then fixed and stained with the indicated primary antibodies. For *in vivo* differentiation assay,  $1 \times 10^6$  of iPSC from different groups were injected into mice with severe combined immunodeficiency (SCID) (Charles River). Teratomas were formed after 4-6 weeks. The animal experimental procedures were approved by the Institutional Animal Care and Use Committee at University of California, Irvine.

### **DNA Methylation**

Genomic DNA was extracted and purified using the Wizard Genomic DNA Purification Kit (Promega) according to the manufacturer's instruction. Bisulfite conversion of DNA was performed using the EZ DNA Methylation Kit (Zymo Research). For maximal conversion, 500 ng genomic DNA was used for bisulfite reaction. Converted DNA was amplified by PCR using primers that are specific for the promoter region of OCT4 and NANOG. Each 50 $\mu$ l PCR reaction mix contained 3  $\mu$ l of bisulfite-treated DNA, 200 nM of forward and reverse primers, 200 $\mu$ M of dNTP, and 0.5 unit Taq DNA polymerase and PCR buffer (Invitrogen). PCR was performed under the following conditions: the initial denaturation of 10 min at 95°C, followed by 35 cycles of 1 min at 95°C, 30 sec at 55°C, and 30 sec at 72°C; and the final extension of 10 min at 72°C. The PCR products were extracted from the gel and purified using QIAquick Gel Extraction Kit (Qiagen). The purified PCR products were subcloned using CloneJET PCR Cloning Kit (Thermo Scientific). For each region, 10 clones were randomly picked and the plasmid DNA was prepared with QuickLyse Miniprep Kit (Qiagen) for DNA sequencing (GENEWIZ).

## **Analysis of Mitochondrial O<sub>2</sub> Respiration by Extracellular Flux Measurement**

To measure mitochondrial function in cells, we employed a Seahorse Bioscience XF24 Extracellular Flux Analyzer (Seahorse Bioscience, North Billerica, MA) and follow the manufacturer's protocol. Briefly, cells were plated in a 0.2% gelatin or Matrigel coated 24-well Seahorse XF-24 assay plate at  $7.5 \times 10^4$  cells/well, and grown for 16 hours before analysis. On the day of metabolic flux analysis, cells were washed once with freshly prepared KHB buffer (111 mM NaCl, 4.7 mM KCl, 2 mM MgSO<sub>4</sub>, 1.2 mM Na<sub>2</sub>HPO<sub>4</sub>, 2.5 mM glucose and 0.5 mM carnitine; pH 7.4) and incubated in KHB buffer at 37°C in a non-CO<sub>2</sub> incubator for 1 hr. Three baseline measurements of oxygen consumption rate (OCR) were taken before sequential injection of following mitochondrial inhibitors and final concentration: oligomycin (1 µg/ml), carbonilcyanide p-triflouromethoxyphenylhydrazone (FCCP) (3 µM) and rotenone (0.1 µM). Three measurements were taken after addition of each inhibitor. OCR values were automatically calculated and recorded by the Seahorse XF-24 software. The basal respiration was calculated by averaging the three measurements of OCR before injection of inhibitors.

## **Statistical Analysis**

Data are presented as mean  $\pm$  SD, unless noted otherwise. FACS data were analyzed with BD FACSDiVa software. Student's t test and one-way repeated measures ANOVA with Holm-Sidak method were performed with SigmaStat 3.11. The statistical significance level was set at  $p < 0.05$ .

## Results

### Mitochondrial Akt1 Signaling Enhanced iPSC Reprogramming Efficiency

Since mitochondrial Akt1 signaling appears to positively affect hESC stemness, mitochondrial Akt1 might have played a role during the reprogramming of somatic cells into iPSCs. To test this hypothesis, we altered mitochondrial Akt1 signaling during reprogramming of somatic cells to iPSCs. We set our iPSC generation protocol similar to the original report<sup>74,75</sup>. In addition to OSKM transductions, the cells were transduced with either a mitochondria-targeting constitutively active Akt1 (mito-Akt1) or a control vector (GFP) as outlined in Materials and Methods (Figure 2.2). The dynamics of iPSC derivation are different in mouse and human. It takes ~20 days to observe the formation of mouse iPSC colonies, whereas it takes ~30 days to observe human iPSC colonies. At the end of the process, the iPSC colonies can be visualized and verified by alkaline phosphatase (AP) staining (Figure 2.3). Studies had shown that the undifferentiated PSCs have elevated expression of alkaline phosphatase<sup>89</sup>, therefore, alkaline phosphatase staining can be used to identify PSCs. The numbers of AP-positive colonies from both groups were counted and summarized in Figure 2.4B. Mito-Akt1 transduced group has more AP-positive colonies than control group in mouse iPSC reprogramming studies (Figure 2.4B). These results suggest that mitochondrial Akt1 signaling either enhances reprogramming of somatic cells to iPSCs or enhances the transduction efficiency of the four reprogramming factors. To determine the effect of mito-Akt1 signaling on transduction efficiency, mito-Akt1 and control Ad-GFP were introduced into a transgenic MEF line that is stably-transduced with a doxycycline-inducible OSKM polycistronic cassette (MEF $\epsilon$ A)<sup>87,86,88</sup>. Reprogramming of MEF $\epsilon$ A was induced with doxycycline and the number of cells that express the murine pluripotency marker SSEA-1 was determined by flow cytometry. On day 18 after induction with

doxycycline, more SSEA-1-positive cells were observed in cells transduced with mito-Akt1 than Ad-GFP control (Figure 2.4C). To determine whether mitochondrial Akt signaling is required for the OSKM reprogramming, mitochondria Akt1 was inhibited using a dominant negative Akt1 construct (mito-dnAkt, Figure 2.1). Transduction of the MEF $\epsilon$ A cells with mito-dnAkt1 significantly reduced the number of SSEA-1 positive, reprogrammed cells significantly, thus confirmed the essential role of mitochondrial Akt signaling during reprogramming (Figure 2.4C). To determine of the effect of mitochondrial Akt1 signaling on human somatic cell reprogramming, mito-Akt1 or control adenoviral vector was introduced into human neonate dermal fibroblasts (HDFN) simultaneously with the OSKM reprogramming factors (Figure 2.4D). An increased number of alkaline phosphatase-positive colonies were observed in the human cells co-transduced with mito-Akt1 as compared to Ad-GFP control suggesting that mitochondrial Akt1 signaling also enhances OSKM reprogramming of human somatic cells. Collectively, these results suggest that mitochondrial Akt1 signaling may modulate iPSC reprogramming resulting in enhanced reprogramming efficiency.

### **The Reprogrammed Cells Expressed Pluripotent Markers**

We next sought to characterize the identities of these reprogrammed cells. As proof of concept, we focused our efforts on the characterization of mouse iPSCs. PSCs have unique markers that distinguish them from somatic cells<sup>89</sup>. Octamer-binding transcription factor 4 (Oct4), Sex determining region Y-box 2 (Sox2), Kruppel-like factor 4 (Klf4), and Nanog are transcription factors predominantly expressed in embryonic cells and whose functions have been demonstrated to be closely associated with pluripotency<sup>90-95</sup>. Stage-specific embryonic antigen-1 (SSEA1), or CD15, is a carbohydrate adhesion molecule located on the cell surface which may

mediate adhesion and migration of the mouse ESCs (mESCs). These markers, therefore, serve as standards to determine the identities of reprogrammed cells. We first compare the morphologies of reprogrammed cells to mESC. The morphologies of these reprogrammed cells resembled mESCs (Figure 2.3A). To determine their marker expression, we performed immunofluorescence staining using specific antibodies for each of the aforementioned markers. We demonstrated that these reprogrammed cells expressed Oct4, Sox2, Klf4, Nanog, c-Myc, and SSEA1 (Figure 2.5) in both control and mito-Akt1 groups. This result suggests that the reprogrammed cells from MEFs are morphologically similar to mESCs and express the examined pluripotent markers, such as Oct4, Sox2, Klf4, Nanog, c-Myc and SSEA1. These results are similar to the original reports<sup>74,75</sup>.

### **The Reprogrammed Cell May Differentiate into Cell Lineages of Three Germ Layers**

Next, we characterized the differentiation capacity of these reprogrammed cells. Growing ESCs in suspension mimics the three dimensional environment of embryo development therefore allowing us to differentiate ESCs into cell lineages of three germ layers in culture dishes, which is called embryoid body (EB) formation<sup>6,96</sup>(Figure 2.6A). Both groups of iPSCs were cultured in suspension without LIF, resulting in the spontaneous differentiation and the loss of ESC morphology. Interestingly, different types of cell emerged from EBs following differentiation (Figure 2.6B). We also observed the formation of bundles of beating cells, which is a common outcome of mESC spontaneous differentiation. To demonstrate the existence of cell lineages of three germ layers, we immunofluorescence-stained the cells emerged from these EBs with germ layer-specific markers. We choose  $\alpha$ -fetoprotein (AFP) for endodermal, desmin for mesodermal, and  $\beta$ -tubulin III for ectodermal lineages as reported in earlier study<sup>75</sup>. Both groups of EB-

derived cells expressed three germ layers-specific markers (Figure 2.6C). These results suggest that these reprogrammed cells from both groups can form EBs and differentiate into the cell lineages of three germ layers cell *in vitro*, implying they are pluripotent.

On the other hand, the injection of pluripotent stem cell into immunodeficient mice can result in the formation of teratoma. Pathophysiologically, teratomas belong to a class of tumors known as nonseminomatous germ cell tumor and are results of abnormal development of pluripotent cells. Experimentally, it can be used as an alternative method to examine the pluripotency of a cell line<sup>2,97</sup>. To test whether our reprogrammed cells could differentiate *in vivo*, we injected the reprogrammed cells subcutaneously into mice with severe combined immunodeficiency (SCID). Six weeks later, we observed the formation of tumors at the injection sites. From histology analyses, three primary germ layers of cells were observed in these tumors, indicating that these were teratomas (Fig 2.6D). These studies showed that the iPSCs derived with mitochondrial Akt1 activation during reprogramming were capable of differentiating into endoderm, mesoderm and ectoderm *in vitro* and *in vivo*, suggesting their bona fide identity of iPSCs.

### **Mitochondrial Akt1 Modulated DNA Methylation in the Resulting iPSC**

DNA methylation is a chemical reaction that mediates a covalent modification at the 5' position of the cytosine in CpG dinucleotides. Methylation is catalyzed by DNA methyltransferases (DNMTs) with *S*-adenosyl-methionine as the methyl-group donor. In DNA sequences, the distribution of CpG is not homogenous and therefore can be divided into -poor and -enriched regions. The CpG-enriched regions are also named CpG islands, and is usually longer than 500bp, and contain more than 55% GC content<sup>98</sup>. When the CpG islands are located

in promoter regions, DNA methylation may lead to the repression of gene transcription. The mechanisms behind DNA methylation and transcription repression are not fully understood but could be mediated via the interplays between the structures of methylated DNA, chromatin, and chromatin remodeling proteins<sup>99</sup>. During stem cell differentiation, it has been shown that the reduced expression of pluripotent genes is associated with both histone and DNA methylation<sup>100,101</sup>. On the other hand, the process of iPSC reprogramming involves gene expression profile shifting from the somatic cell to the PSCs, which is also accompanied by the DNA methylation changes<sup>102,103</sup>. In previous report, negative regulation of Oct4 and Nanog promoters methylation had been linked to increased pluripotency<sup>104</sup>. We, therefore, analyzed the DNA methylation patterns of Oct4 and Nanog promoters of the reprogrammed cells. From bisulfite sequencing studies, we found that the CpG islands at Oct4 and Nanog promoters are heavily-methylated in MEF, whereas they remained unmethylated in mESCs. Interestingly, analysis of the resulting reprogrammed cells indicated that the CpG islands were more methylated in the control iPSCs (absence of mito-Akt1) than in the mito-Akt1 iPSCs (with mito-Akt1) (Figure 2.7). These data suggest that activation of mitochondrial Akt1 signaling during reprogramming leads to more profound de-methylation of pluripotency gene promoters in the resulting iPSCs.

### **Mitochondrial Akt1 Modulated Cellular Respiration in the Resulting iPSC**

Since somatic cell reprogramming is associated with changes of cellular respiration, we evaluated cellular bioenergetics with a Seahorse analyzer. The oxygen consumption rate (OCR) represents measurements of oxidative respiration and extracellular acidification rate (ECAR) represents magnitudes of glycolysis. The respiration profile (OCR) of the mito-Akt1 iPSCs was

nearly identical to the mESCs, whereas the OCR of the control iPSCs is similar to that of MEFs (Figure 2.8A). In contrast, the glycolysis profile (ECAR) of both mito-Akt1 iPSCs and control iPSCs was similar to mESCs and differed from that of MEFs (Figure 2.8B). MEFs had lower ECAR and higher OCR than the mESCs. These findings suggest activation of mitochondrial Akt1 signaling during reprogramming may modulate cellular respiration and help establish a cellular respiration state in the resulting iPSCs that is closer to ESCs.

## **Discussion**

New insights into the molecular events underlying the maintenance, differentiation and de-differentiation of stem cells could reveal new opportunities for realizing the potential of regenerative medicine. PI3K/Akt signaling pathway has been tightly associated with the stemness of PSCs. Interestingly, a pool of Akt1 translocating into mitochondria upon PI3K activation was demonstrated in several reports from different groups<sup>45,47</sup>. Our preliminary studies also showed the mitochondrial translocation of Akt1 in human ESCs upon serum stimulation, suggesting a role of Akt1 in the mitochondria of human ESCs. A mitochondria-targeting constitutively active Akt1 expression increased the protein amounts of Oct4 and Sox2 in human ESCs and sustained its pluripotency, implying that mitochondrial Akt1 signaling may regulate the stemness of human ESCs. The underlying mechanism, however, is poorly understood.

Gurdon et al. demonstrated the basic concept that somatic cells could be reprogrammed to pluripotency in 1958<sup>105</sup>. The reprogramming factors were defined by Takahashi and Yamanaka in 2006. Using the four factors, Oct4, Sox2, Klf4, and c-Myc, they created iPSCs from somatic cells<sup>74,75</sup>. Subsequently, various laboratories developed different protocols and vehicles to



produce iPSCs by genetically manipulating critical transcription factors or with small molecule chemical compounds. However, the exact signaling network underlying reprogramming remains elusive and the efficiency of reprogramming is relatively low. Our study indicates that mitochondrial Akt1 is involved in the signaling network regulating somatic cell reprogramming.

In our previous DNA microarray analysis, the top ranking genes positively modulated by activation of mitochondrial Akt1 in hESCs were those regulating nucleosome positioning and chromatin organization. Chromatin remodeling through changing nucleosome positioning and histone modification is a critical mechanism that modulates gene transcription. Nucleosome positioning and DNA methylation are important components of epigenetic regulation of transcription initiation and gene expression. While the pattern of nucleosome positioning and regulators of positioning are just beginning to be recognized, its role in cell fate decision in ESCs and iPSCs are not fully understood. Recent studies suggested that nucleosome occupancy correlated with histone modification and the length of nucleosome occupancy increased with differentiation<sup>106</sup>. Our group recently completed a map of genome-wide nucleosome positioning in hESC (<http://www.dtd.nlm.nih.gov/geo/query/acc.cgi?acc=GSE49140>)<sup>107,108</sup>, future studies may reveal the mechanisms through which growth factor signaling such as Akt1 modulates nucleosome organization and regulate cell fate specification.

ESCs and iPSCs shared significant similarity in pluripotency markers and ability to differentiate. But there are distinctive differences in epigenetic signatures between iPSCs and ESCs. Unique patterns of DNA methylation in early passage iPSCs has been reported when compared to ESCs<sup>102,109,110</sup>, and aberrant DNA methylation in iPSCs showed striking resemblance to cancer cells<sup>111,112</sup>. Epigenetic regulation not only played an important role in the reprogramming process, but also affected the quality of iPSCs<sup>113</sup>. The findings in the current

chapter suggest that activation of mitochondrial Akt1 signaling modulated mitochondria respiration during somatic cell reprogramming, increased the efficiency of reprogramming, and promoted demethylation of Oct4 and Nanog promoters in the resulting iPSCs.

Mitochondrial Akt1 regulation of cellular oxidative phosphorylation, ROS, and cell survival was independent of cytosolic Akt1 and nuclear Akt1<sup>70</sup>. Stem cells have lower mitochondrial oxidative phosphorylation and oxidative stress than the differentiated cells<sup>114</sup>. In terminally differentiated cells, glycolysis decreases while mitochondria respiration increases. Reprogramming of fibroblasts into iPSC is accompanied by increased glycolysis and reduced oxidative phosphorylation. However, to support active cell division, embryonic stem cells rely on glycolysis for anabolic biosynthesis, i.e. the classical Warburg effect. Only part of the pyruvate generated from glycolysis enters mitochondria and TCA cycle for oxidative phosphorylation<sup>115</sup>. Recent studies have shown that certain mitochondria metabolites, such as 2-hydroxyglutarate and FAD, modulated DNA and histone methylation and thereby regulated gene transcription<sup>116,117</sup>. Therefore, alteration of metabolism may play a role in modulating gene transcription during the interplay of extrinsic growth factor signaling and intrinsic epigenetic mechanism of reprogramming. Mitochondrial Akt1 signaling lowered oxygen consumption without affecting ECAR and ATP production in MEF, which suggested tighter coupling of oxidative phosphorylation. Although we could not assess how mitochondrial Akt1 signaling affected respiration during reprogramming in each individual cell as it was not possible to identify the specific cell that would reprogram, we had compared the changes of cell respiration before and after reprogramming and confirmed reduction of mitochondria respiration (OCR) and increase of glycolysis (ECAR) in both iPSCs and ESCs.

PI3K/Akt pathway positively regulates embryonic stem cell self-renewal and inhibition of PI3K led to differentiation of hESC. Akt is main downstream effector of PI3K signaling pathway<sup>118</sup>. The activated Akt then interacts with different proteins at different subcellular localizations to exert different cellular functions. Activation of Akt signaling increased the pro-stemness Nanog expression in hESCs<sup>119</sup>. These observations suggested that Akt signaling was involved in the extrinsic mechanisms modulating cell renewal and cell fate determination in stem cells. However, previous studies on PI3K/Akt pathway used tools that altered global Akt signaling in stem cells, whereas our study focused on the effect of mitochondrial Akt1 signaling without changing cytosolic Akt actions. Our group and other laboratories identified Akt translocation to mitochondria as a key component of Akt signaling in cells<sup>46,47,61,69,85</sup>. Akt family has three members Akt1, Akt2 and Akt3, but only Akt1 can be translocated to mitochondria<sup>120</sup>. When we inhibited mitochondrial Akt1 signaling with the mitochondria-targeting dominant negative construct, fibroblasts failed to reprogram with the four factors. This suggests that activation of mitochondrial Akt1 signaling is required for somatic cell reprogramming. In summary, our work in current chapter indicated the significance of mitochondrial Akt1 signaling in the somatic reprogramming. Although the mechanistic details are not yet clear, our results suggested that mitochondrial Akt1 may regulate somatic cell reprogramming via modulating mitochondria respiration and epigenetics. Understanding the mechanisms underlying the signaling network that modulates cell metabolism and epigenetic regulation of gene transcription will help develop new strategy to control somatic cell reprogramming and stem cell differentiation.

## Figures

Figure 2.1

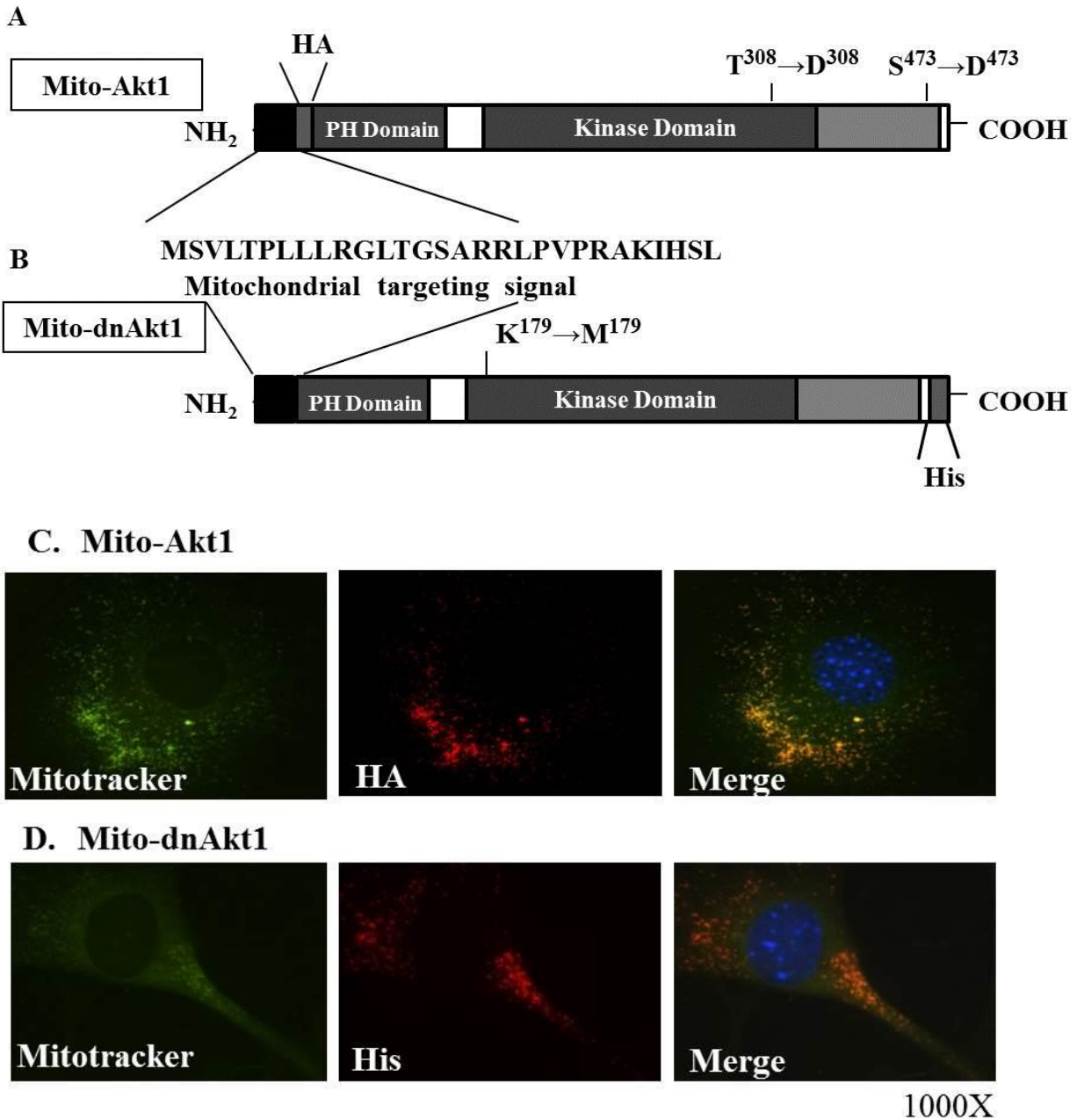


Figure 2.1. The two mitochondria-targeting Akt constructs used in this study. (A) An HA-tagged constitutively active Akt1 (adenoviral vector) and (B) A His-tagged dominant negative Akt1 (Tet-on inducible lentiviral vector), both fused with mitochondria targeting sequence at the N terminus. (C) MEFs were transduced with designated viral vector. 72 hour after transduction,

cells were fixed and subjected to immunofluorescence staining using anti-HA tag or anti-His tag antibodies and MitoTracker® Green FM.

Figure 2.2

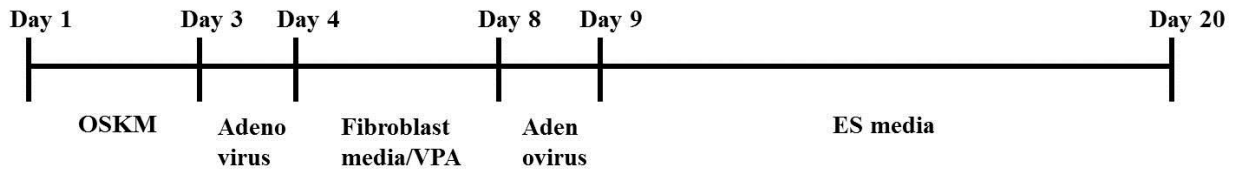


Figure 2.2. The scheme of mouse iPSC induction procedure. O: Oct4. S: SOX2. K: Klf4. M: c-Myc. VPA: valproic acid. Detailed reprogramming protocol is described in the Materials and Methods.

Figure 2.3

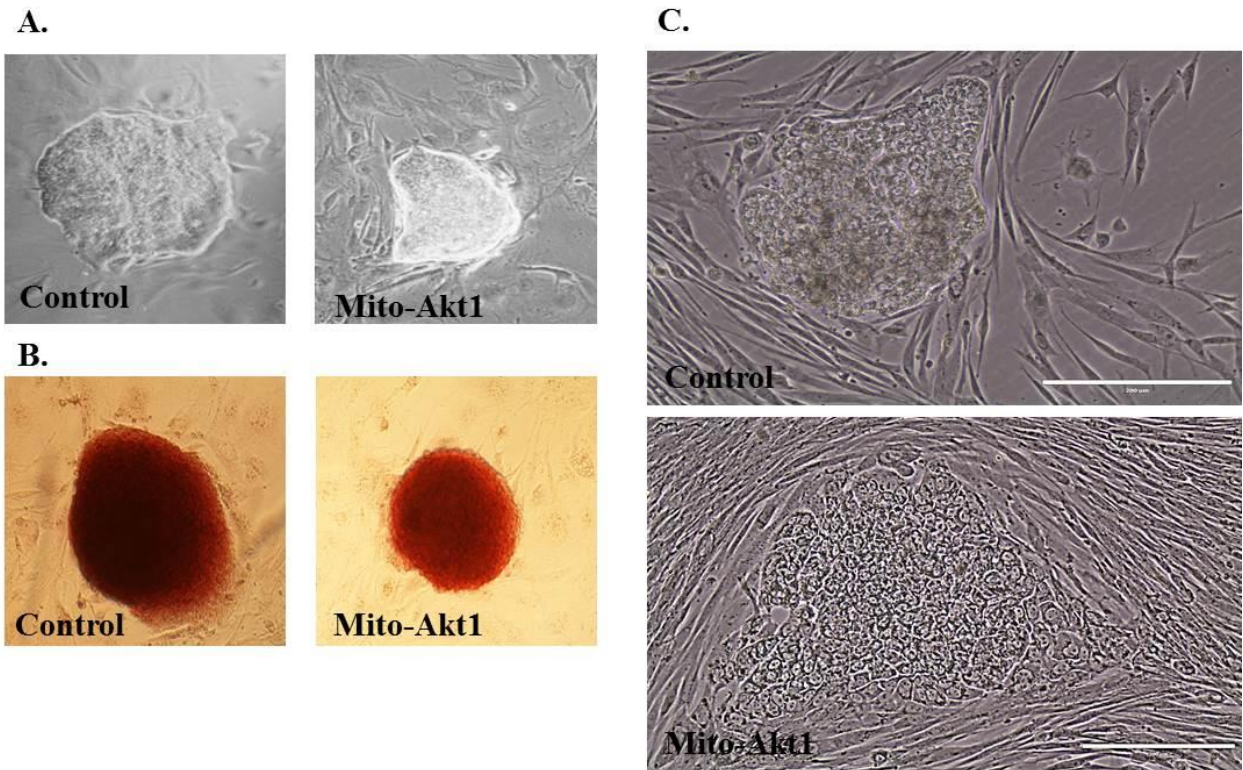


Figure 2.3. Morphologies of reprogrammed cells from MEF or HDF-N. (A) Morphologies of reprogrammed cells from OSKM-transduced MEFs with either Ad-GFP (Control) or mito-Akt1. (B) Representative pictures of alkaline phosphatase staining of the reprogrammed cell colonies from MEFs. (C) Morphologies of reprogrammed cells from OSKM-transduced HDF-N with either Ad-GFP (Control) or mito-Akt1.

Figure 2.4

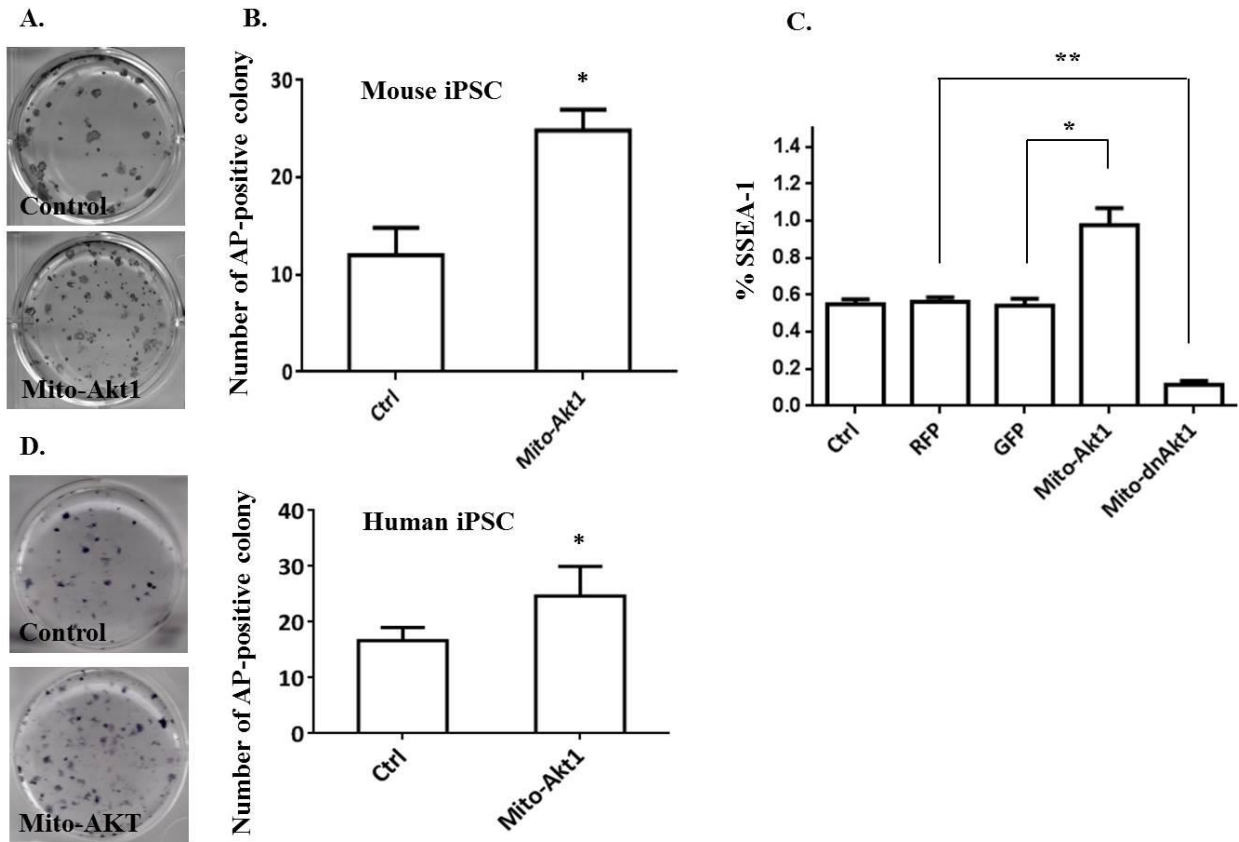


Figure 2.4. Mitochondrial Akt1 enhanced mouse iPSC reprogramming efficiency. (A) Representative pictures of AP-staining of mouse iPSC from either control or mito-Akt1 groups.

(B) The number of mouse iPSC colonies was determined by counting the number AP-positive colonies in each well on day 20. Bar graph represents the results summarized from 3 independent experiments in triplicates. \*  $p < 0.0001$ . (C) Reprogramming efficiency analyzed by SSEA1 positive cells. Mito-Akt significantly increased the number of cells stained positive for SSEA1, while mito-dnAkt reduced SSEA1 staining to background level. Ctrl: control media. RFP: lenti-RFP virus. GFP: Ad-GFP virus. The percentage of SSEA1-positive cell was determined by flow cytometry on day 21. Bar graph represents the results summarized from 3 independent experiments in triplicates. \*  $p < 0.005$ , \*\*  $p < 0.0001$ . (D) The number of human iPSC colonies was determined by counting the number of alkaline phosphatase-positive colonies in each well on day 30. Representative photo of AP staining is shown here. Bar graph represents the results summarized from 3 independent experiments in triplicates. \*  $p < 0.01$ .



Figure 2.5

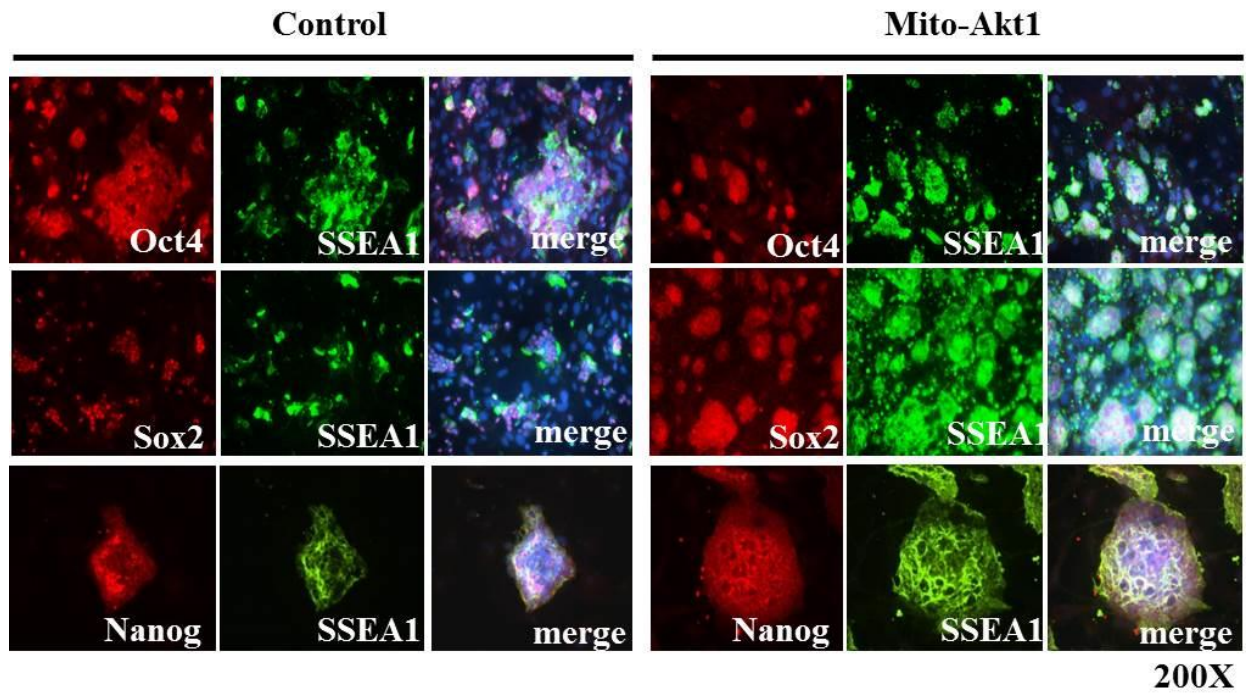
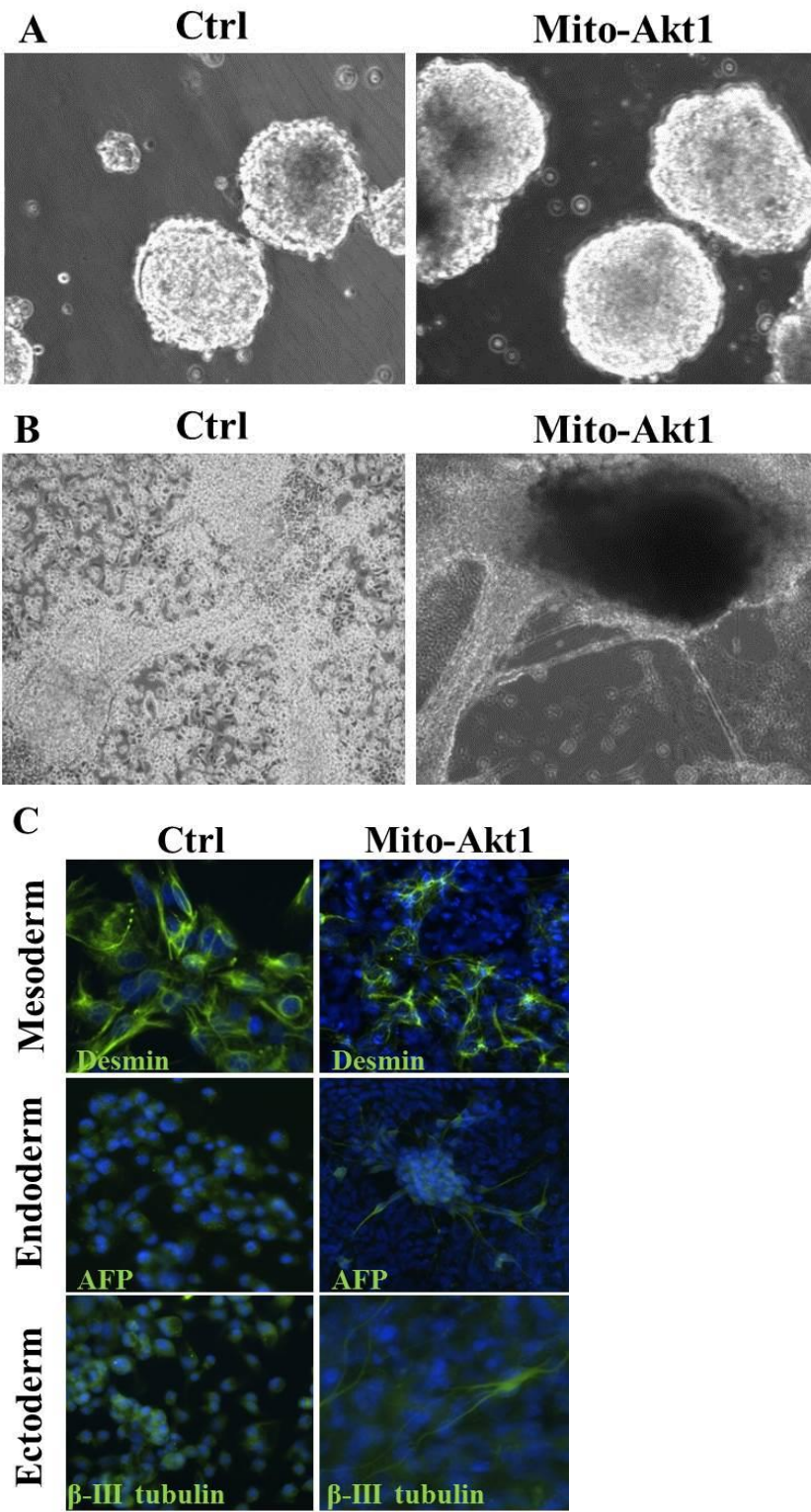


Figure 2.5. The mouse iPSCs expressed embryonic stem cell markers. Mouse iPSC colonies derived from both groups (Control and mito-Akt1) were stained for SSEA1, Oct4, Sox2, and Nanog. Pictures were taken at 200x magnification with Eclipse Ti fluorescence microscope (Nikon).



Figure 2.6



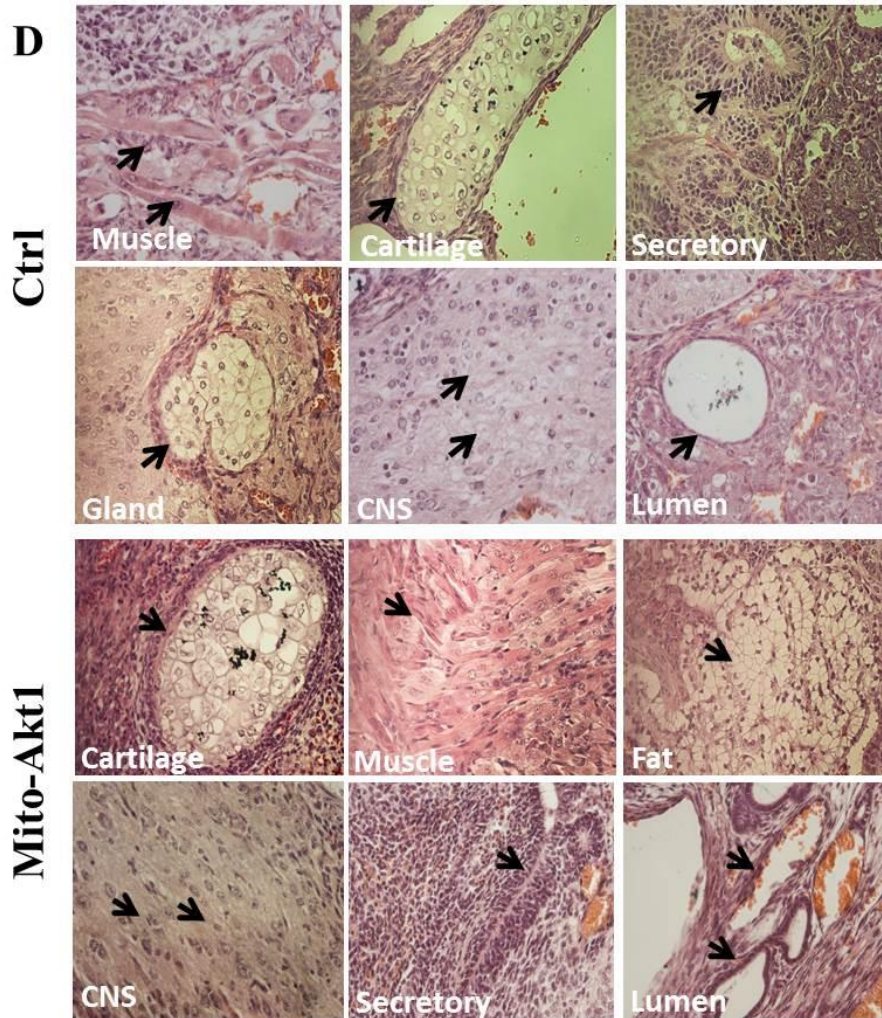


Figure 2.6. The reprogrammed cells may differentiate into cell lineages of three germ layers. (A) iPSCs from both groups (control and mito-Akt1) formed into EBs in suspension culture. (B) Various cell types emerged from EBs of both groups. Some cells organized into bundles. (C) Cells emerged from EBs of both groups were fixed and immunofluorescence-stained with designated three germ layers markers.  $\alpha$ -fetoprotein (AFP) is used for endoderm,  $\beta$ -III tubulin is used for ectoderm and Desmin is used for mesoderm. (D) Teratomas formed in SCID mice were collected and subjected to tissue fixing, embedding, and section. Hematoxylin and eosin staining analysis of teratomas from both groups (control and mito-Akt1) were shown. Cells with morphologies similar to each tissues were shown and indicated with black arrows.

Figure 2.7

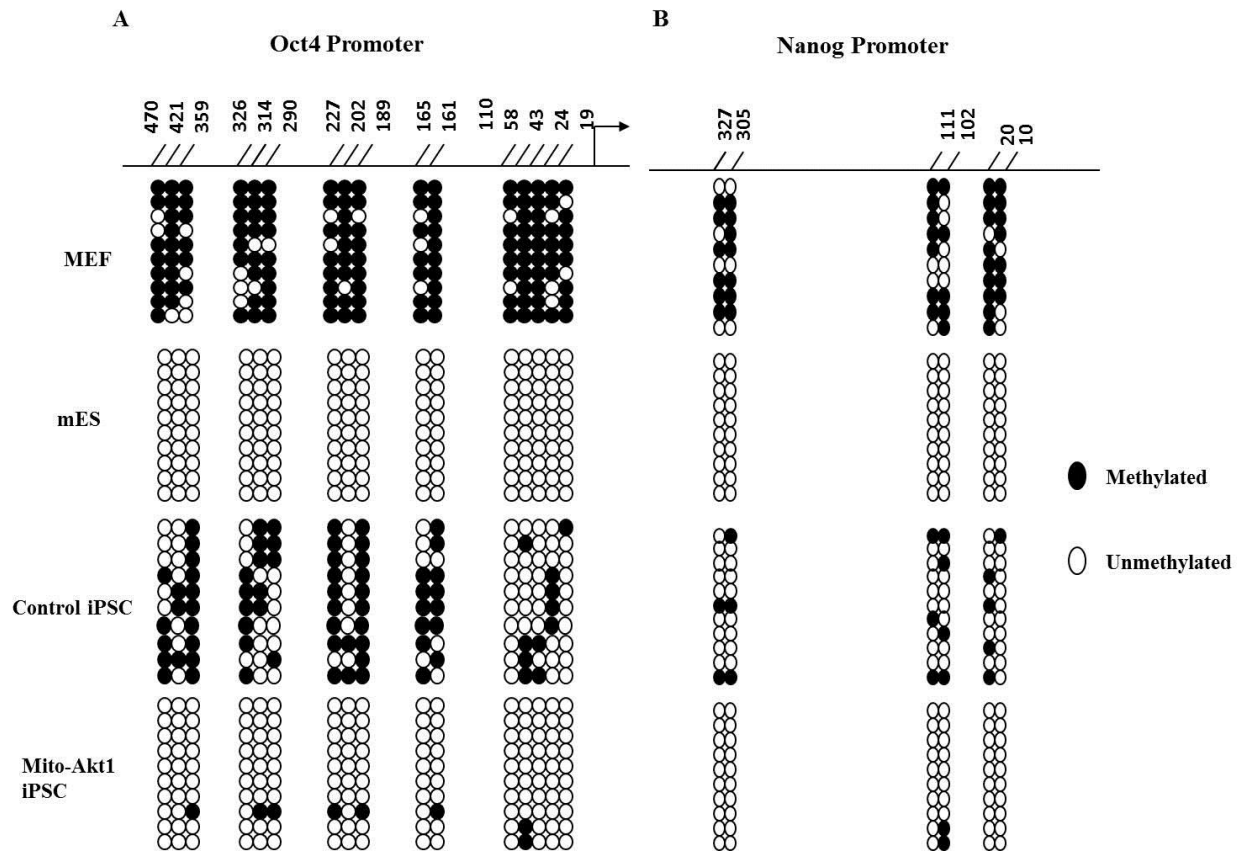


Figure 2.7. Methylation of Oct4 and Nanog promoters in mouse iPSCs. (A) Bisulfite sequencing of the promoter region of Oct4. (B) Bisulfite sequencing of the promoter region of Nanog. Genomic DNA were extracted from MEF, mouse ESC and iPSCs for bisulfite sequencing to determine the methylation status of the CpG islets at Oct4 and Nanog promoters. 10 random colonies from each group were used for this assay.

Figure 2.8

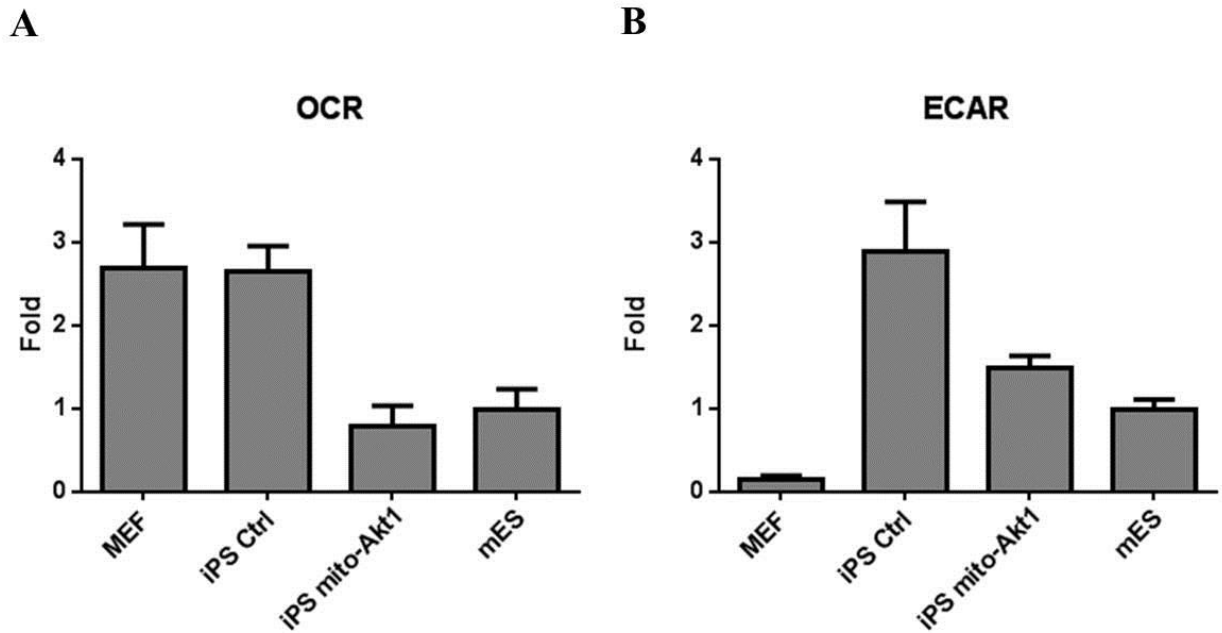


Figure 2.8. Mitochondrial Akt1 modulated cellular respiration in the resulting iPSC. (A) Basal oxygen consumption rate (OCR) in MEF, mESC, and iPSC. (B) Basal extracellular acidification rate (ECAR) in MEF, mESC, and iPSC. Bar graph represents the results summarized from 3 independent experiments in triplicates.

## CHAPTER 3

### Mitochondrial Akt1 Modulated Cellular Metabolism

#### Introduction

The mitochondrion is a unique organelle that regulates various cellular functions<sup>121</sup>. The roles of mitochondria in pluripotent stem cells (PSCs) remain elusive; however, increasing efforts have been made towards understanding the role of mitochondria in regulating metabolism in PSCs. As mentioned in the previous chapter, the immature morphology of mitochondria in PSCs suggests their role may not just be simply providing the energy source for the cell uses. In differentiated cells, mitochondria produce massive amounts of ATP as an energy source through the TCA cycle and electron transport chain (ETC). The process requires oxygen as a final electron acceptor; and is also named aerobic respiration or oxidative phosphorylation (OXOPHOS). The capacity of mitochondria to produce massive amounts of ATP fulfills the energy demands of differentiated cells such as neurons and muscles, allowing them to exert specialized cellular functions. In contrast, glycolysis produces much less ATP and generates lactic acid as a byproduct. Glycolysis, however, also provides nutrient precursors for the biosynthesis of macromolecules through the pentose phosphate pathway. For example, the ribose-5-phosphate can be used to synthesize purines and pyrimidines, NADPH may be used to synthesize fatty acids and erythrose 4-phosphate can be used to synthesize aromatic amino acids.

In rapidly dividing cells, such as cancer cells, the high nutrient demand for cell proliferation and growth shifts metabolic balance towards glycolysis and away from OXOPHOS<sup>115</sup>. In this respect, PSCs resemble cancer cells in that they rapidly divide and therefore require a metabolic balance that favors glycolysis<sup>115,122</sup>. From both the metabolomics

and cellular bioenergetics analyses of iPSCs, Panopoulos demonstrated that somatic cells changed from an oxidative state to a glycolytic state following the shift to pluripotency. Interestingly, they further demonstrated that iPSC reprogramming efficiency is associated with the cellular bioenergetics of the parental cells<sup>123</sup>, meaning the closer a somatic cell's overall bioenergetics is to pluripotent cells, the higher its reprogramming efficiency. This suggests that metabolic profile may represent a “barrier” to efficient reprogramming. Similarly, our study indicated that the activation of mitochondrial Akt1 signaling enhanced iPSC reprogramming and modulated cellular bioenergetics in the resulting iPSCs. This suggests that mitochondrial Akt1 signaling may modulate cellular metabolism.

Besides cellular bioenergetics, the mitochondrion has an additional role in reactive oxygen species (ROS) regulation<sup>124</sup>. ROS are generated from the one-electron reduction of molecular oxygen, and can be categorized into three forms: superoxide anions ( $O_2^-$ ), hydrogen peroxide ( $H_2O_2$ ) and hydroxyl radicals ( $OH^-$ ). The accumulation of ROS in the cell is thought to be detrimental; therefore, various enzymes and systems have evolved to modulate the level of intracellular ROS. Superoxide anion can be reduced to hydrogen peroxide by superoxide dismutase (SOD) and hydrogen peroxide can be reduced to water and oxygen by catalase. The hydroxyl radicals can be eliminated through glutathione system. The imbalance between ROS generation and elimination may result in excessive ROS accumulation leading to the damage of DNA, proteins and lipids in the cell, which is called oxidative stress. Severe oxidative stress can lead to cell death via apoptosis or necrosis. Studies have shown that PSCs consume less oxygen and grow better in a hypoxic environment. This requirement for low oxygen reduces ROS generation in PSCs, suggesting that excessive ROS may be detrimental to PSCs. In support, Wu

et al. demonstrated that oxidative stress may induce apoptosis and senescence of induced pluripotent stem cells<sup>125</sup>.

On the other hand, ROS have also been demonstrated to be secondary messengers in cell signaling transductions<sup>126-128</sup>. In ROS-inducing conditions, Ji et al. showed that the expression of pluripotency markers was decreased in human ESC, and result in increased expression of mesodermal and endodermal markers. This suggests that increased ROS generation may trigger differentiation of PSCs. This is supported by the studies in ESC differentiation. For example, Crespo et al. demonstrated that mitochondrial ROS may mediate cardiomyocyte formation from embryonic stem cells<sup>129</sup>. Zhang et al. also demonstrated that the increase of ROS level was accompanied by human ESC spontaneous differentiation, probably through UCP2 repression<sup>130</sup>. In contrast, the iPSC reprogramming process was shown to be accompanied by increased oxidative stress<sup>131,132</sup> and that the administration of the antioxidant, vitamin C, reduced the level of ROS during reprogramming and enhanced iPSC colony formation<sup>132</sup>. The mechanistic details behind elevated ROS levels during reprogramming are still not understood, but Esteban et al. demonstrated that ROS levels are different in either 3 factors (OSK) or 4 factors (OSKM) reprogrammed cells. This suggests that the ROS level might be associated with the genes that are regulated by these transcription factors. Collectively, lowering the ROS production may be beneficial to the early stages of reprogramming by preventing ROS-induced damage, therefore increasing the efficiency of reprogramming. While we demonstrated that activation of mitochondrial Akt1 during iPSC reprogramming enhanced its efficiency, the role of mitochondrial Akt1 in the regulation of ROS levels, requires more investigation.



## **Materials and Methods**

### **Analysis of Mitochondrial O<sub>2</sub> Respiration by Extracellular Flux Measurement**

To measure mitochondrial function in cells, we employed a Seahorse Bioscience XF24 Extracellular Flux Analyzer (Seahorse Bioscience, North Billerica, MA) and follow the manufacturer's protocol. Briefly, cells were plated in a 0.2% gelatin or Matrigel coated 24-well Seahorse XF-24 assay plate at  $7.5 \times 10^4$  cells/well, and grown for 16 hours before analysis. On the day of metabolic flux analysis, cells were washed once with freshly prepared KHB buffer (111 mM NaCl, 4.7 mM KCl, 2 mM MgSO<sub>4</sub>, 1.2 mM Na<sub>2</sub>HPO<sub>4</sub>, 2.5 mM glucose and 0.5 mM carnitine; pH 7.4) and incubated in KHB buffer at 37°C in a non-CO<sub>2</sub> incubator for 1 hr. Three baseline measurements of oxygen consumption rate (OCR) were taken before sequential injection of following mitochondrial inhibitors and final concentration: oligomycin (1 µg/ml), carbonilcyanide p-triflouromethoxyphenylhydrazone (FCCP) (3 µM) and rotenone (0.1 µM). Three measurements were taken after addition of each inhibitor. OCR values were automatically calculated and recorded by the Seahorse XF-24 software. The basal respiration was calculated by averaging the three measurements of OCR before injection of inhibitors.

### **Metabolites Extraction**

Cellular metabolites were extracted with 80% HPLC grade methanol (Fisher Scientific) using a previously described method<sup>133</sup>. In brief, 72 hours after adenoviral transduction, cells were collected by trypsinization and cell numbers were counted.  $1 \times 10^6$  MEFs were aliquoted in 100µL MEF medium and gently mixed with ice-cold quenching solution (60% methanol, 0.85% ammonium bicarbonate (pH7.4)). Cells were then pelleted down at 1000g for 1 min at 4°C. The supernatant was removed and the cell pellet was resuspended in 500µL ice-cold 100% methanol.



The cell suspension was snap-frozen in liquid nitrogen for 5 min and thawed on ice. The thawed cell suspension was then vortexed for 30 seconds and pelleted down at 800g for 1 minute at 4°C. The supernatant was collected and transferred to another new tube. The cell pellet was put through another cycle of 100% methanol extraction following the same procedure, and then the supernatant was combined with the previous extracts. The cell pellet was then resuspended in 250µL ddH<sub>2</sub>O and snap-frozen as above. The thawed cell suspension was vortexed for 30 seconds and pelleted down at 15,000g for 1 minute at 4°C. The supernatant was collected and combined with the previous extracts. Final methanol concentration was 80%. The extracts (in 80% methanol) were dried in a vacuum centrifuge at 30°C until a fully dried pellet was obtained (Figure 3.1).

### **ATP Assay**

The obtained metabolite pellet was reconstituted with 50% Acetonitrile (Sigma Aldrich) containing 0.1% trifluoroacetic acid for ATP (  $m/z=506$ ) and NADH ( $m/z=664$ ) quantification with MALDI TOF/TOF as we previously reported<sup>85</sup>. The cellular ATP level was normalized to an external loading control (Adenosine 5'-[ $\gamma$ -thio] triphosphate, ATP- $\gamma$ -S,  $m/z=522$ , Sigma Aldrich). We tested the effect of adding an external control by adding same amount (1mM) of ATP- $\gamma$ -S into metabolite extraction procedure in each group in fibroblasts and ESCs. The introduction of ATP- $\gamma$ -S into each group resulted in altered pattern in mass spectrum and is repeatedly detected in fibroblasts and ESCs (Figure 3.2), suggesting the feasibility of using it as an external control. Several mass spots (including ATP- $\gamma$ -S,  $m/z=522$ ) only show up or higher levels in the groups with ATP- $\gamma$ -S addition (indicating with red arrows), suggesting they are originated from ATP- $\gamma$ -S. They could be the impurities in the purchased ATP- $\gamma$ -S, as indicated in

the product description. We choose to use mass point of 835 ( $m/z=835$ ) for normalization purpose because we do not see much signal in the cell alone extract and that ATP- $\gamma$ -S ( $m/z=522$ ) is itself potentially overlapped and interfered by cellular Guanosine triphosphate (GTP).

### **FACS Analysis of Superoxide and Apoptosis**

To measure mitochondria superoxide, the cells were loaded with  $1\mu\text{M}$  MitoSOX Red (Molecular Probes) at  $37^\circ\text{C}$  for 30 minutes and then washed 3 times with PBS. The cells were analyzed with a BD LSR II Flow Cytometer (excitation at 514 nm and emission at 575 nm). To measure apoptosis, an Annexin V Apoptosis kit (MitoTracker Red and Alexa Fluor 488 Annexin V) was purchased from Invitrogen. MEFs were stained according to the instructional manual, and their fluorescence was measured with a BD LSR II Flow Cytometer (excitation at 488 nm, emission at 525 and 575 nm). Although apoptotic cells showed green fluorescence with reduced red fluorescence, live cells showed minimal green fluorescence and bright red fluorescence, and necrotic cells showed neither. The FACS measurement was gated according to the positive (doxorubicin treated) and negative controls (no death-inducing agent). The analysis was presented as the percentages of apoptotic cells. BD FACSDiVa software was used to analyze the data.

### **Statistical Analysis**

Data are presented as mean  $\pm$  SD, unless noted otherwise. FACS data were analyzed with BD FACSDiVa software. Student's t test and one-way repeated measures ANOVA with Holm-Sidak method were performed with SigmaStat 3.11. The statistical significance level was set at  $p < 0.05$ .

## **Result**

### **Mitochondrial Akt1 Modulated Cellular Bioenergetics of Mouse Embryonic Fibroblast**

Cellular bioenergetics is the study of energy flow within the cell and the relationships between the cell's different metabolic pathways. There are two main pathways that cells use to produce energy: Oxidative phosphorylation and glycolysis. Oxidative phosphorylation consists of multiple biochemical reactions that lead to the establishment of a proton gradient across the mitochondrial inner membrane. This proton gradient can then drive Complex V of ETC to generate massive amounts of ATP. The process needs an oxygen molecule as the final electron acceptor. Therefore, by measuring the change in oxygen concentration, one can quantify the amount of oxidative phosphorylation occurring in a given cell. On the other hand, glycolysis can also contribute to energy production, albeit to a lesser extent. A glucose molecule can go through glycolysis to generate pyruvate. In the cytosol, pyruvate can be converted to lactate, leading to changes in cellular pH. Thus, by measuring the pH, one can tell how a cell is using glycolysis to generate energy and intermediate metabolites.

Since the metabolic profile of somatic cells changes during iPSC reprogramming and the reprogramming efficiency is associated with the "metabolic status" of the parental cells<sup>123</sup>, we hypothesize that activation of mitochondrial Akt1 may modulate cellular bioenergetics of MEF. To study the effect of mitochondrial Akt1 signaling on cellular bioenergetics in MEF, we use the Seahorse XF Extracellular Flux Analyzer to measure oxygen consumption rate (OCR) and extracellular acidification rate (ECAR) 72 hours after adenoviral vector transductions (mito-Akt1 vs. Control). Although mito-Akt1 did not alter ECAR, it significantly reduced OCR (Figure 3.3A and B). Interestingly, however, the ATP levels in these cells were not altered (Fig 3.3C), suggesting a better ATP production efficiency in mitochondria. On the other hand, the activation

of mitochondrial Akt1 reduced cellular NADH level (Figure 3.3D), suggesting that the metabolic profile of cell may be altered.

### **Mitochondrial Akt1 Regulated Reactive Oxygen Species and Apoptosis under Stress in MEF**

iPSC reprogramming involves the change of gene expression profile from somatic cell to pluripotent stem cell. Although the mechanistic details behind transcription factor mediated reprogramming are still not clear, studies have shown that the process can cause oxidative stress to cells. Elevated oxidative stress could lead to cell death via apoptosis or necrosis and may result in low reprogramming efficiency. The mitochondrion is the main cellular location that produces massive ROS and cause oxidative stress. We demonstrated that the activation of mitochondrial Akt1 signaling reduced oxygen consumption in MEF. Therefore, we sought to investigate if the ROS production in mitochondria is also modulated by mitochondrial Akt1 signaling. In unstressed conditions, the levels of mitochondrial ROS were similar in all groups and mitochondrial Akt1 did not alter ROS levels. To mimic the condition of increased oxidative stress during iPSC reprogramming, we treated MEFs with doxorubicin, which is a chemotherapeutic agent for cancer known to induce ROS production and leading to cell apoptosis<sup>134,135</sup>. When the MEFs were under stress, mitochondria ROS was lowered in the MEFs transduced with mito-Akt1 (Figure 3.4A), suggesting that the activation of mitochondrial Akt1 signaling may prevent ROS production under stress. The lower level of ROS under stress conditions may prevent the apoptosis induced by ROS-mediated damage. Indeed, an apoptosis study showed that mito-Akt1 reduced apoptosis level in doxorubicin-treated conditions (Figure 3.4B). Collectively, it is possible that activation of mitochondrial Akt1 reduced mitochondrial

oxidative stress in MEFs during reprogramming and led to reduced apoptosis and increased reprogramming efficiency.

## **Discussion**

We demonstrated enhanced iPSC reprogramming efficiency via activation of mitochondrial Akt1 signaling in the previous chapter. We also provided evidence indicating that mitochondrial Akt1 may modulate cellular respiration and epigenetics. In the current chapter, we followed up on this evidence to show that activation of mitochondrial Akt1 signaling reduced oxygen consumption of the cell, supporting our hypothesis that mitochondrial Akt1 may modulate cellular respiration and cellular metabolism.

Increasing attention has been directed to cellular metabolism in PSCs. PSCs maintain a glycolytic metabolic profile to support the high nutrient requirement for rapidly growing and dividing cells, known as Warburg effect<sup>115,122</sup>. Although the mechanistic details of PSC pluripotency regulation by cellular metabolism are still not clear, studies have shown that the loss of this glycolytic profile may result in loss of pluripotency. 2-deoxy-D-glucose (2-DG) is an analog of glucose which cannot be catabolized through glycolysis and therefore serves as a competitive inhibitor for glucose utilization. Treatment of cancer stem cells with 2-DG reduced cell viability and significantly hindered colony formation<sup>136</sup>. In another report, treatment of human hematopoietic progenitors with 2-DG enhanced rEPO-induced erythroid commitment<sup>137</sup>. These studies indicate that PSCs require a glycolytic profile to maintain differentiation competence.

Conversely, pushing a cell's metabolic balance toward glycolysis may facilitate pluripotency and impede PSC differentiation. Uncoupling proteins (UCPs) are mitochondrial inner membrane proteins that may disrupt the proton gradient established across the mitochondrial inner membrane by the ETC. The normal physiological role of UCPs is to dissipate the proton gradient across the mitochondrial inner membrane and direct the energy stored in chemical bonds into thermogenesis, therefore reducing mitochondrial ATP production. Interestingly, UCP2 is highly expressed in human PSCs and ectopic UCP2 expression suppressed differentiation<sup>130,138</sup>. These studies imply that “metabolic modulators” exist in PSCs and that their functions are tightly associated with PSC pluripotency. Understanding of the mechanisms regulating the expression and activity of these metabolic modulators may help to link cellular metabolism to cell fate specification.

Our previous<sup>85</sup> and current studies indicate that activation of mitochondrial Akt1 signaling reduced cardiomyocyte and MEF oxygen consumption, suggesting that mitochondrial Akt1 may serve as a metabolic modulator in cells. Interestingly, Varum et al. demonstrated that human ESCs had a lower oxygen consumption rate, a lower mitochondrial membrane potential, and had increased levels of glycolytic enzymes<sup>139</sup>. We observed similar effects in previous studies that activation of mitochondrial Akt1 signaling in cardiomyocytes led to lower oxygen consumption, elevated glycolysis, lower mitochondrial membrane potential and increased ATP production<sup>85</sup>. This supports the notion that mitochondrial Akt1 may act as a metabolic modulator in cells. However, more studies are needed to establish the role of mitochondrial Akt1 as a metabolic modulator in PSCs.

On the other hand, although we observed reduced oxygen consumption upon activation of mitochondrial Akt1 signaling, the overall ATP level remained unchanged. The level of

glycolysis did not change either, suggesting that either the cell reduced its energy expenditure or overall, cellular energy production was more efficient. Although the mechanistic details remain unclear, we previously showed that constitutively active mitochondria-targeting Akt1 also enhanced Complex V activity<sup>69</sup> suggesting mitochondrial Akt1 may enhance ATP production efficiency by regulating Complex V activity. Our recent mitochondrial proteomics study also revealed that Complex V was differentially phosphorylated after acute insulin stimulation<sup>140</sup>. It implies that complex V may be a substrate for Akt1. Indeed, Bijur et al. has reported the interaction between Akt and Complex V<sup>61</sup>. Interestingly however, Complex V does not contain a consensus Akt phosphorylation motif. This implies that an intermediary between Complex V and Akt1 may be involved. Intriguingly, protein kinase C $\alpha$  has been reported to interact and phosphorylate complex V resulting in the prevention of ATP reduction in renal proximal tubule cell injured by hypoxia and oxidant<sup>141</sup>. Moreover, several studies also indicated that an interaction exists between protein kinase C and Akt<sup>142-145</sup> and that the mitochondrial translocation of protein kinase C has also been reported<sup>146,147</sup>. Although these interactions might be tissue/cell-, subcellular location-specific and may only occur after injury, they present interesting points for further investigation.

In the current chapter, we also demonstrated that activation of mitochondrial Akt1 signaling reduced cellular NADH levels, suggesting that mitochondrial Akt1 may act as a metabolic modulator. Reduced NADH levels might attenuate the electron flow generated from complex I, ultimately leading to reduced oxygen consumption. Mitochondria are an important source of ROS within most mammalian cells. Complex I uses NADH as a substrate to transfer electrons (reduction) to its cofactor flavin mononucleotide (FMN) which then pass through a chain of seven FeS (iron-sulfur) centres to the CoQ reduction site<sup>148</sup>. Oxygen's ability to access

the FMN and CoQ site electron carriers leads to the production of ROS. Reduced NADH levels resulting from activation of mitochondrial Akt1 signaling may therefore reduce the production of ROS. Indeed, Kussmaul et al. and Hirst et al. demonstrated that increased ROS production is associated with a higher NADH/NAD<sup>+</sup> ratio<sup>149,150</sup>.

Although the mechanistic details are not completely understood, a previous study showed that the levels of ROS appear to increase during iPSC reprogramming<sup>131</sup>. ROS production is reduced in hypoxic conditions and has been demonstrated to enhance iPSC reprogramming<sup>151</sup>. Furthermore, elevated ROS levels may cause DNA damage and lead to cell senescence which, has been shown to impair somatic cell reprogramming to PSCs<sup>152</sup>. Therefore, the reduced ROS levels mediated by activation of mitochondrial Akt1 signaling may enhance iPSC reprogramming efficiency by modulating ROS production and result in reduced apoptosis during the reprogramming process.

In summary, we studied the activation of mitochondrial Akt1 signaling's effects on somatic cells in this chapter. Our results indicated that mitochondrial Akt1 may act as a metabolic modulator that reduces oxygen consumption. The unchanged ATP level and reduced NADH levels suggest a mechanistic role of mitochondrial Akt1 in regulating OXOPHOS. Reduced NADH levels support the results of reduced ROS production and oxygen consumption. Overall, this leads to a better "primed condition" for cells to endure the stress caused by OSKM-mediated reprogramming, which is evident by lower apoptosis levels under stress conditions. Future efforts will need to be focused on the targets of Akt1 in the mitochondria to elucidate the molecular map of mitochondrial Akt1 mediated enhancement of iPSC reprogramming.



**Figure**  
Figure 3.1

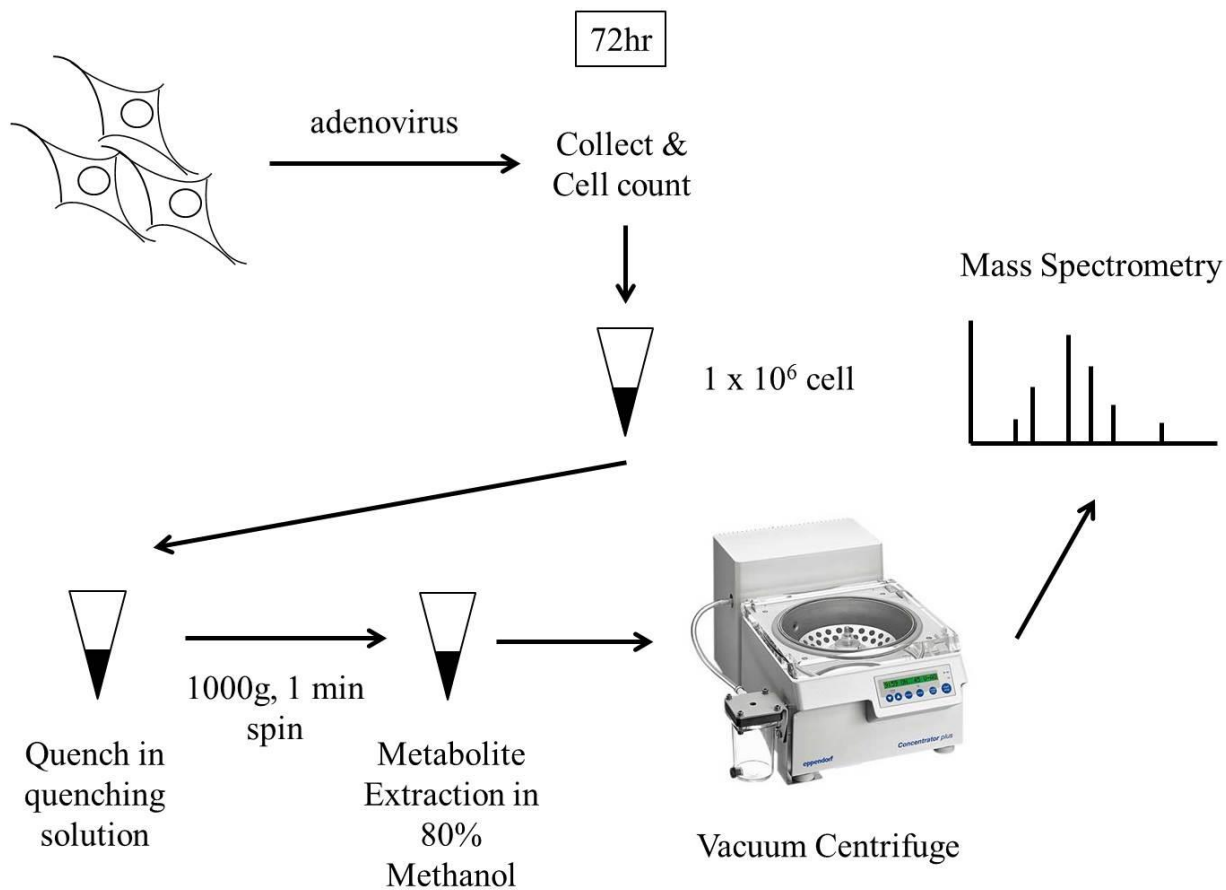
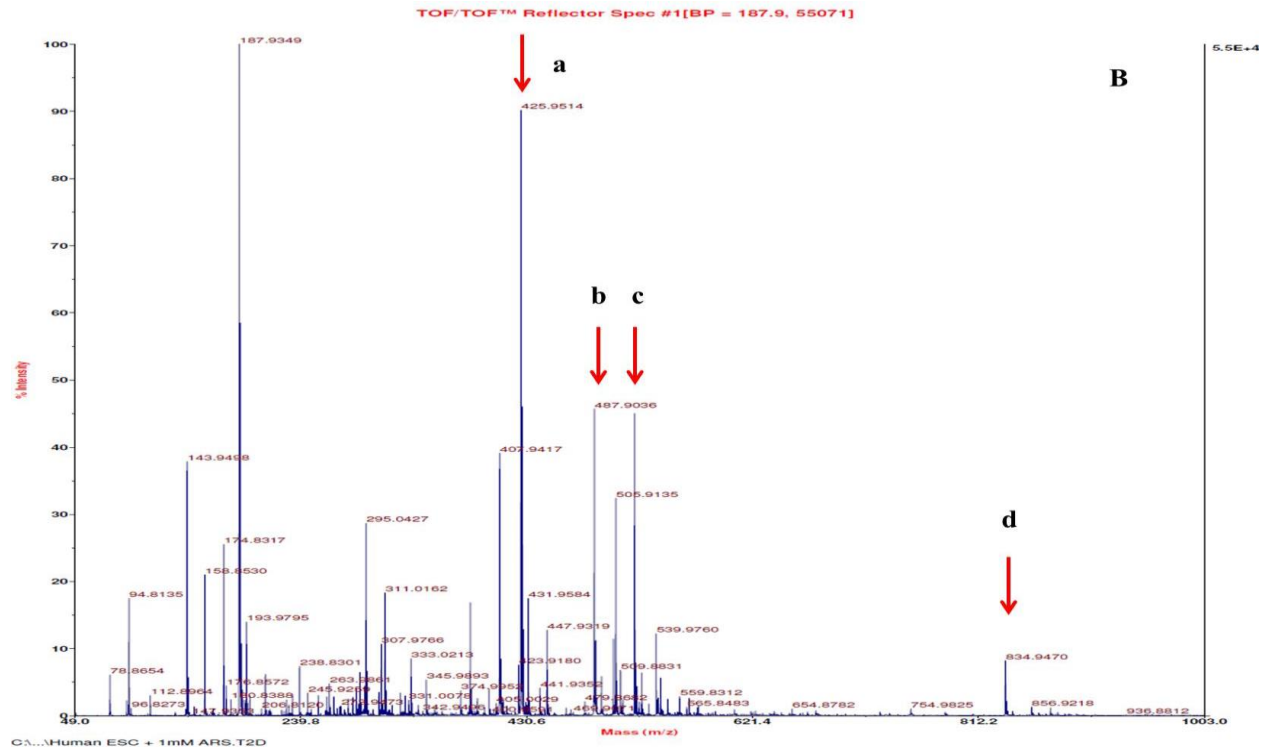
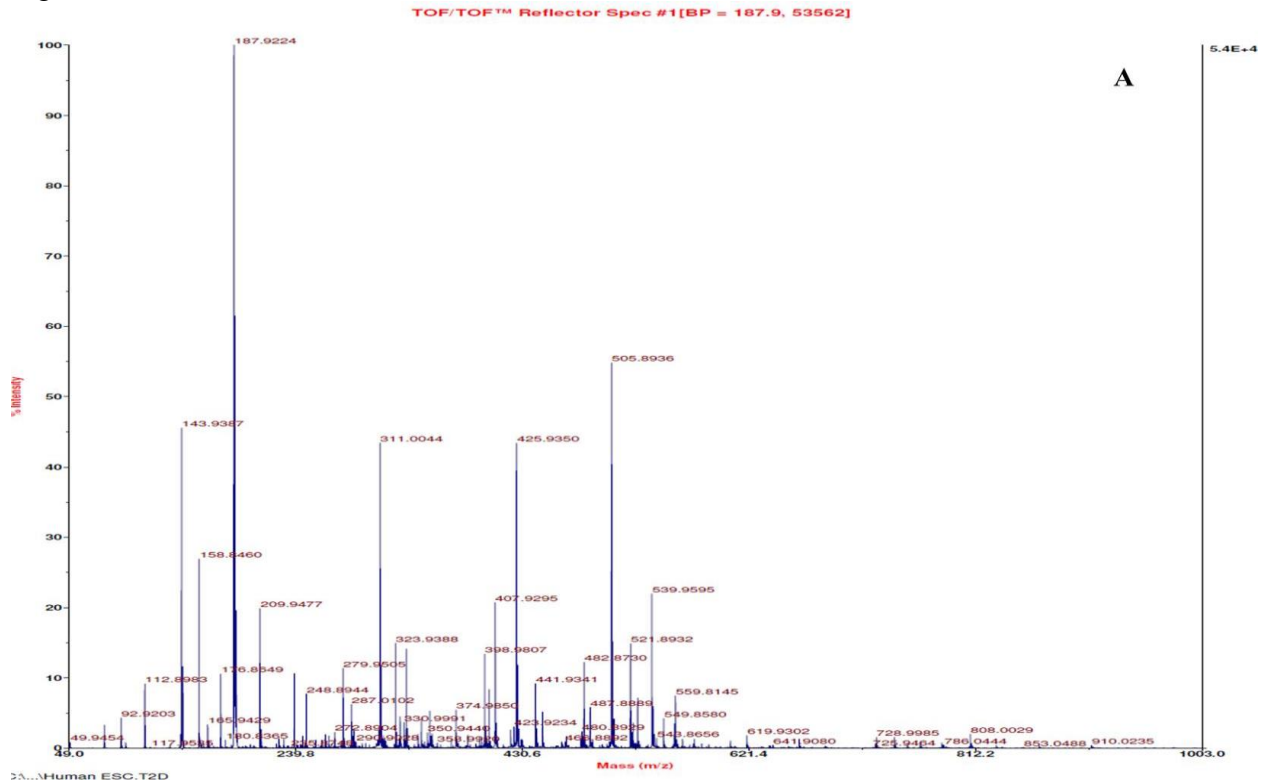


Figure 3.1. The scheme of metabolite extraction from mouse embryonic fibroblast.  $1 \times 10^6$  cells were subjected to metabolite extraction with 80% methanol following quenching step. The detailed procedure is described in the “Materials and Methods” section of this chapter.

Figure 3.2



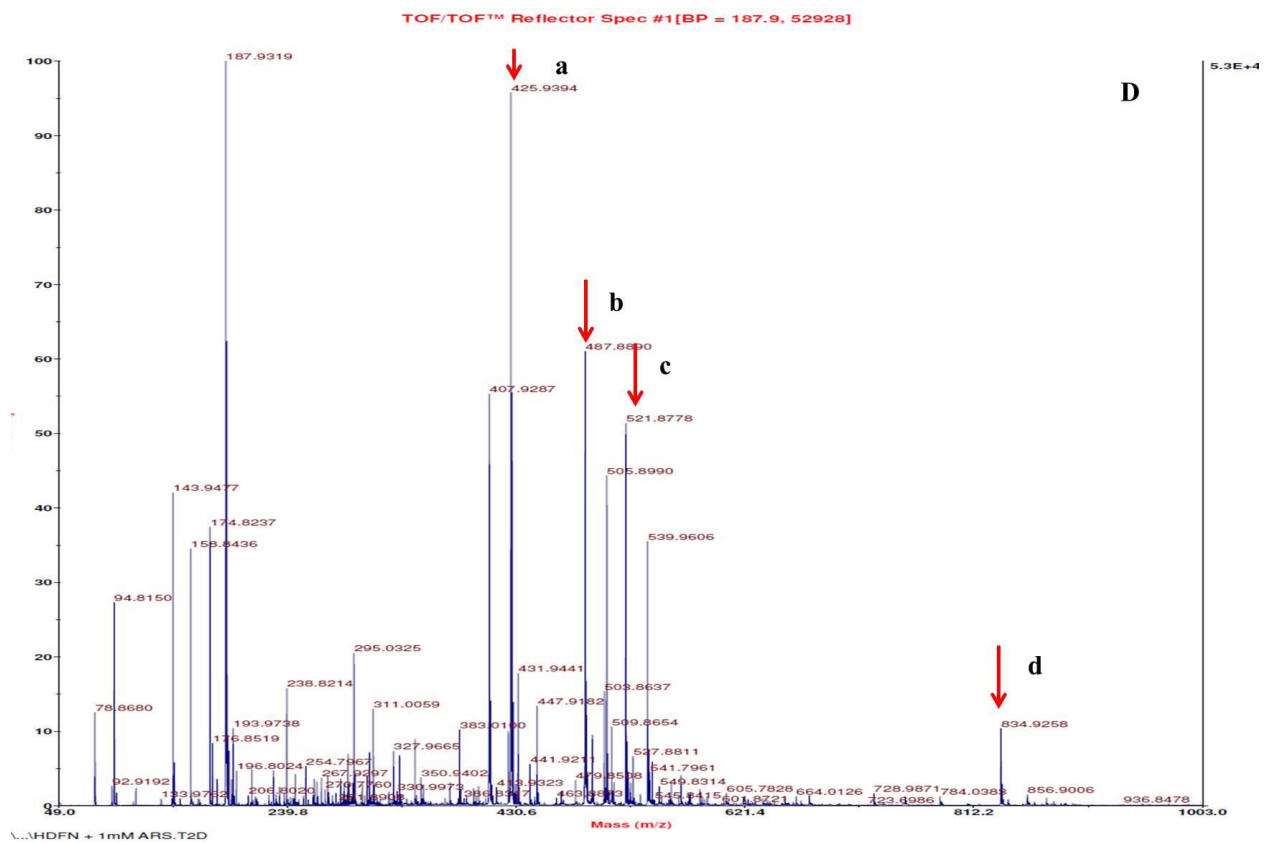
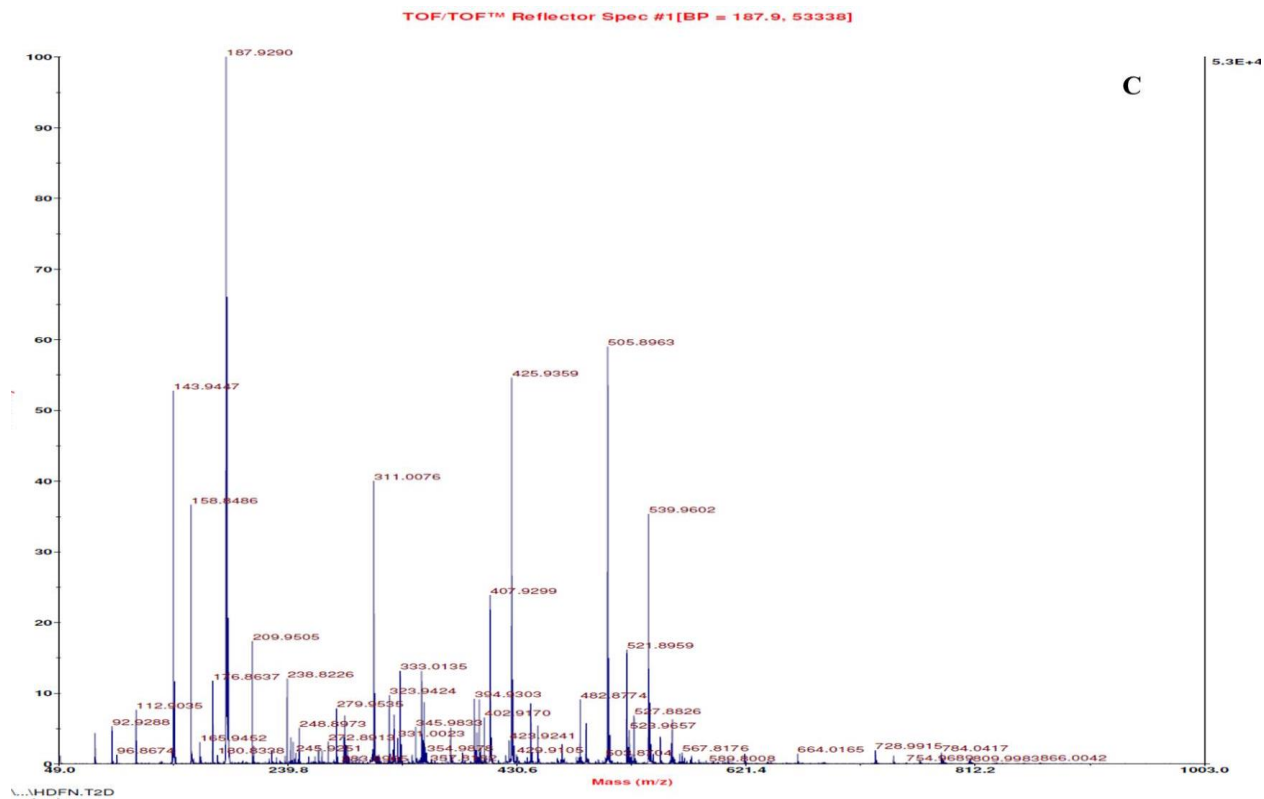


Figure 3.2. The mass spectrums of extracted metabolites from cells with or without external control. ATP- $\gamma$ -S was purchase from Sigma Aldrich and dissolved in ddH<sub>2</sub>O to final stock concentration of 1M. A 20  $\mu$ L of diluted final concentration of 1mM of ATP- $\gamma$ -S was used to resuspend cell pellet, followed by 80% methanol extraction procedure as described in materials and methods. A 20  $\mu$ L of ddH<sub>2</sub>O was used as control to resuspend the cell pellet and subjected to metabolite extraction. Both dried metabolite pellets were reconstituted with 50% acetonitrile (0.1% TFA) as described in materials and methods and subjected to mass spectrometry. (A) The mass spectrum of extracted metabolites from human ESC without ATP- $\gamma$ -S addition. (B) The mass spectrum of extracted metabolites from human ESC with ATP- $\gamma$ -S addition. (C) The mass spectrum of extracted metabolites from human neonate dermal fibroblast without ATP- $\gamma$ -S addition. (D) The mass spectrum of extracted metabolites from human neonate dermal fibroblast with ATP- $\gamma$ -S addition. Red arrows indicate the mass spots that display different intensities between ATP- $\gamma$ -S-addition and control groups. 4 mass spots are identified with differentially intensities between the two groups. a: m/z: 426, b: m/z: 488, c: m/z: 522, d: m/z 835. The peak with highest intensity with a mass value of 188 corresponding to the MALDI matrix  $\alpha$ -Cyano-4-hydroxycinnamic acid (CHCA) used. The peak intensities for CHCA are similar in both ATP- $\gamma$ -S-addition and control groups to control the loading for mass spectrometry.

Figure 3.3

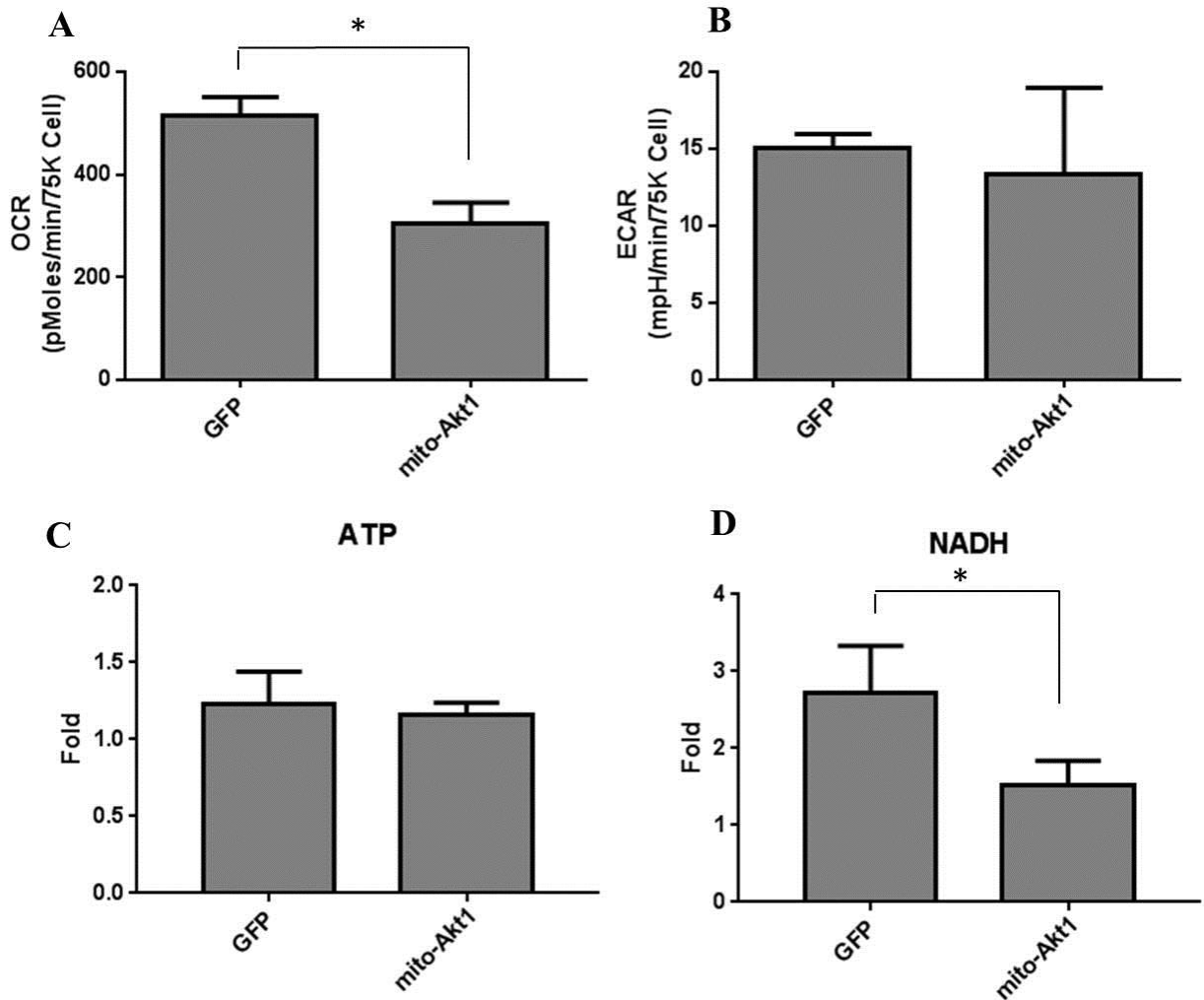


Figure 3.3. Mitochondrial Akt1 modulated cellular bioenergetics of MEF. (A) The effect of mitochondrial Akt1 activation on OCR in MEFs. The cells were transduced with Ad-mito-Akt1 (mito-Akt1) or Ad-GFP (control). 72 hours after transduction, cells were studied with a Seahorse XF24 analyzer. Bar graph represents the results summarized from 3 independent experiments in triplicates. \*  $p < 0.005$  (B) The effect of mitochondrial Akt1 activation on ECAR in MEF. The cells were transduced with Ad-mito-Akt1 (mito-Akt1) or Ad-GFP (control). 72 hours after transduction, cells were studied with a Seahorse XF24 analyzer. (C) Cellular ATP contents in

MEF. ATP level was quantified by mass spectrometry as described in Materials and Methods of this chapter. (D) Cellular NADH contents in MEF. NADH level was quantified by mass spectrometry as described in Materials and Methods. Bar graph represents the results summarized from 3 independent experiments in triplicates. \*  $p < 0.05$

Figure 3.4

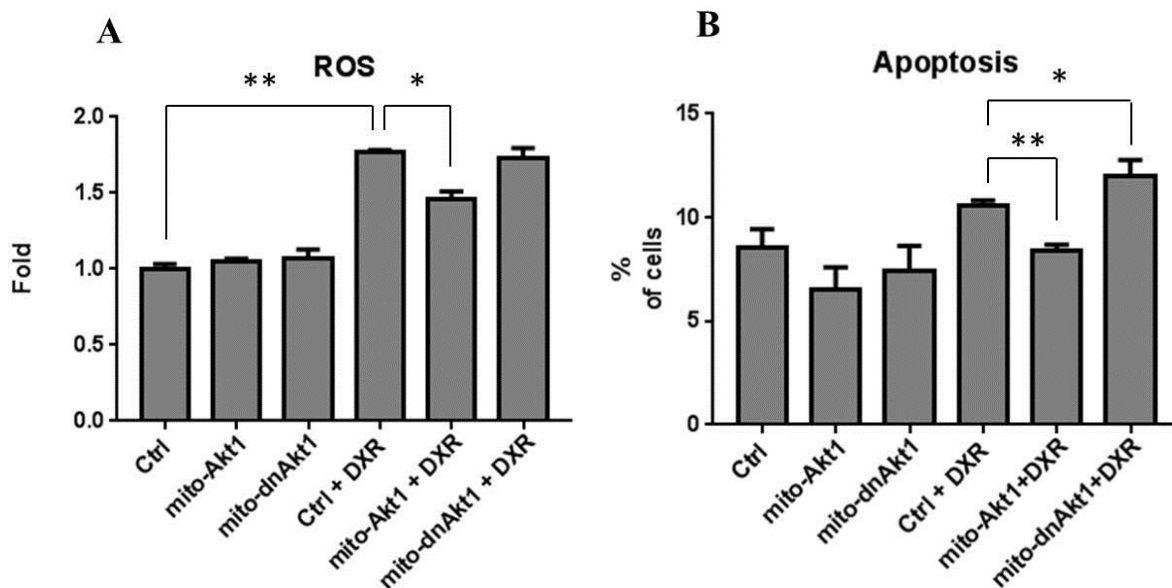


Figure 3.4. Activation of mitochondrial Akt1 signaling reduced ROS and apoptosis levels under stress conditions. (A) The effect of mito-Akt1 on oxidative stress in MEF. Mitochondrial ROS was analyzed with MitoSOX Red and quantified by flow cytometry. (B) The effect of mito-Akt1 on apoptosis in MEF. Apoptosis level was detected using Annexin V apoptosis kit and quantified by flow cytometry described in Materials and Methods. The analysis was presented as the percentages of apoptotic cells. Bar graph represents the results summarized from 3 independent experiments in triplicates. \*  $p < 0.005$ . DXR: Stress induction with  $2\mu\text{M}$  doxorubicin.

## CHAPTER 4

### Mechanism of Mitochondrial Akt1-PDH E3 subunit Interaction

#### Introduction

Pyruvate dehydrogenase is a mitochondrial multi-enzyme complex that consists of three catalytic enzymes : pyruvate dehydrogenase (E1), dihydrolipoyl transacetylase (E2), dihydrolipoamide dehydrogenase (E3) and a non-catalytic enzyme: E3 binding protein (E3bp). The three catalytic enzymes catalyze distinct reactions that all contribute to converting pyruvate into acetyl-CoA, a process called pyruvate decarboxylation. The acetyl-CoA can then fuel the TCA cycle and lead to the production of ATP via the electron transport chain. The enzyme complex is well-conserved from prokaryotes to eukaryotes albeit with slightly different composition of the enzyme complex and the structure. This suggests it is functionally significant across the entire spectrum of living organisms<sup>153</sup>.

Pyruvate dehydrogenase complex (PDC) is the gatekeeper enzyme of the TCA cycle linking glycolysis to oxidative phosphorylation. It is therefore deeply involved in the regulation of metabolic pathways associated with cellular bioenergetics. The significance of PDC has been demonstrated in various pyruvate dehydrogenase deficiencies<sup>154</sup>, which cause the buildup of lactic acid (lactic acidosis) in the body and result in a variety of neurological problems. Symptoms of the deficiency can appear shortly after birth, but varies between individuals. Since the sever outcomes of its deficiency, individuals with the condition usually do not survive through childhood.

As the linker of glycolysis and the TCA cycle, the activity of pyruvate dehydrogenase (PDH) is critical for diverting the metabolic flux from and to various metabolic pathways. PDH inactivation is crucial for glucose conservation if glucose is in limited supply, whereas proper PDH activity is required to allow both ATP and fatty acid production from glucose. The activity of pyruvate dehydrogenase is well-regulated by phosphorylation of the pyruvate dehydrogenase (E1 $\alpha$ )<sup>155,156</sup>. Pyruvate dehydrogenase kinase (PDK) phosphorylates E1 $\alpha$  at Ser293, Ser300 and Ser232<sup>157</sup>, leading to the inactivation of the enzyme. In contrast, pyruvate dehydrogenase phosphatase (PDP) dephosphorylates E1 $\alpha$ , resulting in the activation of the enzyme. Beside covalent modifications of PDH, allosteric effects mediated by the substrates and products of PDH have also been indicated in the regulation of the enzyme activity<sup>158–160</sup>. In addition, PDH activity can also be regulated through the expression of its regulators, e.g. PDK and PDP, under different stimuli<sup>161,162</sup>. Collectively, these studies suggest that PDH activity responds to various environmental cues and is fine-tuned via PDK and PDP.

In our previous studies, we demonstrated that Akt1 interacts with the PDC in mitochondria. In our follow up study using different antibodies specific to each subunit of the PDC, E1 $\alpha$ , E1 $\beta$ , E2, and E3, we also demonstrated that Akt1 preferentially bound to the E3 subunit. Moreover, we further demonstrated that the expression of a constitutively active, mitochondria-targeting Akt1 (mito-Akt1) increased basal PDH activity<sup>85</sup>. This results prompted us to hypothesize that Akt1 may bind to E3 and regulate PDH activity. Understanding of Akt1-E3 interaction may provide a mechanism of the regulation of PDH activity. However, the Akt1-E3 interaction has not yet been investigated, therefore, we first need to establish their interaction.



## **Materials and Methods**

### **Plasmid DNA**

Human DLD clone was purchased from OriGene (SC126940). Mouse AKT1 clone was purchased from Addgene.

### **Site-directed Mutagenesis**

To mimic the protein interaction of E3 in mitochondria, the mitochondria targeting sequence (MTS) was removed from E3. We designed primers that clones out the DLD cDNA fragment without MTS (Forward primer: 5'-GGGGGATCCATGGCAGATCAGCCGATTGATGCTGAT-GTAACAGTTATAGGTTCTG-3'; Reverse primer: 5'-GGGAAAGTTGATTGATTTGCCAA-ATGACGCAGCAAGATTTGCTTCTC-3'). This will generate a PCR product of 1.4kb ( $\Delta$ MTS-DLD). The PCR product was then inserted into pBluescriptII KS vector and subjected to site-directed mutagenesis. Arginine 228 (R228) and Lysine 385 (K385) of DLD (E3) were mutated to alanine. Site-directed mutagenesis was performed via QuikChange II XL Site-Directed Mutagenesis Kit (Stratagene) according to manufacturer's manual. Plasmid DNA were then isolated after mutations and sent to sequencing facility (GENEWIZ) for DNA sequencing. DNA sequences of mutated clones were compared with human DLD cDNA sequence using BLAST and the corresponding mutations were verified. For constitutively Akt1 construction, Thr308 and Ser473 of mouse AKT1 were mutated to glutamate (D) using QuikChange II XL Site-Directed Mutagenesis Kit (Stratagene) according to manufacturer's manual. Plasmid DNA after mutations were isolated and sent to sequencing facility (GENEWIZ) for DNA sequencing. DNA sequence of mutated clones was compared with mouse AKT1 cDNA sequence using BLAST and the corresponding mutations were verified.

## **Protein Expression and Purification**

### **Recombinant Constitutively Active AKT1**

We continually had difficulties in purifying constitutively active Akt1 in prokaryotic expression system. Therefore we shifted to the baculovirus expression system for constitutively active Akt1 expression and purification. Since we do not have the corresponding materials, the recombinant mouse Akt1 protein expression and purification were assisted from West Bioscience. We sent the mutated Akt1 construct to West Bioscience for the preparation of expression construct in eukaryotes expression system. After expression in Sf9 insect cell, the recombinant Akt1 was purified using Ni-NTA affinity column.

### **Recombinant Dihydrolipoamide Dehydrogenase (E3)**

The wild type and mutated E3 (R228A and K385A) cDNA was inserted to pBEn-SBP-SET1a expression vector (Stratagene) and transformed into *E. coli* BL21 competent cell. The ampicillin-resistant clones were selected and checked for correct insert. The correct clones were stored as glycerol stock in -80°C for long term storage. To express the proteins, single colony from the designated clones was picked and inoculated in 5 ml and grow in suspension culture for 16 hours at 37°C. The overnight culture were inoculated to 500 mL culture until OD<sub>600</sub> reaches 0.2-0.3 and incubate at 37°C until OD<sub>600</sub> reaches 0.6-0.8. The culture was then cooled to room temperature and protein expression was induced with 0.5mM IPTG at room temperature for 3 hours.

To purify both wild type and mutant E3 recombinant proteins, the induced culture was centrifuged at 3000 rpm for 30 min at 4°C to collect cell pellet. The cell pellet was resuspended

in streptavidin binding buffer (10 mM Tris HCl, pH 8.0, 150 mM NaCl) supplemented with protease inhibitor cocktails (SIGMAFAST<sup>TM</sup>), 20mM NaF, and 2mM Na<sub>3</sub>VO<sub>4</sub> and 1ug/ml lysozyme. The cell suspension was then subjected to freeze/thaw cycle to lyse cell. Genomic DNA was sheared by sonication, followed by centrifuging at 10,000g for 30min at 4°C. Cell lysate was obtained from the clear suspension, aliquoted and stored at -80°C. The clear cell lysate was first precipitated with ammonium sulfate at 40% at 4°C. The precipitated proteins were re-dissolved in original volume of streptavidin binding buffer supplemented with protease inhibitors as described above. Both the SBP tag-conjugated wild type and mutant E3s were purified with streptavidin agarose resin (Thermo Fisher) and eluted with biotin elution buffer (10 mM Tris HCl, pH 8.0 150 mM NaCl, 2 mM biotin). The eluted protein was subjected to SDS-PAGE and protein amount was estimated by comparing the intensity of Coomassie-Brilliant Blue-stained protein band to bovine serum albumin standards.

### **Neonatal Primary Cardiomyocyte Isolation**

Primary cultures of neonatal cardiomyocytes were prepared from Sprague-Dawley rats according to a protocol we previously described<sup>70</sup>. In brief, neonatal hearts were collected from decapitated new born rat and minced. The minced heart chunks were subjected to 10 cycles of dissociation with pancreatin buffer (0.0014g/ml pancreatin, 2% HEPES, 0.008g/ml sodium chloride, 0.002g/ml dextrose, 0.2mg/ml potassium chloride, 0.0575mg/ml Sodium phosphate monobasic monohydrate, 0.001g/ml sodium bicarbonate, 0.02mg/ml phenol red). The dissociated cells were collected after pelleting down at 900rpm for 6 minutes and subjected to differential plating to remove fibroblasts. The obtained neonatal cardiomyocytes were plated at a density of 6-8 x 10<sup>6</sup>

cells/100mm plate. The animal experimental procedures were approved by the Institutional Animal Care and Use Committee at University of California, Irvine. Cardiomyocytes were maintained with DMEM containing 10% FBS and 1% penicillin/streptomycin and incubated at 37°C, 5% CO<sub>2</sub>.

### **Experimental Animals**

The rats (Sprague Dawley) were fasting for 16 hours before acute insulin stimulation. For acute insulin stimulation, recombinant human insulin (50U/kg) was injected intraperitoneally without anesthesia. The rats were euthanized 30 minutes after insulin injection. Hearts were collected from the rats and subjected to mitochondrial preparation. The animal experimental protocol was approved by the Institutional Animal Care and Use Committee at University of California, Irvine.

### **Adenoviral Vectors Transduction and Antibodies**

To transduce adenoviral, cardiomyocytes were incubated with equal amounts of viral vectors in DMEM containing 10% FBS for 48–72 hours. An adenoviral vector expressed a mitochondria-targeting constitutively active Akt1 (Ad-mito-Akt1). Mitochondrial targeting was achieved by fusing a mitochondria-targeting sequence (MSVLTPLLLRGLTGSARRLPVPRAKIHSL) to the N terminus. The control adenovirus expresses green-fluorescent protein (GFP). Ad-mito-Akt1 achieved more than 95% transduction efficiency in the primary cardiomyocytes. Rabbit anti-pyruvate dehydrogenase subunits E3, and AKT1 (E45) were purchased from Genetex. Anti-rabbit HRP-conjugated secondary antibody was purchased from Santa Cruz (sc-2004).

## **Mitochondria Preparation**

Cells were harvested by scraper after ice-cold PBS washed 3 times and suspended in mitochondria isolation buffer (20 mM HEPES-KOH, pH 7.2, 10 mM KCl, 1.5 mM MgCl<sub>2</sub>, 1.0 mM sodium EDTA, 1.0 mM sodium EGTA, 1.0 mM dithiothreitol and 250 mM sucrose), supplemented with 3 µg/ml aprotinin, 3 µg/ml leupeptin, 2 mM phenylmethylsulfonyl fluoride, 20 mM NaF, 10 mM NaPP, and 2 mM Na<sub>3</sub>VO<sub>4</sub>. After incubating on ice for 30 min, the cells were homogenized with 20 strokes of loose pestle and 50 strokes of tight pestle. The nuclei and cell debris were removed by centrifugation at 1,000g for 15 min at 4°C. The supernatants were centrifuged at 10,000g for 15 min at 4°C, and the resulting mitochondrial fractions were re-suspended with mitochondria isolation buffer. The supernatants were further centrifuged at 100,000g for 1 hour at 4°C. The supernatants (S-100) and mitochondrial fractions were stored at -80°C.

## **BD Simulation of Akt1-E3 Interaction**

This part of analysis was assisted by our collaborators in Dr. Douglas Tobias group at Department of Chemistry at University of California, Irvine. In brief, Brownian dynamics simulations model of Akt1-E3 interaction was conducted using Simulation of Diffusional Association (SDA) program. The SDA program makes use of the BD algorithm to simulate diffusional association, calculating the potential energy from electrostatic and hydrophobic interactions in an implicit solvent. Molecular dynamics was run utilizing the CHARMM force field and the NAMD 2.9 simulation package. MD simulations were run in order to relax a

clustered complex model generated from highly-populated Brownian dynamics states. In silico mutations were produced using the CHARMM force field model.

### **Akt1-E3 *in vitro* Pulldown Assay**

Both the purified wild type and mutant E3s were attached on streptavidin agarose. The purified Akt1 was incubated with either wild type or mutant E3 in phosphate buffer saline (PBS) supplemented with 3mM NADH and protease inhibitor cocktails on a rotating device at room temperature for 2 hours. The unbound Akt1 was washed off with three times of PBS. The amount of bound Akt1 was determined with SDS-PAGE, followed by western blot using anti-AKT1 antibody (E45) (Genetex, GTX61035).

### **Identification of binding site on Akt1 using FBS**

This part of analysis was conducted via our collaborators in Dr. Nagarajan Vaidehi group at Department of Immunology at City of Hope. The Akt1 PH out crystal structures pdbID 3MVH and 4GV1 were selected for use with FBS. First the structures were prepared using MODELLER to add in missing regions of the kinase domain of each structure. The resulting structures were selected using DOPE score<sup>163</sup>. The 60,000 compounds subset of the National Cancer Institute (NCI) open database of compounds was screened against the entire surface of the modeled protein using Glide<sup>164-166</sup>. Both ligand and receptor van der Waal radii scaling was set at 0.5 and a single pose for each ligand was saved for evaluation using FBS<sup>167</sup>.

## Screening of Small Molecular Compounds

This part of analysis was conducted by our collaborators in Dr. Nagarajan Vaidehi group at Department of Immunology at City of Hope. Using the second ranked site identified by FBS as the center of the docking box, the library of 10,000 diverse fragments was screened at the FBS site shown in Figure 4.4. The docking was performed using the SP precision setting of Glide<sup>164-166</sup>. Docking the library of 10,000 diverse fragments resulted in 931,000 poses. These poses were then sorted by emodel score and the 1000 poses extracted from the results. Using these top 1000 poses, Phase was used to develop a 5 point pharmacophore with at least 10 members<sup>168-170</sup>. The screening resulted in 62 and 36 hypotheses for the crystal structures 3MVH and 4GV1 respectively. Top 3 pharmacophore hypotheses for each structure, 7435 compounds were identified and extracted from NCI open compound database (<https://cactus.nci.nih.gov/download/nci/>). The top 1000 compounds were used for secondary analysis. The bindings of 1000 compounds were then optimized via side chain composition, binding energy via Prime<sup>171-173</sup> and Macromodel<sup>174</sup>. The top 100 compounds were then further evaluated to maximize favorable residue ligand contacts and hydrogen bonding interactions. This revealed a list of 33 compounds as shown in Table 4.1.

## Small Molecular Compounds Reconstitution and Storage

Small molecular compounds were requested as powder from National Cancer Institute Developmental Therapeutics Program (NCI/DTP) Open Chemicals Repository. These small molecular compounds were reconstituted in DMSO at 10mM stock and stored at -80°C.

## **Pyruvate Dehydrogenase Enzyme Activity Assay**

Pyruvate Dehydrogenase (PDH) Enzyme Activity Microplate Assay Kit was purchased from abcam (ab109902). 72 hours after adenoviral vectors transduction, cells were incubated with hypotonic solution (250mM sucrose, 20mM HEPES pH7.4, 10mM KCl, 1.5mM MgCl<sub>2</sub>, 1mM EGTA, 1mM EDTA, 1mM DTT) and mitochondria fraction was isolated. The mitochondria were then solubilized with detergent according to the manufacturer's manual. Same amount of solubilized mitochondrial lysate was loaded into each well of the provided anti-PDC antibody-coated microplate. Substrates were added after 3-hour incubation at room temperature. The OD at 450 nm was measured using a Synergy HT multi-detection microplate reader. Enzyme activities were calculated and presented as  $\Delta OD_{450}/\text{min}$ . Triplicate measurements were done for each sample, and three biological replicates were repeated.

## **Western Blots**

Equal amounts of proteins from each sample were separated by SDS-PAGE and transferred to polyvinylidene difluoride membrane, and incubated with a blocking buffer (3% BSA in 20mM Tris-HCl [pH7.5], 137 mM NaCl, and 0.1% Tween 20) for 1 hour at room temperature. The membranes were incubated sequentially with primary antibodies overnight at 4°C, washed three times with TBS-T (20mM Tris - HCl [pH7.5], 137mM NaCl, and 0.1% Tween 20), incubated with respective horseradish peroxidase-conjugated secondary antibodies (1:5000 to 1:20,000 dilution in TBS-T), washed three times with TBS-T, and then incubated with West Pico Chemiluminescent Substrate to visualize the proteins (Thermo Scientific, Pittsburgh, PA)



## **Result**

### **Akt1-E3 Interaction Simulation Model**

To understand the interaction between Akt1 and E3, we first sought to establish an Akt1-E3 interaction model. Through our collaborator, Akt1-E3 interaction was simulated with Brownian dynamics (BD)<sup>175</sup>. The BD method simulates the rigid protein structures and does not account for the flexibility of protein-protein interaction structures. In contrast, fully-atomistic molecular dynamics (MD) simulates the dynamics of all atomic degrees of freedom and may provide structural flexibility. Our collaborators therefore, ran MD simulations to relax a clustered complex model generated from highly-populated BD states. The Akt1-E3 interaction is mediated via seven amino acid pairs forming salt-bridge interaction shown in Figure 4.1. Further computational mutation studies indicated that arginine 228 (R228) and lysine 385 (K385) of E3 and the corresponding amino acid residues of Akt1 are the most significant interaction mediators between the two proteins.

### **R228 and K385 Mutations to Alanine Do not Disrupt AKT1-E3 Interaction**

To demonstrate that the Akt1-E3 interaction is mediated through these amino acid residues, we sought to disrupt their interactions and determine whether the interaction was altered. To achieve this, we performed site-directed mutagenesis at R228 and K385 in E3, the two most significant amino acid residues identified in the computational model. To disrupt the salt-bridge interaction, the two amino acid residues were mutated to alanine to eliminate the original positive charges. The DNA sequences of E3 mutants were run through BLAST with human DLD cDNA sequences and the correct mutations were verified. Both the wild type and

mutant E3 constructs were then inserted into an expression construct and the recombinant proteins were expressed in an *E. coli* BL21 strain. The recombinant E3 proteins (both wild type and mutant) were purified and immobilized on agarose beads. To mimic the structure of phosphorylated Akt1, threonine 308 (T308D) and serine 473 (S473D) were mutated to aspartate. The expression of recombinant Akt1 (Akt1CA) were carried out in a baculovirus expression system and the protein was purified through His-tagged protein purification. The protein purification results are summarized in Figure 4.2.

We first examined their interactions by pulldown assay with the recombinant E3s attached to the agarose beads and the recombinant Akt1CA in suspension (Figure 4.3A). Consistent with previous studies<sup>85</sup>, the purified Akt1CA bound to purified recombinant wild type E3 (E3WT) (Figure 4.3B). However, to our surprise, the E3 mutations of R228A and K385A did not reduce the amount of bound Akt1 to E3 in the pulldown assay (Figure 4.3B). This result confirms that Akt1 may directly interact with E3, but suggests that additional amino acid residues may be required to mediate Akt1-E3 interactions.

### **Alternative Identification of binding site on Akt1 using FindBindSite**

We next sought to reveal the significance of other amino acid residues in the context of Akt1-E3 interaction. However, considering that the mutations of additional amino acid residues of E3 might effect on the formation of PDC, we adopted an alternative computational method to predict protein-protein interaction (PPI) sites on Akt1. FindBindSite (FBS) was previously developed to identify potential PPIs on given proteins by docking a small and diverse library of

small molecules to the entire protein structure. It had been shown to correctly predict the PPIs on 41 selected proteins with a hit rate of 71%<sup>167</sup>.

Using FBS, our collaborators revealed one high confidence consensus site allosteric to the ATP binding site by screening against both pleckstrin homology (PH) domain out structures of Akt1, represented by the yellow spheres of Figure 4.4. The identified site is located in an area of the protein exposed by the movement of the PH domain to the out orientation. Using this site as the center, they mapped the regions of lower ligand density to map the potential interaction interface between Akt1 and the E3 component of the PDC. The surface of the mapped interaction is shown in Figure 4.4 represented by the dark blue area. The predicted potential interaction interface between Akt1 and E3 with FBS also partially agrees with the earlier BD simulation model (Figure 4.5).

### **FindBindSite Revealed A list of Small Molecular Compounds That May Bind to the FBS-Predicted Allosteric Site**

Since we could not determine the interaction between Akt1 and E3 via the BD simulation model and since FBS predicted a new interaction interface between Akt1 and E3, we decided to focus on FBS for Akt1-E3 interaction. The PPIs predicted via FBS can also be used to determine how small molecular compounds might bind to our protein of interest<sup>167</sup>. Since the FBS-predicted binding site is in close proximity to the Akt1-E3 interaction interface, we hypothesize that the binding of small molecular compounds to the predicted allosteric site may potentially modulate the Akt1-E3 interaction. To reveal this idea, we first need to screen and identify the

potential small molecular compounds that may bind to the allosteric site predicted by FBS. Using the second ranked site identified by FBS (yellow sphere in Figure 4.4), our collaborators identified a list of 33 small molecular compounds that may bind to Akt1-E3 interface using additional computational analyses (Table 4.1, see materials and methods of this chapter for details).

### **Two Small Molecular Compounds Showed Potentially Inhibited Akt1-E3 Interaction in a Pulldown Assay**

33 potential small molecular compounds were identified from a pool of 60,000 in the National Cancer Institute Developmental Therapeutics Program (NCI/DTP) Open Chemicals Repository. From the 33, we obtained 19 from the NCI/DTP (Table 4.2). We next set up a pulldown assay to study the effects of these compounds on Akt1-E3 interaction. As discussed previously, agarose bead-attached wild type E3 with an SBP-tag pulled down Akt1CA. We then incubated these small molecular compounds with the two proteins and used western blotting to determine the amount of Akt1 remained bound to E3. Figure 4.6 shows the results western blot results. To summarize and quantitate the effects of each small molecular compound on Akt1-E3 interaction, we normalized the signal intensity of bound Akt1 from each group to that of a mock control treated with DMSO (Table 4.2). Red colors indicate the binding of Akt1 and E3 still exist, while blue colors suggest the binding was attenuated. In support of our hypothesis, some of the small molecular compounds disrupted the Akt1-E3 interaction and some of them, NSC 34766 for example, disrupted the interaction in a dose-dependent manner, suggesting high specificity. However, we also observed that some small molecular compounds show little to no effect on

Akt1-E3 interaction. Noticeably, not all small molecular compounds that showed reduced the amount of bound Akt1 disrupted the interaction in a dose dependent manner. From the 19 screened small molecular compounds, only compound NSC 34766 and NSC 628725 reduced Akt1-E3 interaction in a dose-dependent manner, suggesting that these two small molecular compounds may specifically disrupt the Akt1-E3 interaction in the current experimental set up.

### **Compound NSC 34766 and NSC 628725 Disrupted Akt1-E3 Interaction in Mitochondria**

We previously reported the translocation of Akt1 into mitochondria upon stimulation<sup>47</sup> and that Akt1 preferentially interacted with the E3 subunit of PDC in mitochondria<sup>85</sup>. With this knowledge, we next examined whether the two small molecular compounds identified in the current study could also disrupt the Akt1-E3 interaction in the mitochondria. Our co-immunoprecipitation study indicated that Akt1 interacted with E3 in mitochondria (Figure 4.7, DMSO), and that the incubation of these two small molecule compounds reduced the amount of bound Akt1 on E3 in a dose-dependent manners. This result advances our discovery of inhibitive small molecular compounds from *in vitro* biochemical assay to *in vivo* mitochondrial physiological environment. It also suggests that these small molecular compounds may modulate the effect of Akt1 on E3 in mitochondria physiologically.

## **The Expression of A Constitutively Active Mitochondria-Targeting Akt1 Increased PDH Activity**

The pyruvate dehydrogenase complex resides in the mitochondrial matrix and catalyzes pyruvate decarboxylation. The product, acetyl-CoA, then enters TCA cycle where it fuels the energy production. Therefore, the PDC activity is tightly associated with oxidative phosphorylation and cellular bioenergetics. We previously identified both the association of Akt1 with PDC<sup>85</sup> and that the expression of mitochondrial Akt1 reduced cellular oxygen consumption (Chapter 3). We next sought to determine the regulation of PDC activity via mitochondrial Akt1 signaling. To address this, we adopted a PDH-specific enzyme activity assay that pulls down PDC prior to the measurement of PDH activity. By doing so, cleaner and more reliable signals can be obtained. 72 hours after adenoviral vector transduction, mitochondria fraction was isolated from each group (No viral vector control, GFP and mito-Akt1). Equivalent quantities of mitochondrial lysate were used for the quantification of PDH activity. The result indicates that the adenoviral control (GFP) reduced PDH activity, and that the expression of constitutively active mitochondrial Akt1 (mito-Akt1) increased PDH activity (Figure 4.8) suggesting that mitochondrial Akt1 signaling may increase PDH activity.

## **Small Molecular Compound NSC 628725 Incubation Reduced PDH Activity**

Akt1 is phosphorylated and translocates into mitochondria after insulin stimulation and PI3K activation<sup>45,47</sup>. Current work demonstrates that Akt1 interacts with PDH in mitochondria and regulates its activity. The small molecular compounds screening revealed that two potential

compounds NSC 34766 and NSC 628725 might disrupt Akt1-E3 interaction (Table 4.2). To determine if Akt1-E3 interaction is required for the regulation of PDH activity via Akt1, we sought to apply these two small molecular compounds to the PDH activity quantification study.

The delivery of small molecular compounds to mitochondria requires specific structures and design on the structure features of the compounds itself, which may require more structural modifications and studies<sup>176-178</sup>. Our goal was to determine whether Akt1-E3 interaction is necessary for the modulation of PDH activity via Akt1. Based on the significance of both Akt1 and E3 in various cellular functions, knocking down their expression levels seemed inappropriate. Moreover, the need for a specific mitochondrial Akt1 as well as the lack of specific mitochondrial Akt1 modulators for the study further complicated matters. We therefore adopted an alternative method to skip the delivery process and took advantage of our small molecular compounds screening discovery to prove the concept. Directly solubilizing mitochondria under the condition that PDC remains intact, we incubated mitochondria lysate with designated small molecular compounds as in the previous co-immunoprecipitation study. These conditions resemble a similar environment to the mitochondrial matrix after the small molecular compounds are delivered there. From the observation that compound NSC 628725 disrupted the Akt1-E3 interaction more efficiently (Figure 4.7), we focused our PDH activity study on compound NSC 628725.

We first determined the effect of compound NSC 628725 on cultured cells. 72 hours after adenoviral transduction, mitochondria fractions were isolated from the cell lysate. The mitochondria lysate was incubated with compound NSC 628725 and later subjected to PDH activity quantification. The results show that PDH activity increases in mito-Akt1-transduced

cells compared to the control. Incubation with compound NSC 628725 reduced the effect of mito-Akt1 on PDH activity (Figure 4.9A), supporting our hypothesis that mitochondrial Akt1 signaling may regulate PDH activity, probably is through Akt1-E3 interaction.

To advance our finding to physiological conditions, we set up similar study in a rat model. Mitochondrial Akt1 translocation was induced via intraperitoneal injection of insulin, which had been reported earlier<sup>47</sup>. The mitochondria from the whole heart of either mock (PBS)- or insulin-injected rats were isolated and the mitochondria lysates were obtained as described above. The same amount of mitochondrial lysate was incubated with compound NSC 628725 and subjected to PDH activity quantification. Our results indicate that IP-injection of insulin increases PDH activity ~1.5 fold, which is consistent with several previous reports<sup>179</sup>. Incubation of low to high doses of compound NSC 628725 reduced the effect of insulin on PDH activity in a dose-dependent manner (Figure 4.9B), similar to our previous study on cultured cells (Figure 4.9A). To exclude the false positive effect of small molecular compound incubation, we select a compound (NSC 21697) that previously showed no effect on Akt1-E3 interaction (Table 4.2) as a control study. In contrast, compound NSC 21697 did not reduce the effect of insulin on PDH activity (Figure 4.9C), suggesting the inhibition on Akt1-E3 interaction via compound NSC 628725 was specific. Collectively, these results indicate that insulin increased PDH activity, probably through Akt1 as an effector. The disruption of Akt1-E3 interaction via compound NSC 628725 resulting in reduced PDH activity also suggests that the regulation of PDH activity via insulin-Akt1 signaling axis may be mediated through the E3 subunit of PDC.



## Discussion

Cells require sufficient energy to support their regular cellular activities. Mitochondria serve as the major cellular organelle that directs various nutrients and metabolites for the purpose of producing energy. The regulation of metabolic flow in mitochondria, is therefore, significantly associated with energy production efficiency. Inefficient energy production or impaired metabolic flow may be the cause of different diseases<sup>180</sup>. The pyruvate dehydrogenase complex links the metabolic flow from glycolysis to the TCA cycle, in order to produce NADH and succinate. NADH and succinate are respectively used as substrates by Complex I and Complex II to pump protons ( $H^+$ ) into the mitochondrial intermembrane space. The electron flow from complex I and II then proceeds to Complex III, then Complex IV and finally to oxygen molecules leading to the production of reactive oxygen species. The process establishes a proton ( $H^+$ ) gradient across inner membrane space driving Complex V to generate ATP.

In this process, PDH activity is well regulated by pyruvate dehydrogenase kinase and pyruvate dehydrogenase phosphatase. The phosphorylation of PDH by PDK reduces its activity, while the dephosphorylation of PDH by PDP increases its activity. The loss of function of either PDK or PDP may cause PDH deficiency and results in metabolic disorders<sup>181,182</sup>. Previous studies showed that insulin may regulate PDH activity through the translocation of protein kinase C (PKC) into mitochondria of liver and skeletal muscle cells<sup>183,184</sup>. They further showed molecular resolution that PKC phosphorylated PDP and led to the activation of PDP and an increase in PDH activity. Our work demonstrated a similar phenomenon in which, protein kinase B/Akt translocated into mitochondria under insulin activation regulating PDH activity through the E3 subunit of PDH. The current study provides an alternative method by which insulin

signaling directs metabolic flow by regulating PDH activity. However, whether different downstream effectors of insulin signaling on the regulation of PDH activity in different cell types exist requires more investigation. On the other hand, our work showed the effects of Akt1 and E3 interactions on PDH activity, but did not look into other isoforms of Akt. Akt1 and Akt2 are the major isoforms in skeletal muscle and cardiac muscle. Knockout mouse studies showed that Akt1<sup>-/-</sup> mice exhibited intra-uterine growth retardation and Akt2<sup>-/-</sup> mice were hyperglycemic and insulin resistant<sup>185-187</sup>. Our previous work indicated that Akt1 is the major isoform that mediates insulin signaling to mitochondria, but Akt2 helped to compensate when Akt1 was missing<sup>69</sup>. While Akt1 and Akt2 were assigned distinctive physiological roles, they might serve as compensate for each other in isoform-specific knockout mice. Interestingly, the roles of Akt isoforms in somatic cell reprogramming have been reported recently<sup>188</sup>. The ectopic expression of three isoforms all lead to enhanced iPSC reprogramming. However, the use of myristoylated Akt isoforms may generate different effects from mitochondrial Akt. The roles of different Akt isoforms in mitochondria in the context of cell fate regulation, therefore, require more sophisticated studies.

We previously identified several potential Akt1 associated proteins in mitochondria and also revealed that Akt1 preferentially binds to the E3 subunit of PDC. Current work extends our finding by providing two different computational methods that revealed the interactions between Akt1 and E3. A Brownian dynamics model simulated Akt1-E3 interaction by rigid protein structures with some aid in protein structural flexibility via molecular dynamics simulation. The provided model revealed 7 interaction pairs between Akt1 and E3. In an effort to disrupt the two most important ones, we failed to see any effect on their interaction. This suggests that either additional interaction pairs are required or the provided interaction prediction was inappropriate.

The FindBindSite<sup>167</sup> method predicted an alternative interaction interface between Akt1 and E3. Although it showed partial agreement with the BD model, they represented two distinct interaction models. Considering the effects of amino acid residue mutations on protein structure complex, we chose to focus on the FBS method. Using FBS, our collaborators identified 33 compounds from a library of 60,000 compounds. Combined with more efficient bench study, FBS may be a useful tool for new small molecular compounds identification and represents a quick platform for drug development.

By using compound NSC 628725 identified from FBS, we observed the disruption of Akt1-E3 interactions and the effect of insulin on PDH activity. The results suggest that the effect of the insulin-mitochondrial Akt1 signaling axis on PDH activity is probably through the E3 subunit of PDC. Interestingly, the E3 subunit contains no Akt consensus phosphorylation site sequence<sup>189</sup>. However, the authentic phosphorylation sites of the substrates do not always conform to the consensus sequence<sup>190-192</sup>. Future study will need to focus on the regulatory mechanisms of PDH activity via Akt1. Is Akt1 activation (phosphorylation at T308 and S473) required for the Akt1-E3 interaction and the regulation of PDH activity? Using a wild type or dominant negative Akt1 in both the pulldown interaction assay and PDH assay should help to address these questions. Moreover, the current literature states that PDH activity is regulated via its phosphorylation status<sup>155-157</sup>. Therefore, further studies need to be done to reveal the effect of Akt1-E3 interactions on the phosphorylation status of PDH. On the other hand, the complex formation of PDC involves multiple enzyme subunits. The effects of Akt1-E3 interaction in the regulation of PDC complex formation is poorly understood and requires more investigation. However, the lack of proper tools for studying mitochondrial Akt1 signaling may hinder progress toward this goal. With the identification of potential inhibitors for Akt1-E3 interactions, the

current work presents a useful research tool for studying mitochondrial Akt1 signaling. With the development of proper tools for studying mitochondrial Akt1 signaling, we may then apply these small molecular compounds to the iPSC reprogramming study to reveal the role of Akt1-E3 interaction in iPSC reprogramming.

In summary, our work provides a molecular level resolution of Akt1 signaling in mitochondria that may regulate mitochondrial metabolism through the pyruvate dehydrogenase complex. The increased PDH activity should fuel the TCA cycle and hence result in increased ATP production and oxygen consumption. However, to our surprise, we demonstrated that the cellular ATP level was not altered and the cellular oxygen consumption reduced upon activation of mitochondrial Akt1 signaling. This suggests that additional regulation points or mechanisms exist along the way to the last step of oxidative phosphorylation. The indirect regulations of enzyme activities in the TCA cycle and ETC via metabolite levels have recently been reported. Future metabolomics study may provide mechanistic cues regarding the regulation of cellular metabolism through mitochondrial Akt1 signaling.

## Figures

Figure 4.1

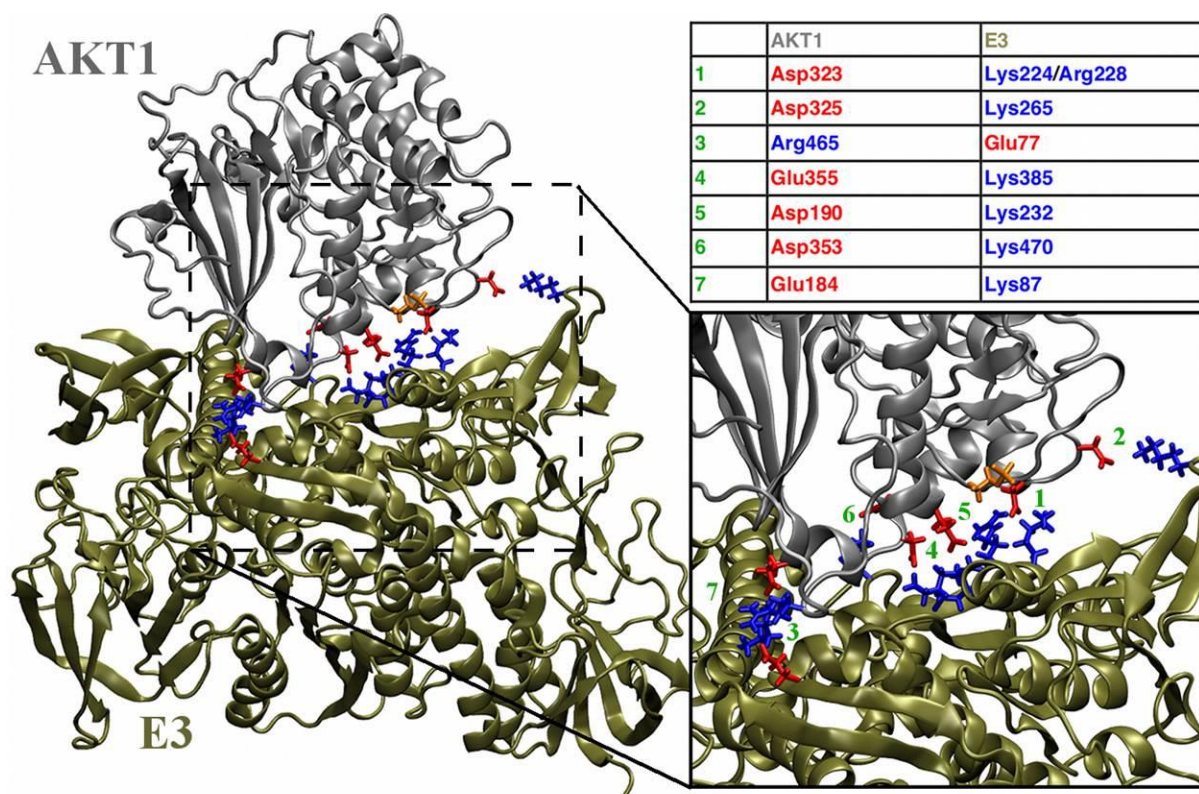


Figure 4.1. The simulation model of interaction of Akt1–E3 by Brownian dynamics. The interaction interface possesses significant electrostatic interactions. Interactions 6 and 7 were formed during the 10 ns MD simulation. Interactions 1 through 5 are conserved from BD clustering. Positively charged amino acid side chains are shown in blue, negative in red, and the T308 phosphate in orange. E3 is shown in gold, Akt1 in silver.

Figure 4.2

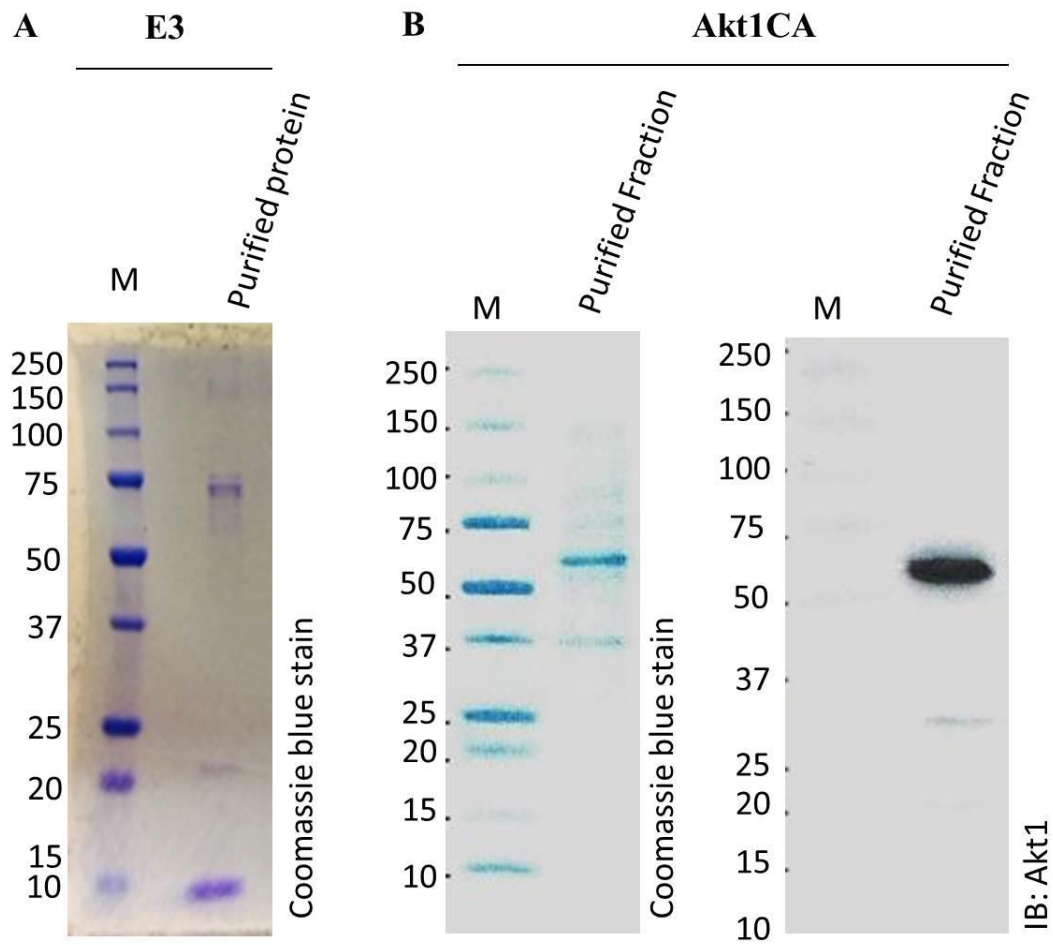


Figure 4.2. The results of recombinant protein purifications. (A) Recombinant human E3 was expressed in *E. coli* BL21 strain and purified with streptavidin agarose. Coomassie blue staining was used to visualize the purified protein. (B) Recombinant mouse constitutively active Akt1 was expressed in baculovirus expression system and purified with Ni-NTA affinity purification. Coomassie blue staining was used to visualize the purified protein. Western blot using anti-Akt1 antibody was used for verification.

Figure 4.3

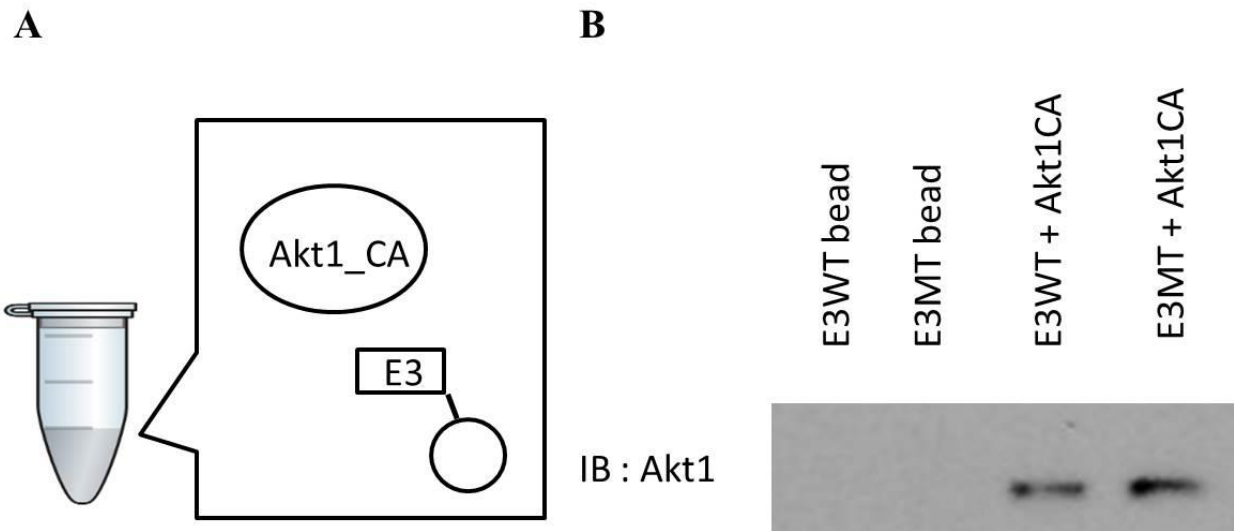


Figure 4.3. Both recombinant wild type and mutant E3s bind to recombinant constitutively active Akt1 in a pulldown assay. (A) The scheme illustrates the in vitro pulldown assay. (B) After 2 hours incubation at room temperature, the bound proteins on E3 beads were subjected to western blotting with Akt1 antibody.

Figure 4.4

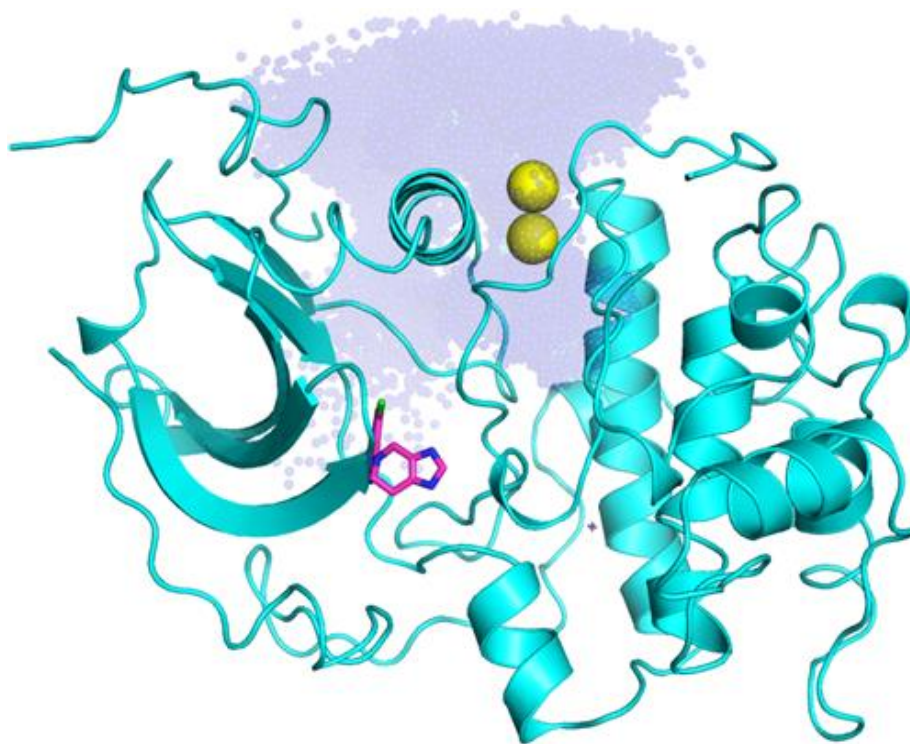


Figure 4.4. Binding region mapped by FBS. The pink ligand is an ATP derived inhibitor found in the crystal structure. The top scoring site identified by FBS is marked with the yellow spheres and represents a druggable pocket identified using FBS. The transparent blue colored region is the interface area mapped by FBS and is demarks the boundaries at which the docking box was set.



Figure 4.5

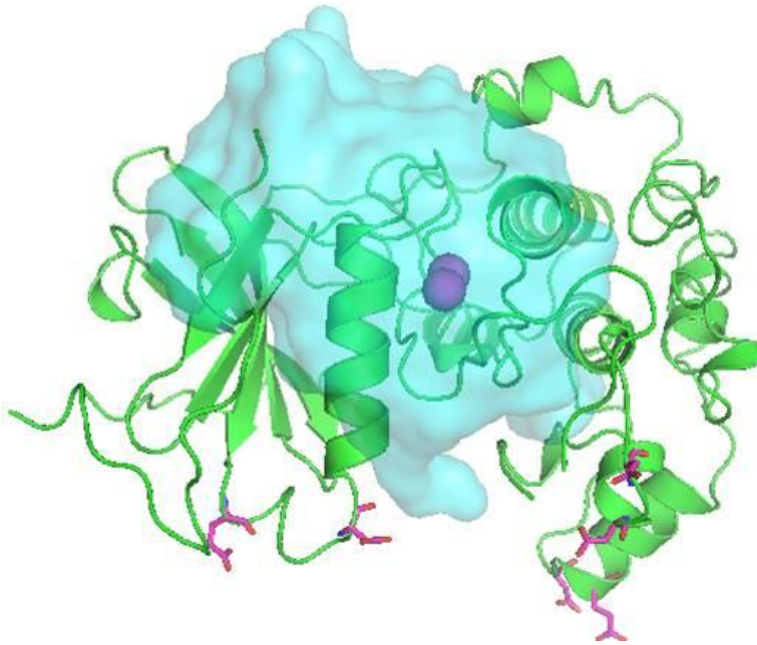


Figure 4.5. FindBindSite predicted interaction model shows partial agreement with Brownian Dynamics simulated model. The surface shown in Cyan corresponds to the prediction from FBS, while amino acid residue showing in pink representing those identified from BD model.

Figure 4.6

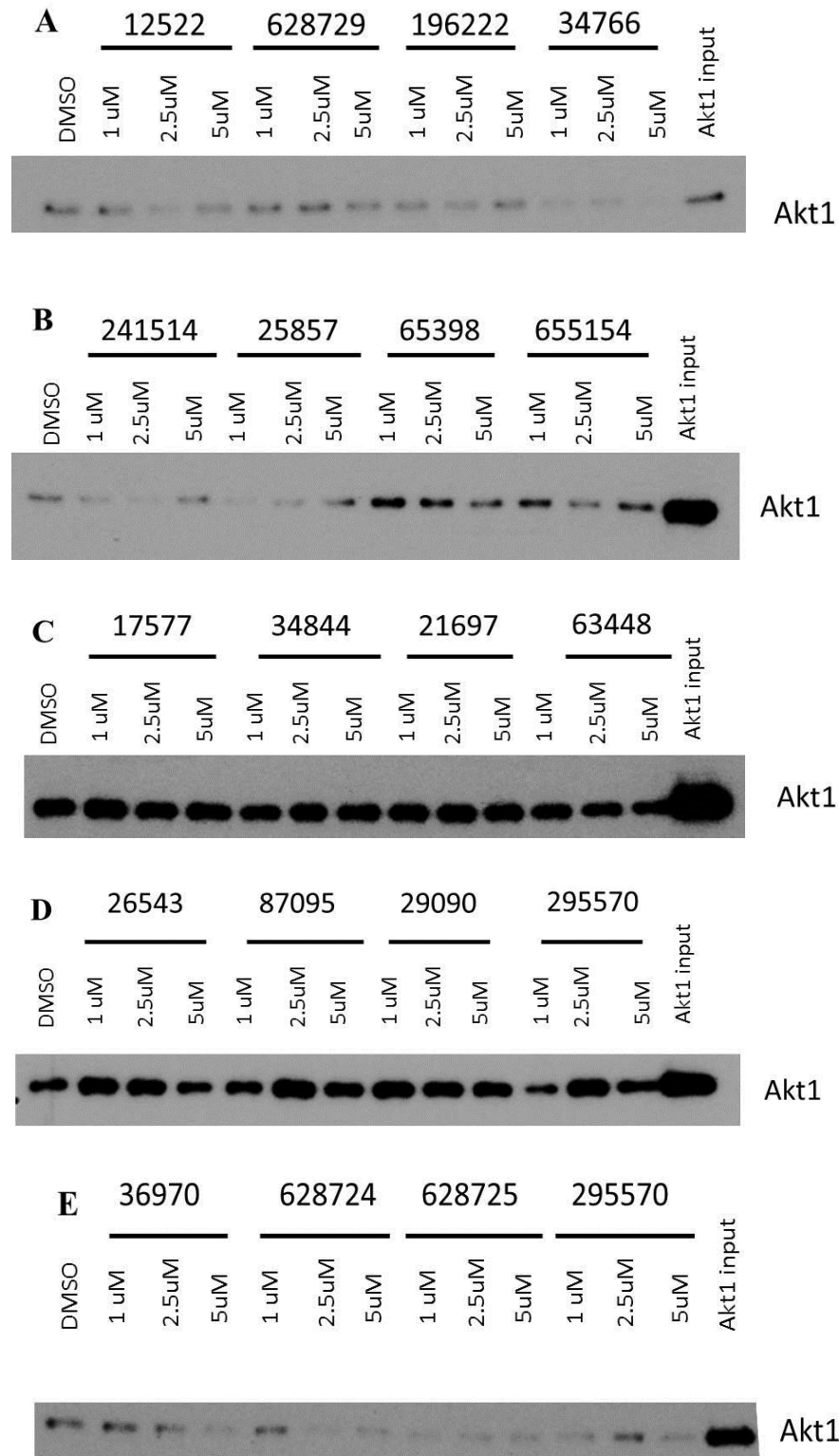


Figure 4.6. *In vitro* pulldown assay reveals some small molecule compounds disrupted Akt1-E3 interaction. (A-E) 19 small molecule compounds were reconstituted in DMSO and diluted to the designated concentrations in each Akt1-E3 pulldown assay. The amount of Akt1 remained bound to E3 was detected using anti-Akt1 (E45) antibody (Genetex). The signal intensities of bound Akt1 were normalized to that of DMSO control and summarized in Table 4.3.

Figure 4.7

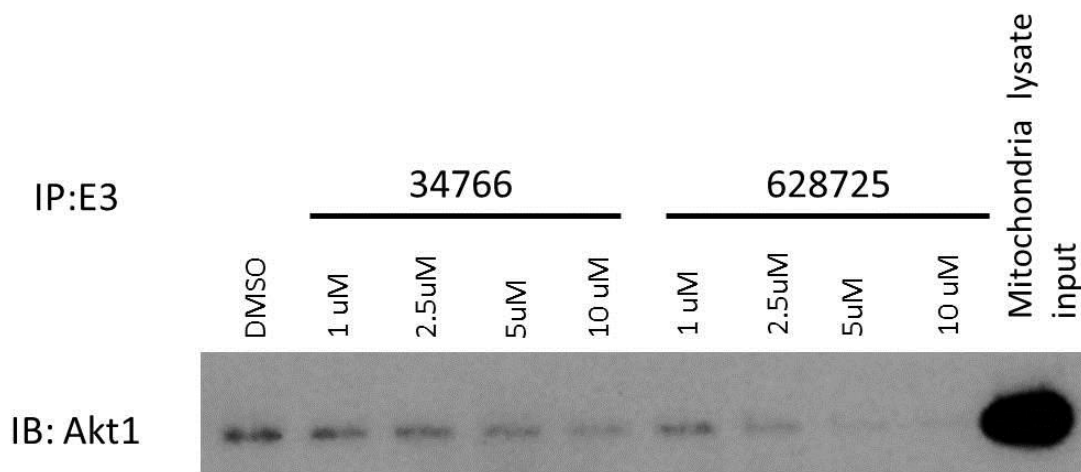


Figure 4.7. Compound NSC 34766 and NSC 628725 reduced the amount of bound Akt1 on E3. Mitochondria were isolated from rat whole heart and subjected to solubilization with detergent. Same amount of mitochondrial lysate were incubate with either NSC 34766 or NSC 628725 at designated concentration at room temperature for 2 hours. After 2 hours incubation, same amount of E3 antibody (Genetex) was added into each group and incubate overnight. The immunocomplex was pulled down with protein A agarose bead (Sigma Aldrich) and subjected to western blot.

Figure 4.8

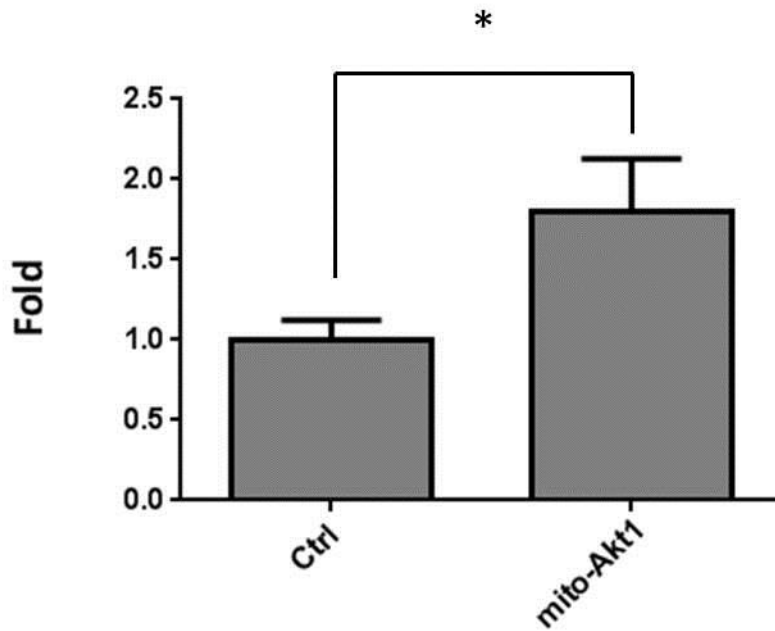
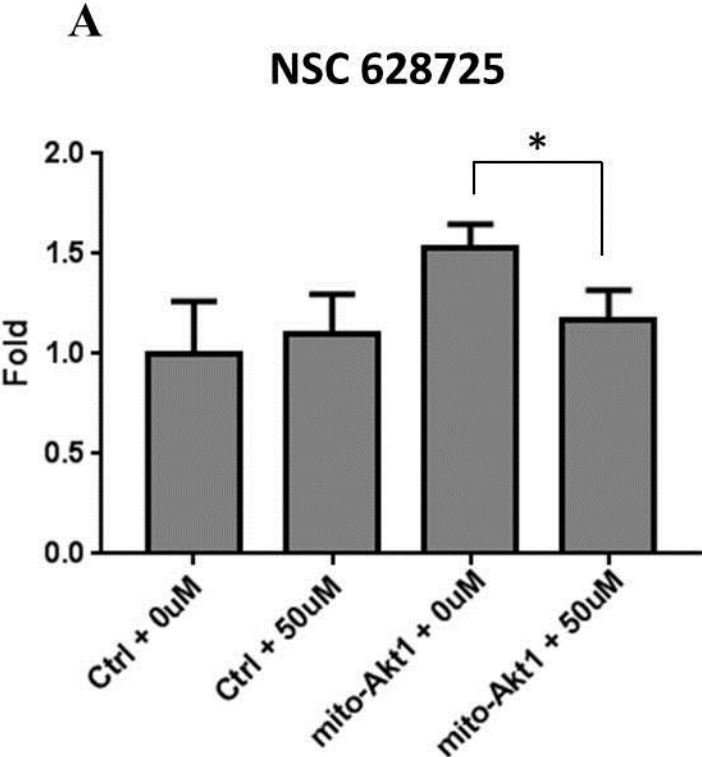
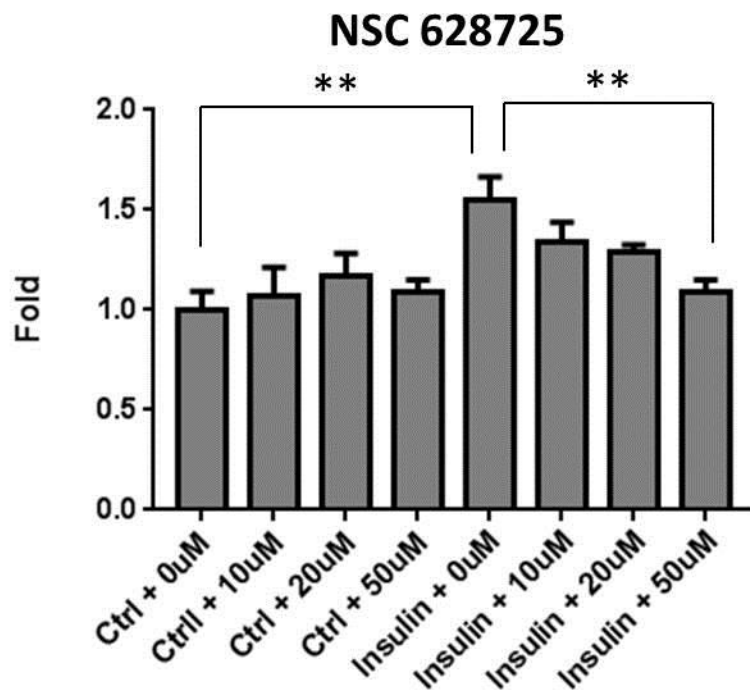


Figure 4.8. The expression of a constitutively active mitochondria-targeting Akt1 increased PDH activity. Cardiomyocytes were transduced with designate adenoviral vectors (Ctrl: Ad-GFP or Ad-mito-Akt1) or no vector control (WT). 72 hours after transduction, mitochondria were isolated and subjected to PDH assay. \*  $p < 0.05$ .

Figure 4.9



**B**



**C**

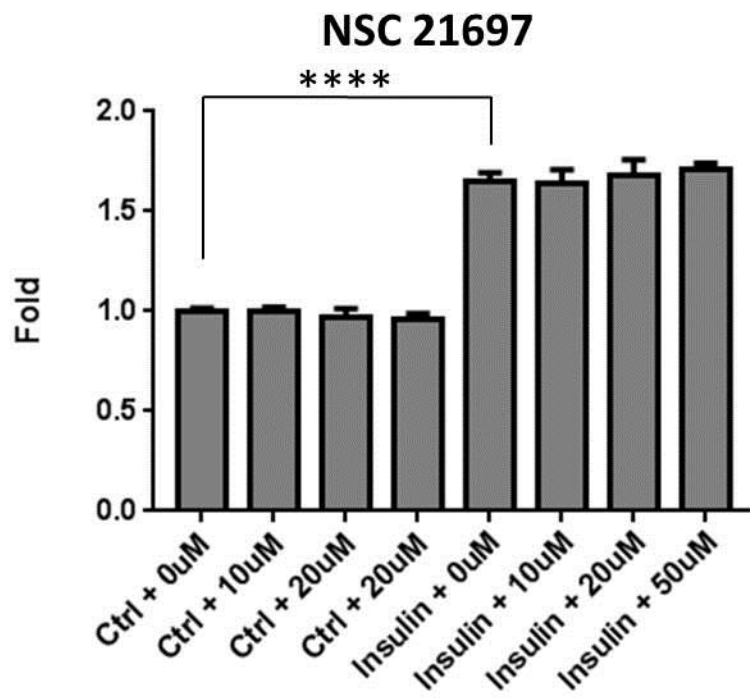


Figure 4.9. Compound NSC 628725 Incubation Reduced PDH Activity. (A) 72 hours after adenoviral vectors transductions, mitochondria were isolated and subjected to the incubation of NSC 628725 at designated concentration. PDH assay was measured as described in materials and methods. Ctrl: Ad-GFP viral vector; mito-Akt1: Ad-mito-Akt1. Mitochondria were isolated from the hearts of either PBS-(Ctrl) or insulin-injected rats and subjected to the incubation of (B) NSC 628725 or (C) NSC 21697. PDH assay was measured as described in materials and methods. Bar graph represents the results summarized from 3 independent experiments in triplicates. \* $p < 0.05$ , \*\* $p < 0.005$ , \*\*\*\* $P < 0.0001$ .

Table 4.1

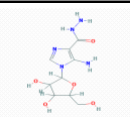
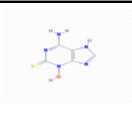
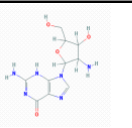
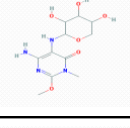
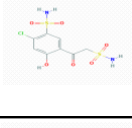
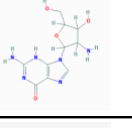
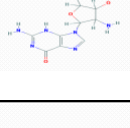
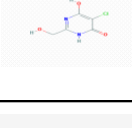
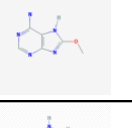
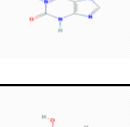
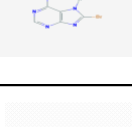
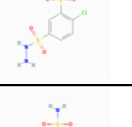
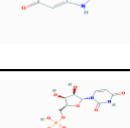
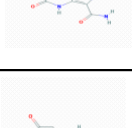
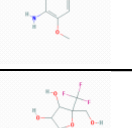
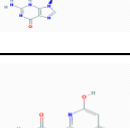
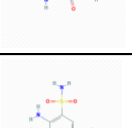
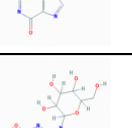
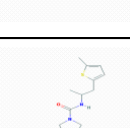
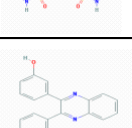
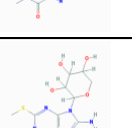
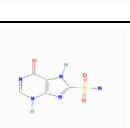
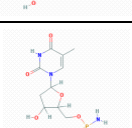
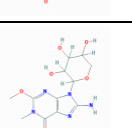
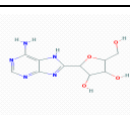
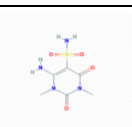
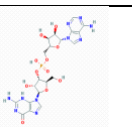
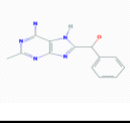
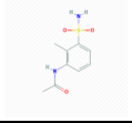
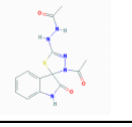


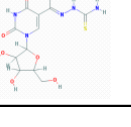

2D structure	NSC#				
	<b>NSC34844</b>		<b>NSC526486</b>		<b>NSC241514</b>
	<b>NSC655154</b>		<b>NSC156244</b>		<b>NSC26543</b>
	<b>NSC241514</b>		<b>NSC31714</b>		<b>NSC25642</b>
	<b>NSC527452</b>		<b>NSC21697</b>		<b>NSC12522</b>
	<b>NSC34766</b>		<b>NSC624641</b>		<b>NSC36970</b>
	<b>PubChem CID: 14629610</b>		<b>NSC680466</b>		<b>NSC690199</b>
	<b>NSC17577</b>		<b>NSC25857</b>		<b>NSC628724</b>
	<b>PubChem CID: 71866410</b>		<b>PubChem CID: 54581247</b>		<b>NSC628729</b>
	<b>NSC63448</b>		<b>NSC295570</b>		<b>NSC628725</b>
	<b>NSC196222</b>		<b>NSC65398</b>		<b>PubChem CID: 93033</b>
	<b>NSC87095</b>		<b>NSC29090</b>		<b>NSC666387</b>
					<b>NSC627859</b>



Table 4.1. List of small molecular compounds obtained via FBS and pharmacophore studies.

Table 4.2

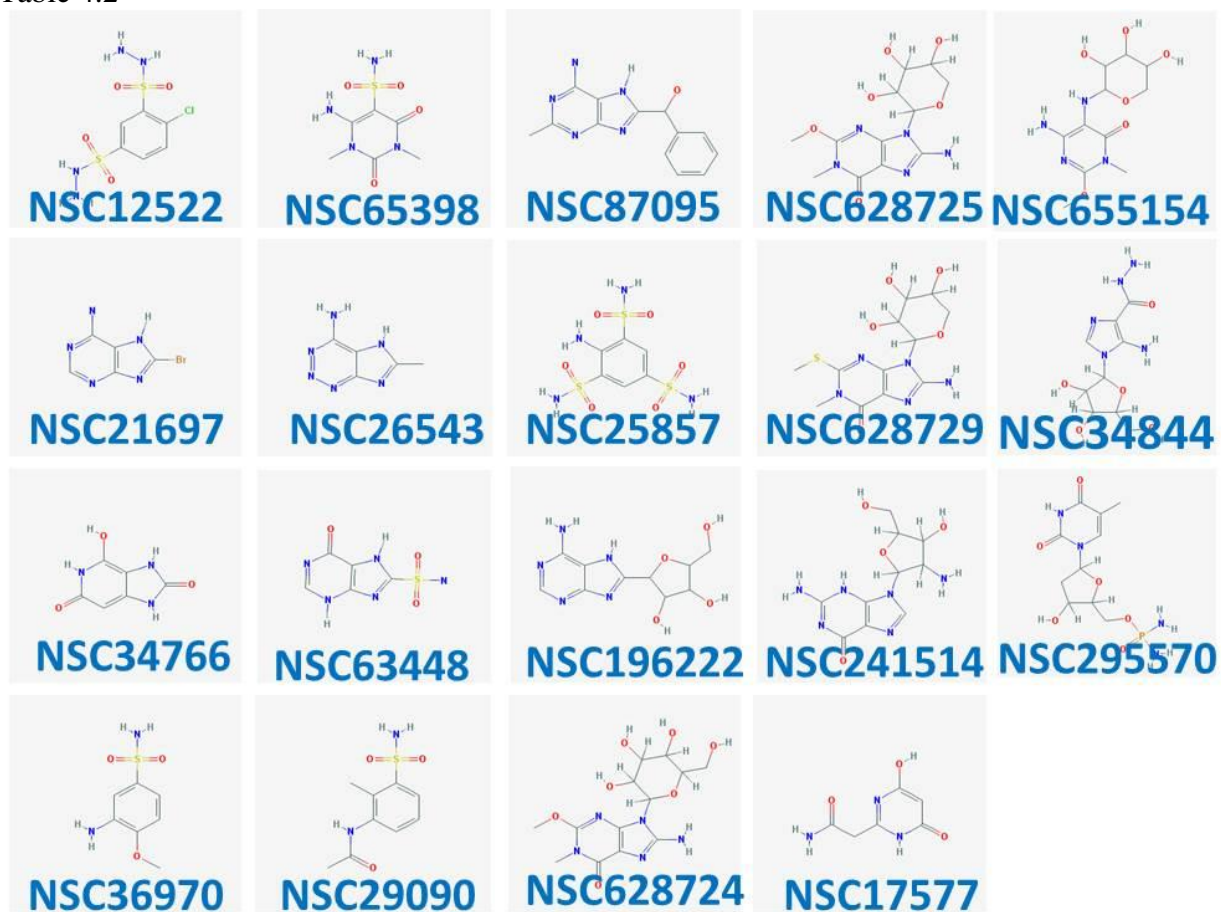


Table 4.2. List of 19 compounds obtained from NCI/DTP for Akt1-E3 pulldown assay.

Table 4.3

Compound	1uM	2.5uM	5uM
12522	0.762335	0.237815	0.473332
17577	1.169341	0.971619	1.088019
34766	0.195935	0.232823	0.119232
34844	0.838566	0.972119	1.001061
21697	0.987984	1.001941	0.933939
26543	1.785891	1.68672	0.921151
29090	1.876798	1.73619	1.539124
63448	0.835094	0.660035	0.372674
65398	2.664136	2.010051	1.363523
25857	0.25777	0.340049	1.009806
36970	1.051037	0.690901	0.233489
87095	1.082564	2.267052	1.40809
196222	0.641321	0.519828	0.781739
241514	0.369234	0.073702	0.746148
295570	0.465372	0.777732	0.301727
628724	0.763288	0.183137	0.324132
628725	0.201853	0.337032	0.362725
628729	0.823309	1.043358	0.703619
655154	1.824032	0.93388	1.551032

Table 4.3. The effects of small molecular compounds on Akt1-E3 interaction. The effects of each small molecular compound on Akt1-E3 interaction was determined by western blot described in Figure 4.6. The signal intensity from western blot was normalized to that of control (DMSO) and then summarized and color-coded in this table. Red colors indicate strong binding, while blue colors indicated reduced binding.

## CONCLUSION

Stem cell's merits rest on their potential to differentiate into cell lineages from all three germ layers. Recent advances in stem cell research have also urged its application in human trials; the quality and safety of stem cells therefore, become important considerations for their further applications. While the mechanistic details behind the regulation of stem cell pluripotency and differentiation remain unclear, the discovery of iPSCs has inspired researchers to study these mechanisms and thus understand both how iPSC reprogramming works and how it can be applied in the future.

The studies in this dissertation highlight the significance of PI3K/Akt signaling to the regulation of somatic cell reprogramming. Particularly, we demonstrated the importance of mitochondria in somatic cell reprogramming by modulating mitochondrial performance through mitochondrial Akt1 signaling, which resulted in enhanced reprogramming efficiency. We postulated that Akt1 interacts with unknown targets resulting in the repression of TCA cycle, and lower cellular NADH levels. This leads to less substrate being directed to complex I of the electron transport chain, reducing generation of reactive oxygen species. The lower ROS levels may improve ATP production efficiency via Complex V. Therefore, it maintains ATP levels, supporting energy expenditures and reducing oxidative stress that may be caused during iPSC reprogramming.

The second part of this dissertation investigated the interaction between Akt1 and the E3 subunit of the TCA cycle's gatekeeper enzyme, PDH. The activation of mitochondrial Akt1 signaling increased PDH activity, similarly to acute insulin stimulation. Using FBS, our collaborators identified a novel site for protein-protein interaction and selected out small

molecular compounds that fit this binding pocket. In vitro pulldown studies identified compounds NSC 34766 and NSC 628725 as potential inhibitors for Akt1-E3 interactions. The application of compound NSC 628725 further disrupted the effects of mitochondrial Akt1 and insulin on PDH activity. Therefore, we have identified a new regulatory mechanism of PDC activity through Akt1 signaling in mitochondria. This mechanism is different from the pathway mediated through PDK. However, metabolic pathways in mitochondria are complex and interconnected. By quantification of only individual metabolites level, e.g. ATP, NADH, may not conclude the mechanistic details of Akt1 signaling in mitochondria on cellular metabolism. Therefore, a thorough metabolomics study should be conducted to summarize the net effect of mitochondrial Akt1 signaling on cellular metabolism. This may help to conclude the mechanism of mitochondrial Akt1 on the TCA cycle and mitochondrial metabolism.

E3 is actually a subunit of multiple mitochondrial enzyme complexes, such as pyruvate dehydrogenase complex,  $\alpha$ -ketoglutarate dehydrogenase complex, and branched-chain amino acid-dehydrogenase complex, and is also involved in the glycine cleavage system. Here we showed that Akt1 increased PDH activity through E3 binding, but we did not determine the effects of Akt1 on other enzymes' activities. In addition, E3 has been reported to have cryptic protease activity and is physiologically participates in processing mitochondrial iron chaperone frataxin<sup>193</sup>. From our experience of purifying constitutively active Akt1 in prokaryotes, we continually observed that Akt1 was processed into smaller fragments, but remained detectable in the fractions containing prokaryotic E3. Whether E3 could process Akt1 under certain conditions and what the consequences of that processing would be not known. Therefore, deeper studies are needed to conclude the role of Akt1-E3 interactions in the regulation of PDH activity.

Overall, it is a very interesting project. Mechanisms for modulating mitochondria performance via mitochondrial Akt1 signaling may be present in many physiological conditions and diseases. The involvement of multiple enzyme complexes and the cryptic function of E3 may further complicate interpretations of Akt1-E3 interactions in various systems chosen to be investigated. This complex biological process allows us to strive, strengthen our skills and minds and expand our patience.

## REFERENCE

1. Pierce, G. B. Teratocarcinoma: model for a developmental concept of cancer. *Curr. Top. Dev. Biol.* **2**, 223–246 (1967).
2. Stevens, L. C. The biology of teratomas. *Adv. Morphog.* **6**, 1–31 (1967).
3. Kleinsmith, L. J. & Pierce, G. B. MULTIPOTENTIALITY OF SINGLE EMBRYONAL CARCINOMA CELLS. *Cancer Res.* **24**, 1544–1551 (1964).
4. Kahan, B. W. & Ephrussi, B. Developmental Potentialities of Clonal In Vitro Cultures of Mouse Testicular Teratoma. *J. Natl. Cancer Inst.* **44**, 1015–1036 (1970).
5. Martin, G. R. & Evans, M. J. The morphology and growth of a pluripotent teratocarcinoma cell line and its derivatives in tissue culture. *Cell* **2**, 163–172 (1974).
6. Martin, G. R. & Evans, M. J. Differentiation of clonal lines of teratocarcinoma cells: formation of embryoid bodies in vitro. *Proc. Natl. Acad. Sci. U. S. A.* **72**, 1441–1445 (1975).
7. Papaioannou, V. E., Mcburney, M. W., Gardner, R. L. & Evans, M. J. Fate of teratocarcinoma cells injected into early mouse embryos. *Nature* **258**, 70–73 (1975).
8. Rosenthal, M. D., Wishnow, R. M. & Sato, G. H. In Vitro Growth and Differentiation of Clonal Populations of Multipotential Mouse Cells Derived From a Transplantable Testicular Teratocarcinoma. *J. Natl. Cancer Inst.* **44**, 1001–1014 (1970).
9. Rossant, J. Investigation of the determinative state of the mouse inner cell mass. II. The fate of isolated inner cell masses transferred to the oviduct. *J. Embryol. Exp. Morphol.* **33**, 991–1001 (1975).
10. Evans, M. J. & Kaufman, M. H. Establishment in culture of pluripotential cells from mouse embryos. *Nature* **292**, 154–156 (1981).
11. Drummond-Barbosa, D. & Spradling, A. C. Stem cells and their progeny respond to nutritional changes during *Drosophila* oogenesis. *Dev. Biol.* **231**, 265–278 (2001).
12. LaFever, L. & Drummond-Barbosa, D. Direct control of germline stem cell division and cyst growth by neural insulin in *Drosophila*. *Science* **309**, 1071–1073 (2005).
13. Hsu, H.-J. & Drummond-Barbosa, D. Insulin levels control female germline stem cell maintenance via the niche in *Drosophila*. *Proc. Natl. Acad. Sci. U. S. A.* **106**, 1117–1121 (2009).
14. Williams, R. L. *et al.* Myeloid leukaemia inhibitory factor maintains the developmental potential of embryonic stem cells. *Nature* **336**, 684–687 (1988).
15. Smith, A. G. *et al.* Inhibition of pluripotential embryonic stem cell differentiation by purified polypeptides. *Nature* **336**, 688–690 (1988).
16. Kidder, B. L., Yang, J. & Palmer, S. Stat3 and c-Myc Genome-Wide Promoter Occupancy in Embryonic Stem Cells. *PLOS ONE* **3**, e3932 (2008).
17. Boeuf, H., Hauss, C., Graeve, F. D., Baran, N. & Kedinger, C. Leukemia Inhibitory Factor–dependent Transcriptional Activation in Embryonic Stem Cells. *J. Cell Biol.* **138**, 1207–1217 (1997).
18. Niwa, H., Burdon, T., Chambers, I. & Smith, A. Self-renewal of pluripotent embryonic stem cells is mediated via activation of STAT3. *Genes Dev.* **12**, 2048–2060 (1998).
19. Bouchard, C., Staller, P. & Eilers, M. Control of cell proliferation by Myc. *Trends Cell Biol.* **8**, 202–206 (1998).
20. Cartwright, P. *et al.* LIF/STAT3 controls ES cell self-renewal and pluripotency by a Myc-dependent mechanism. *Development* **132**, 885–896 (2005).
21. Wnt signalling in stem cells and cancer : Article : Nature. Available at: <http://www.nature.com/nature/journal/v434/n7035/full/nature03319.html>. (Accessed: 8th May 2016)

22. Sato, N., Meijer, L., Skaltsounis, L., Greengard, P. & Brivanlou, A. H. Maintenance of pluripotency in human and mouse embryonic stem cells through activation of Wnt signaling by a pharmacological GSK-3-specific inhibitor. *Nat. Med.* **10**, 55–63 (2004).
23. Reya, T. *et al.* A role for Wnt signalling in self-renewal of haematopoietic stem cells. *Nature* **423**, 409–414 (2003).
24. Levenstein, M. E. *et al.* Basic fibroblast growth factor support of human embryonic stem cell self-renewal. *Stem Cells Dayt. Ohio* **24**, 568–574 (2006).
25. Koivisto, H. *et al.* Cultures of human embryonic stem cells: serum replacement medium or serum-containing media and the effect of basic fibroblast growth factor. *Reprod. Biomed. Online* **9**, 330–337 (2004).
26. Xu, C. *et al.* Basic fibroblast growth factor supports undifferentiated human embryonic stem cell growth without conditioned medium. *Stem Cells Dayt. Ohio* **23**, 315–323 (2005).
27. Xu, R.-H. *et al.* Basic FGF and suppression of BMP signaling sustain undifferentiated proliferation of human ES cells. *Nat. Methods* **2**, 185–190 (2005).
28. Urist, M. R. Bone: formation by autoinduction. *Science* **150**, 893–899 (1965).
29. Zhang, J. & Li, L. BMP signaling and stem cell regulation. *Dev. Biol.* **284**, 1–11 (2005).
30. Brazil, D. P. & Hemmings, B. A. Ten years of protein kinase B signalling: a hard Akt to follow. *Trends Biochem. Sci.* **26**, 657–664 (2001).
31. Alessi, D. R. *et al.* Characterization of a 3-phosphoinositide-dependent protein kinase which phosphorylates and activates protein kinase B $\alpha$ . *Curr. Biol. CB* **7**, 261–269 (1997).
32. Sarbassov, D. D., Guertin, D. A., Ali, S. M. & Sabatini, D. M. Phosphorylation and Regulation of Akt/PKB by the Rictor-mTOR Complex. *Science* **307**, 1098–1101 (2005).
33. Feng, J., Park, J., Cron, P., Hess, D. & Hemmings, B. A. Identification of a PKB/Akt Hydrophobic Motif Ser-473 Kinase as DNA-dependent Protein Kinase. *J. Biol. Chem.* **279**, 41189–41196 (2004).
34. Riley, J. K. *et al.* The PI3K/Akt pathway is present and functional in the preimplantation mouse embryo. *Dev. Biol.* **284**, 377–386 (2005).
35. Paling, N. R. D., Wheadon, H., Bone, H. K. & Welham, M. J. Regulation of Embryonic Stem Cell Self-renewal by Phosphoinositide 3-Kinase-dependent Signaling. *J. Biol. Chem.* **279**, 48063–48070 (2004).
36. Watanabe, S. *et al.* Activation of Akt signaling is sufficient to maintain pluripotency in mouse and primate embryonic stem cells. *Oncogene* **25**, 2697–2707 (2006).
37. Takahashi, K., Mitsui, K. & Yamanaka, S. Role of ERas in promoting tumour-like properties in mouse embryonic stem cells. *Nature* **423**, 541 (2003).
38. Armstrong, L. *et al.* The role of PI3K/AKT, MAPK/ERK and NF $\kappa$ B signalling in the maintenance of human embryonic stem cell pluripotency and viability highlighted by transcriptional profiling and functional analysis. *Hum. Mol. Genet.* **15**, 1894–1913 (2006).
39. Wylie, C. Germ Cells. *Cell* **96**, 165–174 (1999).
40. Stevens, L. Origin of Testicular Teratomas from Primordial Germ Cells in Mice. *J. Natl. Cancer Inst.* **38**, 549- (1967).
41. Molecular biology of embryonic and teratocarcinoma stem cells. Proceedings of an international symposium. Prague, Czechoslovakia, 10-15 September 1984. *Cell Differ.* **15**, 69–279 (1984).
42. Kimura, T. *et al.* Conditional loss of PTEN leads to testicular teratoma and enhances embryonic germ cell production. *Development* **130**, 1691–1700 (2003).
43. Matsui, Y., Zsebo, K. & Hogan, B. L. M. Derivation of pluripotential embryonic stem cells from murine primordial germ cells in culture. *Cell* **70**, 841–847 (1992).
44. Resnick, J. L., Bixler, L. S., Cheng, L. & Donovan, P. J. Long-term proliferation of mouse primordial germ cells in culture. *Nature* **359**, 550–551 (1992).

45. Bijur, G. N. & Jope, R. S. Glycogen synthase kinase-3 beta is highly activated in nuclei and mitochondria. *Neuroreport* **14**, 2415–2419 (2003).
46. Miyamoto, S., Murphy, A. N. & Brown, J. H. Akt mediates mitochondrial protection in cardiomyocytes through phosphorylation of mitochondrial hexokinase-II. *Cell Death Differ.* **15**, 521–529 (2008).
47. Yang, J.-Y., Yeh, H.-Y., Lin, K. & Wang, P. H. Insulin stimulates Akt translocation to mitochondria: implications on dysregulation of mitochondrial oxidative phosphorylation in diabetic myocardium. *J. Mol. Cell. Cardiol.* **46**, 919–926 (2009).
48. Chan, D. C. Mitochondria: Dynamic Organelles in Disease, Aging, and Development. *Cell* **125**, 1241–1252 (2006).
49. Calvo, S. E. & Mootha, V. K. The Mitochondrial Proteome and Human Disease. *Annu. Rev. Genomics Hum. Genet.* **11**, 25–44 (2010).
50. Leese, H. J. & Barton, A. M. Pyruvate and glucose uptake by mouse ova and preimplantation embryos. *J. Reprod. Fertil.* **72**, 9–13 (1984).
51. Brinster, R. L. & Troike, D. E. Requirements for blastocyst development in vitro. *J. Anim. Sci.* **49 Suppl 2**, 26–34 (1979).
52. Merkle, S., Favor, J., Graw, J., Hornhardt, S. & Pretsch, W. Hereditary lactate dehydrogenase A-subunit deficiency as cause of early postimplantation death of homozygotes in *Mus musculus*. *Genetics* **131**, 413–421 (1992).
53. Merkle, S. & Pretsch, W. Characterization of triosephosphate isomerase mutants with reduced enzyme activity in *Mus musculus*. *Genetics* **123**, 837–844 (1989).
54. Pretsch, W. Enzyme-activity mutants in *Mus musculus*. I. Phenotypic description and genetic characterization of ethylnitrosourea-induced mutations. *Mamm. Genome Off. J. Int. Mamm. Genome Soc.* **11**, 537–542 (2000).
55. West, J. D., Flockhart, J. H., Peters, J. & Ball, S. T. Death of mouse embryos that lack a functional gene for glucose phosphate isomerase. *Genet. Res.* **56**, 223–236 (1990).
56. Chung, S. *et al.* Mitochondrial oxidative metabolism is required for the cardiac differentiation of stem cells. *Nat. Clin. Pract. Cardiovasc. Med.* **4 Suppl 1**, S60-67 (2007).
57. Cho, Y. M. *et al.* Dynamic changes in mitochondrial biogenesis and antioxidant enzymes during the spontaneous differentiation of human embryonic stem cells. *Biochem. Biophys. Res. Commun.* **348**, 1472–1478 (2006).
58. Shyh-Chang, N., Daley, G. Q. & Cantley, L. C. Stem cell metabolism in tissue development and aging. *Development* **140**, 2535–2547 (2013).
59. Varum, S. *et al.* Enhancement of human embryonic stem cell pluripotency through inhibition of the mitochondrial respiratory chain. *Stem Cell Res.* **3**, 142–156 (2009).
60. Koehler, C. M. Protein translocation pathways of the mitochondrion. *FEBS Lett.* **476**, 27–31 (2000).
61. Bijur, G. N. & Jope, R. S. Rapid accumulation of Akt in mitochondria following phosphatidylinositol 3-kinase activation. *J. Neurochem.* **87**, 1427–1435 (2003).
62. Linseman, D. A. *et al.* Glycogen Synthase Kinase-3 $\beta$  Phosphorylates Bax and Promotes Its Mitochondrial Localization during Neuronal Apoptosis. *J. Neurosci.* **24**, 9993–10002 (2004).
63. Maurer, U., Charvet, C., Wagman, A. S., Dejardin, E. & Green, D. R. Glycogen Synthase Kinase-3 Regulates Mitochondrial Outer Membrane Permeabilization and Apoptosis by Destabilization of MCL-1. *Mol. Cell* **21**, 749–760 (2006).
64. Juhaszova, M. *et al.* Role of Glycogen Synthase Kinase-3 $\beta$  in Cardioprotection. *Circ. Res.* **104**, 1240–1252 (2009).
65. Martel, C. *et al.* Glycogen synthase kinase 3-mediated voltage-dependent anion channel phosphorylation controls outer mitochondrial membrane permeability during lipid accumulation. *Hepatol. Baltim. Md* **57**, 93–102 (2013).



66. Robey, R. B. & Hay, N. Mitochondrial hexokinases, novel mediators of the antiapoptotic effects of growth factors and Akt. *Oncogene* **25**, 4683–4696 (2006).
67. Roberts, D. J., Tan-Sah, V. P., Smith, J. M. & Miyamoto, S. Akt Phosphorylates HK-II at Thr-473 and Increases Mitochondrial HK-II Association to Protect Cardiomyocytes. *J. Biol. Chem.* **288**, 23798–23806 (2013).
68. Roberts, D. J. & Miyamoto, S. Hexokinase II integrates energy metabolism and cellular protection: Acting on mitochondria and TORCing to autophagy. *Cell Death Differ.* **22**, 364 (2015).
69. Yang, J.-Y. *et al.* Impaired translocation and activation of mitochondrial Akt1 mitigated mitochondrial oxidative phosphorylation Complex V activity in diabetic myocardium. *J. Mol. Cell. Cardiol.* **59**, 167–175 (2013).
70. Su, C.-C., Yang, J.-Y., Leu, H.-B., Chen, Y. & Wang, P. H. Mitochondrial Akt-regulated mitochondrial apoptosis signaling in cardiac muscle cells. *Am. J. Physiol. Heart Circ. Physiol.* **302**, H716–723 (2012).
71. Ahmad, N. *et al.* Cardiac protection by mitoKATP channels is dependent on Akt translocation from cytosol to mitochondria during late preconditioning. *Am. J. Physiol. - Heart Circ. Physiol.* **290**, H2402–H2408 (2006).
72. Arciuch, V. G. A. *et al.* Akt1 Intramitochondrial Cycling Is a Crucial Step in the Redox Modulation of Cell Cycle Progression. *PLOS ONE* **4**, e7523 (2009).
73. Barksdale, K. A. & Bijur, G. N. The basal flux of Akt in the mitochondria is mediated by heat shock protein 90. *J. Neurochem.* **108**, 1289–1299 (2009).
74. Takahashi, K. & Yamanaka, S. Induction of Pluripotent Stem Cells from Mouse Embryonic and Adult Fibroblast Cultures by Defined Factors. *Cell* **126**, 663–676 (2006).
75. Takahashi, K. *et al.* Induction of Pluripotent Stem Cells from Adult Human Fibroblasts by Defined Factors. *Cell* **131**, 861–872 (2007).
76. Zhou, L. & Dean, J. Reprogramming the genome to totipotency in mouse embryos. *Trends Cell Biol.* **25**, 82–91 (2015).
77. Mason, C. & Dunnill, P. A brief definition of regenerative medicine. *Regen. Med.* **3**, 1–5 (2007).
78. Gimble, J. M., Katz, A. J. & Bunnell, B. A. Adipose-Derived Stem Cells for Regenerative Medicine. *Circ. Res.* **100**, 1249–1260 (2007).
79. Goudenege, S. *et al.* Enhancement of Myogenic and Muscle Repair Capacities of Human Adipose-derived Stem Cells With Forced Expression of MyoD. *Mol. Ther.* **17**, 1064–1072 (2009).
80. Wilmut, I., Schnieke, A. E., McWhir, J., Kind, A. J. & Campbell, K. H. Viable offspring derived from fetal and adult mammalian cells. *Nature* **385**, 810–813 (1997).
81. Gurdon, J. B. & Wilmut, I. Nuclear Transfer to Eggs and Oocytes. *Cold Spring Harb. Perspect. Biol.* **3**, (2011).
82. Tada, M., Takahama, Y., Abe, K., Nakatsuji, N. & Tada, T. Nuclear reprogramming of somatic cells by in vitro hybridization with ES cells. *Curr. Biol. CB* **11**, 1553–1558 (2001).
83. Cowan, C. A., Atienza, J., Melton, D. A. & Eggan, K. Nuclear reprogramming of somatic cells after fusion with human embryonic stem cells. *Science* **309**, 1369–1373 (2005).
84. Zhou, B. P. *et al.* HER-2/neu blocks tumor necrosis factor-induced apoptosis via the Akt/NF-kappaB pathway. *J. Biol. Chem.* **275**, 8027–8031 (2000).
85. Deng, W. *et al.* Protein kinase B (PKB/AKT1) formed signaling complexes with mitochondrial proteins and prevented glycolytic energy dysfunction in cultured cardiomyocytes during ischemia-reperfusion injury. *Endocrinology* **155**, 1618–1628 (2014).
86. Stadtfeld, M., Maherali, N., Borkent, M. & Hochedlinger, K. A reprogrammable mouse strain from gene-targeted embryonic stem cells. *Nat. Methods* **7**, 53–55 (2010).
87. Eminli, S. *et al.* Differentiation stage determines potential of hematopoietic cells for reprogramming into induced pluripotent stem cells. *Nat. Genet.* **41**, 968–976 (2009).

88. Polo, J. M. *et al.* Cell type of origin influences the molecular and functional properties of mouse induced pluripotent stem cells. *Nat. Biotechnol.* **28**, 848–855 (2010).
89. appendix [Stem Cell Information]. Available at: <http://stemcells.nih.gov/info/scireport/pages/appendix.aspx>. (Accessed: 8th May 2016)
90. Pesce, M. & Schöler, H. R. Oct-4: gatekeeper in the beginnings of mammalian development. *Stem Cells Dayt. Ohio* **19**, 271–278 (2001).
91. Mitsui, K. *et al.* The homeoprotein Nanog is required for maintenance of pluripotency in mouse epiblast and ES cells. *Cell* **113**, 631–642 (2003).
92. Rodda, D. J. *et al.* Transcriptional regulation of nanog by OCT4 and SOX2. *J. Biol. Chem.* **280**, 24731–24737 (2005).
93. Zaehres, H. *et al.* High-Efficiency RNA Interference in Human Embryonic Stem Cells. *STEM CELLS* **23**, 299–305 (2005).
94. Fong, H., Hohenstein, K. A. & Donovan, P. J. Regulation of self-renewal and pluripotency by Sox2 in human embryonic stem cells. *Stem Cells Dayt. Ohio* **26**, 1931–1938 (2008).
95. Chen, L. & Daley, G. Q. Molecular basis of pluripotency. *Hum. Mol. Genet.* **17**, R23–R27 (2008).
96. Martin, G. R., Wiley, L. M. & Damjanov, I. The development of cystic embryoid bodies in vitro from clonal teratocarcinoma stem cells. *Dev. Biol.* **61**, 230–244 (1977).
97. Stevens, L. C. Origin of testicular teratomas from primordial germ cells in mice. *J. Natl. Cancer Inst.* **38**, 549–552 (1967).
98. Takai, D. & Jones, P. A. Comprehensive analysis of CpG islands in human chromosomes 21 and 22. *Proc. Natl. Acad. Sci. U. S. A.* **99**, 3740–3745 (2002).
99. Miranda, T. B. & Jones, P. A. DNA methylation: The nuts and bolts of repression. *J. Cell. Physiol.* **213**, 384–390 (2007).
100. Coskun, V., Tsoa, R. & Sun, Y. E. Epigenetic regulation of stem cells differentiating along the neural lineage. *Curr. Opin. Neurobiol.* **22**, 762–767 (2012).
101. Kraushaar, D. C. & Zhao, K. The Epigenomics of Embryonic Stem Cell Differentiation. *Int. J. Biol. Sci.* **9**, 1134–1144 (2013).
102. Nishino, K. *et al.* DNA Methylation Dynamics in Human Induced Pluripotent Stem Cells over Time. *PLOS Genet* **7**, e1002085 (2011).
103. Lee, D.-S. *et al.* An epigenomic roadmap to induced pluripotency reveals DNA methylation as a reprogramming modulator. *Nat. Commun.* **5**, 5619 (2014).
104. Young, R. A. Control of the Embryonic Stem Cell State. *Cell* **144**, 940–954 (2011).
105. Gurdon, J. B., Elsdale, T. R. & Fischberg, M. Sexually mature individuals of *Xenopus laevis* from the transplantation of single somatic nuclei. *Nature* **182**, 64–65 (1958).
106. Teif, V. B. *et al.* Genome-wide nucleosome positioning during embryonic stem cell development. *Nat. Struct. Mol. Biol.* **19**, 1185–1192 (2012).
107. Yazdi, P. G. *et al.* Increasing Nucleosome Occupancy Is Correlated with an Increasing Mutation Rate so Long as DNA Repair Machinery Is Intact. *PLOS ONE* **10**, e0136574 (2015).
108. Yazdi, P. G. *et al.* Nucleosome Organization in Human Embryonic Stem Cells. *PloS One* **10**, e0136314 (2015).
109. Doi, A. *et al.* Differential methylation of tissue- and cancer-specific CpG island shores distinguishes human induced pluripotent stem cells, embryonic stem cells and fibroblasts. *Nat. Genet.* **41**, 1350–1353 (2009).
110. Bock, C. *et al.* Reference Maps of Human ES and iPS Cell Variation Enable High-Throughput Characterization of Pluripotent Cell Lines. *Cell* **144**, 439–452 (2011).
111. Planello, A. C. *et al.* Aberrant DNA methylation reprogramming during induced pluripotent stem cell generation is dependent on the choice of reprogramming factors. *Cell Regen. Lond. Engl.* **3**, 4 (2014).

112. Lister, R. *et al.* Hotspots of aberrant epigenomic reprogramming in human induced pluripotent stem cells. *Nature* **471**, 68–73 (2011).
113. Ohi, Y. *et al.* Incomplete DNA methylation underlies a transcriptional memory of somatic cells in human iPS cells. *Nat. Cell Biol.* **13**, 541–549 (2011).
114. Folmes, C. D. L. *et al.* Somatic oxidative bioenergetics transitions into pluripotency-dependent glycolysis to facilitate nuclear reprogramming. *Cell Metab.* **14**, 264–271 (2011).
115. Heiden, M. G. V., Cantley, L. C. & Thompson, C. B. Understanding the Warburg Effect: The Metabolic Requirements of Cell Proliferation. *Science* **324**, 1029–1033 (2009).
116. Karytinis, A. *et al.* A novel mammalian flavin-dependent histone demethylase. *J. Biol. Chem.* **284**, 17775–17782 (2009).
117. Wu, H. & Zhang, Y. Mechanisms and functions of Tet protein-mediated 5-methylcytosine oxidation. *Genes Dev.* **25**, 2436–2452 (2011).
118. Miyamoto, S., Rubio, M. & Sussman, M. A. Nuclear and mitochondrial signalling Akts in cardiomyocytes. *Cardiovasc. Res.* **82**, 272–285 (2009).
119. Storm, M. P. *et al.* Regulation of Nanog expression by phosphoinositide 3-kinase-dependent signaling in murine embryonic stem cells. *J. Biol. Chem.* **282**, 6265–6273 (2007).
120. Santi, S. A. & Lee, H. The Akt isoforms are present at distinct subcellular locations. *Am. J. Physiol. Cell Physiol.* **298**, C580–591 (2010).
121. Osellame, L. D., Blacker, T. S. & Duchen, M. R. Cellular and molecular mechanisms of mitochondrial function. *Best Pract. Res. Clin. Endocrinol. Metab.* **26**, 711–723 (2012).
122. Ito, K. & Suda, T. Metabolic requirements for the maintenance of self-renewing stem cells. *Nat. Rev. Mol. Cell Biol.* **15**, 243–256 (2014).
123. Panopoulos, A. D. *et al.* The metabolome of induced pluripotent stem cells reveals metabolic changes occurring in somatic cell reprogramming. *Cell Res.* **22**, 168–177 (2012).
124. Murphy, M. P. How mitochondria produce reactive oxygen species. *Biochem. J.* **417**, 1–13 (2009).
125. Wu, Y. *et al.* Oxidative stress inhibits adhesion and transendothelial migration, and induces apoptosis and senescence of induced pluripotent stem cells. *Clin. Exp. Pharmacol. Physiol.* **40**, 626–634 (2013).
126. Rhee, S. G. Redox signaling: hydrogen peroxide as intracellular messenger. *Exp. Mol. Med.* **31**, 53–59 (1999).
127. D’Aur aux, B. & Toledano, M. B. ROS as signalling molecules: mechanisms that generate specificity in ROS homeostasis. *Nat. Rev. Mol. Cell Biol.* **8**, 813–824 (2007).
128. Schieber, M. & Chandel, N. S. ROS Function in Redox Signaling and Oxidative Stress. *Curr. Biol.* **24**, R453–R462 (2014).
129. Crespo, F. L., Sobrado, V. R., Gomez, L., Cervera, A. M. & McCreath, K. J. Mitochondrial reactive oxygen species mediate cardiomyocyte formation from embryonic stem cells in high glucose. *Stem Cells Dayt. Ohio* **28**, 1132–1142 (2010).
130. Zhang, J. *et al.* UCP2 regulates energy metabolism and differentiation potential of human pluripotent stem cells. *EMBO J.* **30**, 4860–4873 (2011).
131. Ji, J. *et al.* Antioxidant Supplementation Reduces Genomic Aberrations in Human Induced Pluripotent Stem Cells. *Stem Cell Rep.* **2**, 44–51 (2014).
132. Esteban, M. A. *et al.* Vitamin C Enhances the Generation of Mouse and Human Induced Pluripotent Stem Cells. *Cell Stem Cell* **6**, 71–79 (2010).
133. Sellick, C. A., Hansen, R., Stephens, G. M., Goodacre, R. & Dickson, A. J. Metabolite extraction from suspension-cultured mammalian cells for global metabolite profiling. *Nat. Protoc.* **6**, 1241–1249 (2011).
134. Tsang, W. P., Chau, S. P. Y., Kong, S. K., Fung, K. P. & Kwok, T. T. Reactive oxygen species mediate doxorubicin induced p53-independent apoptosis. *Life Sci.* **73**, 2047–2058 (2003).

135. Kim, S.-Y. *et al.* Doxorubicin-induced reactive oxygen species generation and intracellular Ca<sup>2+</sup> increase are reciprocally modulated in rat cardiomyocytes. *Exp. Mol. Med.* **38**, 535–545 (2006).
136. Shen, Y.-A., Wang, C.-Y., Hsieh, Y.-T., Chen, Y.-J. & Wei, Y.-H. Metabolic reprogramming orchestrates cancer stem cell properties in nasopharyngeal carcinoma. *Cell Cycle* **14**, 86–98 (2015).
137. Oburoglu, L. *et al.* Glucose and Glutamine Metabolism Regulate Human Hematopoietic Stem Cell Lineage Specification. *Cell Stem Cell* **15**, 169–184 (2014).
138. Shyh-Chang, N., Zheng, Y., Locasale, J. W. & Cantley, L. C. Human pluripotent stem cells decouple respiration from energy production. *EMBO J.* **30**, 4851–4852 (2011).
139. Varum, S. *et al.* Energy Metabolism in Human Pluripotent Stem Cells and Their Differentiated Counterparts. *PLOS ONE* **6**, e20914 (2011).
140. Pedersen, B. A. *et al.* Novel remodeling of the mouse heart mitochondrial proteome in response to acute insulin stimulation. *Nutr. Metab. Cardiovasc. Dis. NMCD* **25**, 1152–1158 (2015).
141. Nowak, G. & Bakajsova, D. Protein Kinase C- $\alpha$  Interaction with FOF1-ATPase Promotes FOF1-ATPase Activity and Reduces Energy Deficits in Injured Renal Cells. *J. Biol. Chem.* **290**, 7054–7066 (2015).
142. Bauer, B. & Baier, G. Protein kinase C and AKT/protein kinase B in CD4<sup>+</sup> T-lymphocytes: new partners in TCR/CD28 signal integration. *Mol. Immunol.* **38**, 1087–1099 (2002).
143. Konishi, H., Kuroda, S. & Kikkawa, U. The Pleckstrin Homology Domain of RAC Protein Kinase Associates with the Regulatory Domain of Protein Kinase C  $\zeta$ . *Biochem. Biophys. Res. Commun.* **205**, 1770–1775 (1994).
144. Doornbos, R. P. *et al.* Protein kinase Czeta is a negative regulator of protein kinase B activity. *J. Biol. Chem.* **274**, 8589–8596 (1999).
145. Mao, M. *et al.* Inhibition of growth-factor-induced phosphorylation and activation of protein kinase B/Akt by atypical protein kinase C in breast cancer cells. *Biochem. J.* **352 Pt 2**, 475–482 (2000).
146. Majumder, P. K. *et al.* Targeting of protein kinase C delta to mitochondria in the oxidative stress response. *Cell Growth Differ. Mol. Biol. J. Am. Assoc. Cancer Res.* **12**, 465–470 (2001).
147. Li, L., Lorenzo, P. S., Bogi, K., Blumberg, P. M. & Yuspa, S. H. Protein Kinase C $\delta$  Targets Mitochondria, Alters Mitochondrial Membrane Potential, and Induces Apoptosis in Normal and Neoplastic Keratinocytes When Overexpressed by an Adenoviral Vector. *Mol. Cell. Biol.* **19**, 8547–8558 (1999).
148. Sazanov, L. A. Respiratory complex I: mechanistic and structural insights provided by the crystal structure of the hydrophilic domain. *Biochemistry (Mosc.)* **46**, 2275–2288 (2007).
149. Kussmaul, L. & Hirst, J. The mechanism of superoxide production by NADH:ubiquinone oxidoreductase (complex I) from bovine heart mitochondria. *Proc. Natl. Acad. Sci. U. S. A.* **103**, 7607–7612 (2006).
150. Hirst, J., King, M. S. & Pryde, K. R. The production of reactive oxygen species by complex I. *Biochem. Soc. Trans.* **36**, 976–980 (2008).
151. Yoshida, Y., Takahashi, K., Okita, K., Ichisaka, T. & Yamanaka, S. Hypoxia enhances the generation of induced pluripotent stem cells. *Cell Stem Cell* **5**, 237–241 (2009).
152. Banito, A. *et al.* Senescence impairs successful reprogramming to pluripotent stem cells. *Genes Dev.* **23**, 2134–2139 (2009).
153. Patel, M. S., Nemeria, N. S., Furey, W. & Jordan, F. The Pyruvate Dehydrogenase Complexes: Structure-based Function and Regulation. *J. Biol. Chem.* **289**, 16615–16623 (2014).
154. Patel, K. P., O'Brien, T. W., Subramony, S. H., Shuster, J. & Stacpoole, P. W. The spectrum of pyruvate dehydrogenase complex deficiency: clinical, biochemical and genetic features in 371 patients. *Mol. Genet. Metab.* **105**, 34–43 (2012).

155. Harris, R. A., Bowker-Kinley, M. M., Huang, B. & Wu, P. Regulation of the activity of the pyruvate dehydrogenase complex. *Adv. Enzyme Regul.* **42**, 249–259 (2002).
156. Patel, M. S. & Korotchkina, L. G. Regulation of the pyruvate dehydrogenase complex. *Biochem. Soc. Trans.* **34**, 217–222 (2006).
157. Yeaman, S. J. *et al.* Sites of phosphorylation on pyruvate dehydrogenase from bovine kidney and heart. *Biochemistry (Mosc.)* **17**, 2364–2370 (1978).
158. Behal, R. H., Buxton, D. B., Robertson, J. G. & Olson, M. S. Regulation of the pyruvate dehydrogenase multienzyme complex. *Annu. Rev. Nutr.* **13**, 497–520 (1993).
159. Ravindran, S., Radke, G. A., Guest, J. R. & Roche, T. E. Lipoyl domain-based mechanism for the integrated feedback control of the pyruvate dehydrogenase complex by enhancement of pyruvate dehydrogenase kinase activity. *J. Biol. Chem.* **271**, 653–662 (1996).
160. Yang, D., Gong, X., Yakhnin, A. & Roche, T. E. Requirements for the adaptor protein role of dihydrolipoyl acetyltransferase in the up-regulated function of the pyruvate dehydrogenase kinase and pyruvate dehydrogenase phosphatase. *J. Biol. Chem.* **273**, 14130–14137 (1998).
161. Holness, M. J., Kraus, A., Harris, R. A. & Sugden, M. C. Targeted upregulation of pyruvate dehydrogenase kinase (PDK)-4 in slow-twitch skeletal muscle underlies the stable modification of the regulatory characteristics of PDK induced by high-fat feeding. *Diabetes* **49**, 775–781 (2000).
162. Razeghi, P., Young, M. E., Abbasi, S. & Taegtmeyer, H. Hypoxia in vivo decreases peroxisome proliferator-activated receptor alpha-regulated gene expression in rat heart. *Biochem. Biophys. Res. Commun.* **287**, 5–10 (2001).
163. Shen, M.-Y. & Sali, A. Statistical potential for assessment and prediction of protein structures. *Protein Sci.* **15**, 2507–24 (2006). - Google Search. Available at: [https://www.google.com/search?q=Shen%2C+M.-Y.+%26+Sali%2C+A.+Statistical+potential+for+assessment+and+prediction+of+protein+structures.+Protein+Sci.+15%2C+2507%E2%80%9324+\(2006\).&ie=utf-8&oe=utf-8&channel=fs&trackid=sp-006&gws\\_rd=ssl](https://www.google.com/search?q=Shen%2C+M.-Y.+%26+Sali%2C+A.+Statistical+potential+for+assessment+and+prediction+of+protein+structures.+Protein+Sci.+15%2C+2507%E2%80%9324+(2006).&ie=utf-8&oe=utf-8&channel=fs&trackid=sp-006&gws_rd=ssl). (Accessed: 16th May 2016)
164. Schrödinger - Product Suites - List of All Products - Glide. Available at: <http://www.schrodinger.com/Glide/>. (Accessed: 16th May 2016)
165. Friesner, R. A. *et al.* Glide: a new approach for rapid, accurate docking and scoring. 1. Method and assessment of docking accuracy. *J. Med. Chem.* **47**, 1739–1749 (2004).
166. Halgren, T. A. *et al.* Glide: a new approach for rapid, accurate docking and scoring. 2. Enrichment factors in database screening. *J. Med. Chem.* **47**, 1750–1759 (2004).
167. Li, H., Kasam, V., Tautermann, C. S., Seeliger, D. & Vaidehi, N. Computational method to identify druggable binding sites that target protein-protein interactions. *J. Chem. Inf. Model.* **54**, 1391–1400 (2014).
168. Sastry, G. M., Dixon, S. L. & Sherman, W. Rapid shape-based ligand alignment and virtual screening method based on atom/feature-pair similarities and volume overlap scoring. *J. Chem. Inf. Model.* **51**, 2455–2466 (2011).
169. Dixon, S. L. *et al.* PHASE: a new engine for pharmacophore perception, 3D QSAR model development, and 3D database screening: 1. Methodology and preliminary results. *J. Comput. Aided Mol. Des.* **20**, 647–671 (2006).
170. Dixon, S. L., Smondryev, A. M. & Rao, S. N. PHASE: A Novel Approach to Pharmacophore Modeling and 3D Database Searching. *Chem. Biol. Drug Des.* **67**, 370–372 (2006).
171. Jacobson, M. P. *et al.* A hierarchical approach to all-atom protein loop prediction. *Proteins* **55**, 351–367 (2004).
172. Li, X., Jacobson, M. P. & Friesner, R. A. High-resolution prediction of protein helix positions and orientations. *Proteins Struct. Funct. Bioinforma.* **55**, 368–382 (2004).

173. Jacobson, M. P., Friesner, R. A., Xiang, Z. & Honig, B. On the role of the crystal environment in determining protein side-chain conformations. *J. Mol. Biol.* **320**, 597–608 (2002).
174. Schrödinger - Resources & Downloads - Citations. Available at: <http://www.schrodinger.com/citations/41/11/1/>. (Accessed: 24th May 2016)
175. Gabdouliline, R. R. & Wade, R. C. Brownian dynamics simulation of protein-protein diffusional encounter. *Methods San Diego Calif* **14**, 329–341 (1998).
176. Smith, R. A. J., Porteous, C. M., Gane, A. M. & Murphy, M. P. Delivery of bioactive molecules to mitochondria in vivo. *Proc. Natl. Acad. Sci.* **100**, 5407–5412 (2003).
177. Smith, R. A. J., Hartley, R. C. & Murphy, M. P. Mitochondria-targeted small molecule therapeutics and probes. *Antioxid. Redox Signal.* **15**, 3021–3038 (2011).
178. Han, J., Lee, T. H., Tung, C.-H. & Lee, D. Y. Design and synthesis of a mitochondria-targeting carrier for small molecule drugs. *Org. Biomol. Chem.* **12**, 9793–9796 (2014).
179. Feldhoff, P. W., Arnold, J., Oesterling, B. & Vary, T. C. Insulin-induced activation of pyruvate dehydrogenase complex in skeletal muscle of diabetic rats. *Metabolism* **42**, 615–623 (1993).
180. Zhang, S., Hulver, M. W., McMillan, R. P., Cline, M. A. & Gilbert, E. R. The pivotal role of pyruvate dehydrogenase kinases in metabolic flexibility. *Nutr. Metab.* **11**, 10 (2014).
181. Jeoung, N. H. & Harris, R. A. Pyruvate dehydrogenase kinase-4 deficiency lowers blood glucose and improves glucose tolerance in diet-induced obese mice. *Am. J. Physiol. Endocrinol. Metab.* **295**, E46-54 (2008).
182. Maj, M. C. *et al.* Pyruvate dehydrogenase phosphatase deficiency: identification of the first mutation in two brothers and restoration of activity by protein complementation. *J. Clin. Endocrinol. Metab.* **90**, 4101–4107 (2005).
183. Benelli, C. *et al.* Evidence for a role of protein kinase C in the activation of the pyruvate dehydrogenase complex by insulin in Zajdela hepatoma cells. *Metabolism.* **43**, 1030–1034 (1994).
184. Caruso, M. *et al.* Activation and Mitochondrial Translocation of Protein Kinase C $\delta$  Are Necessary for Insulin Stimulation of Pyruvate Dehydrogenase Complex Activity in Muscle and Liver Cells. *J. Biol. Chem.* **276**, 45088–45097 (2001).
185. Cho, H., Thorvaldsen, J. L., Chu, Q., Feng, F. & Birnbaum, M. J. Akt1/PKB $\alpha$  Is Required for Normal Growth but Dispensable for Maintenance of Glucose Homeostasis in Mice. *J. Biol. Chem.* **276**, 38349–38352 (2001).
186. Cho, H. *et al.* Insulin Resistance and a Diabetes Mellitus-Like Syndrome in Mice Lacking the Protein Kinase Akt2 (PKB $\beta$ ). *Science* **292**, 1728–1731 (2001).
187. JCI - Severe diabetes, age-dependent loss of adipose tissue, and mild growth deficiency in mice lacking Akt2/PKB $\beta$ . Available at: <http://www.jci.org/articles/view/16885>. (Accessed: 18th May 2016)
188. Tang, Y. *et al.* Differential effects of Akt isoforms on somatic cell reprogramming. *J Cell Sci* **127**, 3998–4008 (2014).
189. Obata, T. *et al.* Peptide and protein library screening defines optimal substrate motifs for AKT/PKB. *J. Biol. Chem.* **275**, 36108–36115 (2000).
190. Ubersax, J. A. & Ferrell Jr, J. E. Mechanisms of specificity in protein phosphorylation. *Nat. Rev. Mol. Cell Biol.* **8**, 530–541 (2007).
191. Ubersax, J. A. *et al.* Targets of the cyclin-dependent kinase Cdk1. *Nature* **425**, 859–864 (2003).
192. Manning, B. D. & Cantley, L. C. AKT/PKB signaling: navigating downstream. *Cell* **129**, 1261–1274 (2007).
193. Babady, N. E., Pang, Y.-P., Elpeleg, O. & Isaya, G. Cryptic proteolytic activity of dihydrolipoamide dehydrogenase. *Proc. Natl. Acad. Sci. U. S. A.* **104**, 6158–6163 (2007).